UCRL 8642

UNIVERSITY OF CALIFORNIA
Ernest O. Lawrence
Radiation Laboratory

I. NUCLEAR SPECTROSCOPIC STUDIES IN THE HEAVIEST ELEMENT REGION
II. AN ACCELERATING ELECTRON SPECTROGRAPH

TWO-WEEK LOAN COPY

This is a Library Circulating Copy which may be borrowed for two weeks. For a personal retention copy, call Tech. Info. Division, Ext. 5545

DISCLAIMER

This document was prepared as an account of work sponsored by the United States Government. While this document is believed to contain correct information, neither the United States Government nor any agency thereof, nor the Regents of the University of California, nor any of their employees, makes any warranty, express or implied, or assumes any legal responsibility for the accuracy, completeness, or usefulness of any information, apparatus, product, or process disclosed, or represents that its use would not infringe privately owned rights. Reference herein to any specific commercial product, process, or service by its trade name, trademark, manufacturer, or otherwise, does not necessarily constitute or imply its endorsement, recommendation, or favoring by the United States Government or any agency thereof, or the Regents of the University of California. The views and opinions of authors expressed herein do not necessarily state or reflect those of the United States Government or any agency thereof or the Regents of the University of California.

UCRL-8642
UC-4 Chemistry General
TID-4500 (15th Ed.)

UNIVERSITY OF CALIFORNIA

Lawrence Radiation Laboratory
Berkeley, California

Contract No. W-7405-eng-48

I. NUCLEAR SPECTROSCOPIC STUDIES IN THE HEAVIEST ELEMENT REGION

II. AN ACCELERATING ELECTRON SPECTROGRAPH

Royal G. Albridge, Jr.

(Thesis)

April 1960

Printed in USA. Price $2.50. Available from the
Office of Technical Services
U. S. Department of Commerce
Washington 25, D.C.

Climbers

Moments of time
May be mountains,
Leaning up the long slant of day,
An arduous climb,
And rougher still
The steeper slopes of night.
There are other mountain climbers
Than mountain climbers;
Other summits than peaks.
Sometimes
Even to rise from sleep
Is Everest.

Charles Lee

Contents

Abstract. 3
Part One: Nuclear Spectroscopic Studies in the Heaviest Element Region 4
I. Introduction. 4
II. Experimental Techniques 6
A. Instruments 6
B. Intensity Measurements. 7
C. Source Production and Chemistry 8
III. Decay Scheme Studies. 12
A. Neptunium-238 12
B. Protactinium-233. 29
C. Curium-241. 86
IV. Conclusion. 102

Part Two: An Accelerating Electron Spectrograph. 103
I. Introduction. 103
II. The Instrument. 106
A. Vacuum Chamber and System 106
B. The Camera. 109
C. Instrumentation and High Voltage Supplies 114
III. Radioactive Sources 118
IV. Results 119
A. Preaccelerator. 119
B. Postaccelerator 126
V. Intensity Measurements. 130
VI. Conclusions 133
Acknowledgments 134
Appendix - Calculations of Source Absorption for the Pa^{233} Gamma-Ray Sources. 135
I. Wire Source. 135
II. ThO_2 Source. 138
References. 141

Part One: NUCLEAR SPECTROSCOPIC STUDIES IN THE HEAVIEST ELEMENT REGION

Part Two: AN ACCELERATING ELECTRON SPECTROGRAPH

Royal G. Albridge, Jr.
(Thesis)

Lawrence Radiation Laboratory and Department of Chemistry
University of California, Berkeley, California

April 1960

ABSTRACT

The decays of Np^{238} and Pa^{233} were studied by means of high-resolution spectroscopic instruments. The proposed decay schemes were tested by comparing the experimental data with predictions of the Bohr-Mottelson Theory of Deformed Nuclei. Previously unreported transitions were observed and some of these were used to assign new levels in the daughter nuclei, Pu^{238} and U^{233}. Gamma-gamma coincidence techniques were used to study the electron-capture decay of Cm^{241}. The decay scheme is discussed in the light of data obtained.

An accelerating permanent-magnet electron spectrograph for the detection of low-energy electrons was constructed. The instrument can be used as either a pre- or postaccelerating spectrograph. The equipment was used to study the low-energy electron spectrum of Pa^{233}.

Part One: NUCLEAR SPECTROSCOPIC STUDIES IN THE HEAVIEST ELEMENT REGION
Part Two: AN ACCELERATING ELECTRON SPECTROGRAPH

Royal G. Albridge, Jr.
(Thesis)

Lawrence Radiation Laboratory and Department of Chemistry
University of California, Berkeley, California

April 1960

Part One
NUCLEAR SPECTROSCOPIC STUDIES IN THE HEAVIEST ELEMENT REGION

I. INTRODUCTION

Within the last decade great advances have been made toward the understanding of nuclear structure. A large amount of experimental data has been accumulated in the fields of high-energy nuclear physics, nuclear reactions, and nuclear spectroscopy, and much of this information has been correlated and at least partially explained by theory. Some of the largest strides of this nature have been made in nuclear spectroscopy, a field wherein two theories of nuclear structure have met with remarkable success. (It is certainly unnecessary to do more than mention the nuclear shell model of Mayer,[1] and Haxel, Jensen, and Suess,[2] and the collective model of Bohr and Mottelson.)[3,4]

Because of the great success of the collective model in explaining the dynamical aspects of deformed nuclei, the heaviest element region has become to the spectroscopist a fruitful area of investigation, and much work has already been accomplished in this region. As the theoretical treatments have become more refined it has become increasingly important that the experimentalist obtain correspondingly detailed information about nuclear decay schemes which may serve as a test of the theory and thus lead to better understanding.

Because deformed nuclei possess rotational, vibrational, and intrinsic modes of excitation, spectroscopic studies in the regions of deformation attempt to discern the natures of the observed studies and to classify them with appropriate quantum numbers. To this end such data as energy spacings, transition multipolarities, relative transition probabilities, and transition rates are required.

This study has been undertaken to obtain information about the decay schemes of some heaviest element nuclei and to analyze these data for the above purposes. The techniques employed and the analysis undertaken are typical of those used in the fiels of nuclear spectroscopy. For this reason it is felt unnecessary to present a detailed general discussion of such topics as the application of the Bohr-Mottelson theory to the heavy element region. For a general reference of this nature a report by Hyde is recommended.[5]

II. EXPERIMENTAL TECHNIQUES

A. Instruments

The instruments used in this study have all been described in previous publications; therefore only a brief description will be given and references cited.

1. Permanent-Magnet Spectrographs

Permanent magnet spectrographs[6] with field strengths of 52, 99, 160, 216, and 350 gauss were used for the detection of conversion electrons. These spectrographs have a resolution of ~0.1% and a transmission of the order 0.1% to 0.01%.

2. Accelerating Spectrograph

A permanent-magnet preaccelerating spectrograph was used to study the low-energy electron spectrum of Pa^{233}. This instrument is described in Part Two of this dissertation.

3. Double-Focusing Spectrometer

Conversion electrons and continuous beta spectra were measured by means of a double-focusing spectrometer[7] of 0.3% resolution and 0.1% transmission. A VYNS film of ~ 100 $\mu g/cm^2$ thickness was used as the counter window.

4. Bent-Crystal Spectrometer

The DuMond transmission-type bent-crystal spectrometer Mark I[8] (located at the California Institute of Technology, Pasadena, California) was used for precision measurements[9] of the energy and intensities of gamma rays resulting from the decay of Pa^{233}. This instrument measures the wave length of gamma rays by means of direct crystalline diffraction in a bent quartz crystal. A thallium-activated sodium iodide crystal serves as the primary detector. Two different detector arrangements were used. The initial experiment employed a 3-inch-diameter by 2-inch cylindrical sodium iodide crystal connected to a single-channel pulse-height analyzer with chart recorder. Later, a 5-inch-diameter by 3-inch

long cylindrical sodium iodide cyrstal was used with the single-channel analyzer for energy determinations and with a 100-channel Penco Gamma Analyzer for intensity measurements. The pulse-height analyzers were used to reduce the background counting rate by distinguishing those pulses arising from radiations whose energies differed from that of the photons being focused on the detector by the bent quartz crystal.

The instrument is such that the width at half maximum of the recorded peak ($\Delta\lambda$) is constant over the wave length range; $\Delta\lambda$ is of the order of 0.28 x-unit. The resolution, defined as $\Delta\lambda/\lambda$, varies with λ (and hence with energy). The resolution is of order 0.2% at 100 kev and 0.9% at 400 kev. The transmission is approximately the solid angle subtended by an 0.008-inch source at 2 meters.

5. Lens Spectrometer

A thick-lens solenoidal-type spectrometer[10] with 2% resolution and 2% transmission was used for certain phases of the work.

6. Penco Gamma Analyzer

A 100-channel pulse-height gamma analyzer[11] with a 3 x 3-inch thallium-activated sodium iodide crystal was used for the detection of gamma rays. The resolution was 8% at 560 kev and 10% at 280 kev.

7. Gamma-Gamma Coincidence Apparatus

A fast-slow type of coincidence apparatus was used in the study of the decay of Cm^{241}. Thallium-activated sodium iodide crystals (1-1/2 x 1-inch) were the detectors, and the data were recorded by a 50-channel pulse-height analyzer. A block diagram of the apparatus is given by Pilger.[12]

B. Intensity Measurements

The relative intensities of the conversion lines recorded photographically by the permanent-magnet spectrographs were obtained by two different means -- densitometer tracings and visual estimates. A Dietart ARL Recording Densitometer[13] was used to trace the photographic plates,

and these tracings were analyzed by the method of Mladjenovic and Slatis.[14] Standard sources had previously been used at this laboratory to determine the relation between the exposure and photographic darkening for the film used, which was Kodak no-screen x-ray emulsion (25μ) on glass backing.

In some instances the ratio of background to line intensity was too high to permit an accurate analysis by means of densitometry. In these cases relative intensities were obtained from visual comparisons of plates exposed for different periods of time. Two photographic plates differing in exposure by a known factor were placed one on top of the other with emulsions touching, and were viewed over a diffuse source of light. Two lines that were to be analyzed were lined up beside each other and their relative intensities compared. If, under these conditions, the intensities of the lines appeared to be equal, then the absolute intensities of the lines were assumed to differ by the same factor as the exposures. By superimposing the plates in this manner one hopes to cancel differences in the backgrounds of the plates, because both lines are viewed through the same background. This method proved so useful that a set of standard-intensity plates was prepared by making several exposures of a Pa^{233} source, the exposure time varying from 2 to 80 hours. In those cases in which comparison could be made the agreement between intensities obtained by densitometry and visual estimates was good to within 10%. In all cases corrections were made for instrument geometry (by multiplying by the radius of curvature of the electron path[14]) and for film efficiency. The relationship between film efficiency and energy is discussed in Part Two.

C. Source Production and Chemistry

1. Neptunium-238

The Np^{238} spectrograph samples were prepared by irradiating ≈ 100-μg quantities of Np^{237} in the Materials Testing Reactor, Arco, Idaho. Capsules prepared by heat-sealing both ends of 1-1/2-inch pieces of 6-mm quartz tubing held the target material. After one end of the tubing had been sealed, the Np^{237}, dissolved in a drop of hydrochloric

acid, was introduced and centrifuged to the bottom. the acid was evaporated, then the tube baked dry and the other end sealed. An irradiation time of 5 hr at a flux of 2×10^{14} neutrons/cm^2/sec was chosen in order to obtain a large ratio of Np^{238} to Np^{239} activity.

The following chemistry, similar to that described by Gibson,[15] was used for purifying the sample:

(a) The sample was dissolved in concentrated HCl containing a small amount of concentrated HNO_3.

(b) Approximately 3-mg quantities of carriers were added: Zr(IV) to carry the neptunium, and Ba, Sr, Cd, and La as hold-back carriers.

(c) Fe^{++} was added and the solution warmed to reduce the neptunium to the (IV) state.

(d) The Np(IV) was carried on $Zr_3(PO_4)_4$ precipitated by the addition of concentrated H_3PO_4.

(e) The $Zr_3(PO_4)_4$ precipitate was dissolved in 1 M HNO_3, 4 M HF, and lanthanum carried added to precipitate LaF_3 which carried the Np.

(f) LaF_3 was dissolved in an H_3BO_3-HNO_3 solution and $La(OH)_3$ precipitated by the addition of NH_4OH.

(g) The $La(OH)_3$ was dissolved in concentrated HCl and passed through a Dowex A-1 column (6 cm x 3 mm). The La passed through and the Np was adsorbed.

(h) The Np was eluted with 1 M HCl.

The TTA (thenoyltrifluoracetone) extraction used by Gibson was replaced by the anion column, because of difficulties encountered in back-extracting the neptunium from the TTA. The anion column is not as selective as the TTA, and would not have removed any Zr(IV) or Fe(III,II) that might have reached the final step.

An Np^{238} sample was also prepared for measuring the spin of Np^{238} by the atomic beam technique. The spin measurement was performed in co-operation with Richard Marrus and Jack Hubbs. The sample was made by neutron irradiation of a mixture of 3 mg of Np^{237} and 10 mg of U^{238} oxides for 72 hr at a flux of 2×10^{13} neutrons/cm^2/sec. The target was prepared by coprecipitating neptunium and uranium hydroxides by the addition of NH_4OH to a HCl solution of the metals. The hydroxides were converted to

the oxides by heating. The U^{238} was added to serve as a carrier for the small quantity of Np^{237}.

Following the irradiation no purification chemistry was performed. The oxides were mixed with an excess of graphite powder, which served to reduce the oxide to the metal, and placed in the oven of the atomic beam apparatus.

2. Protactinium-233

Production of Pa^{233} was accomplished by neutron irradiation of 0.5- to 1.0-g quantities of Th^{232} metal foil in the Materials Testing Reactor. The foil was sealed in quartz capsuls and irradiated for 24 to 72 hr at a flux of 2×10^{14} neutrons/cm^2/sec.

The chemistry performed was similar to that reported by Hill.[16] The Th^{232} was dissolved in 10 M HCl and ≈ 0.1 M HF and the sample passed through a Dowex A-1 column after the fluoride had been complexed by means of H_3BO_3. The protactinium was eluted with 3 M HCl, extracted from 6.9 M HCl into di-isoptopyl ketone, and back-extracted into 2 M HCl. Again the protactinium was adsorbed onto a Dowex A-1 column from 10 M HCl and possible zirconium impurities eluted with 6.0 M HCl. The protactinium was then eluted in 9.0 M HCl and 0.1 M HF.

One Pa^{233} sample for the bent-crystal spectrometer was prepared by irradiating 3.5 mg of ThO_2 in a 0.008-inch quartz capillary in the lattice position of the MTR (flux ≅ 3×10^{14} neutrons/cm^2/sec) for 2 months. No chemistry was performed on this sample; the ThO_2 capillary served as the spectrometer source.

3. Curium-241

Bombardment of 80 mg of Pu^{239} with 48-Mev alpha particles in the 60-inch Crocker cyclotron produced Cm^{241} by reaction $Pu^{239}(\alpha,2n)Cm^{241}$. The plutonium was bombarded in the form of the fluoride, which was slurried into a platinum "boat" and baked dry.

The chemistry used has been described by Glass.[17] The sample was dissolved by digesting in hot aqua regia. The bulk of the Pu^{239} was removed from the sample by adsorbing it on a large Dowex A-1 column.

Partial purification of the sample was achieved by coprecipitation with LaF_3. The fluoride was dissolved in borate and a $La(OH)_3$ coprecipitation performed. The $La(OH)_3$ was then dissolved in HCl and the actinides were separated from the lanthanides on an alcoholic-HCl column with an eluting agent of 80% concentrated HCl and 20% absolute alcohol. The resin used was a colloidal Dowex-50 resin. Final separation of the curium from other actinides was obtained on a Dowex-50 cation column (5 cm x 2 mm) with an elution agent of 0.4 M ammonium alpha-hydroxyisobutyrate (pH 4.4).

III. DECAY-SCHEME STUDIES

A. Neptunium-238

1. Introduction

The levels of Pu^{238} have been studied previously[18] from the decay[19,20] of Cm^{242} and the decay[21-25] of Np^{238}. The alpha decay of Cm^{242} leads to a well-defined ground-state rotational band, a state of 605 kev which has been assigned[19] as (1-, 0),[26] and two states of 937 kev and 1030 kev. The high-energy states of Pu^{238} are populated by only a very small fraction of the total alpha decay, and (selection rules permitting) are studied more easily through the beta decay of Np^{238}. The spectroscopic studies of this nuclide by Rasmussen et al.[21,22] and by Baranov and Shlyagin[25] have defined levels at about 988, 1030, and 1076 kev; these levels are of theoretical interest because of their tentative interpretation[18,22] as vibrational states.

Certain features of the decay scheme suggested further experimental work. In the earlier studies, the two prominent transitions of about 1030 kev energy had never been completely resolved and the transition between the (2+, 2) and (4+, 0) states had not been reported; therefore, it had not been possible to make a complete comparison of the experimental transition intensities with those predicted by theory. In addition, the tentative assignments of vibrational levels in this nucleus offered the hope of finding additional data concerning this mode of excitation.

2. Source Preparation

The sample was electroplated onto a 0.010-in.-diameter platinum wire from a solution of ammonium oxalate,[27] and the conversion-electron spectrum studied on permanent-magnet spectrographs with field strengths of 52, 99, and 350 gauss.

3. Experimental Results

The experimental results are summarized in Table I. The reported transition energies (E_γ) are weighted averages of the results of several

Table I

Np^{238} Conversion Electron Data

Electron energy (kev)	Conversion shell	Transition energy[a] (kev)	Selected transition energy[b] (kev)	Abundances per 100 beta disintegrations: Freedman et al.[c]	Slätis et al.[d]	Rasmussen et al.[e]	Relative intensities[g]: Baranov and Shlyagin[f]	This work
21.76	L_{II}	44.01		38	28.7	---	23.1	---
25.96	L_{III}	44.02		20	21.0	---	21.1	---
38.44	M_{II}	44.00		14	---	---	11.6	---
39.40	M_{III}	43.96		---	---	---	5.72	---
42.58	N_{II}	43.96		---	15.2	---	3.71	---
42.84	N_{III}	43.97		3.2	---	---	---	---
43.71	O	~44.0		---	---	---	---	---
			(44.11)[h]					
79.52	L_{II}	101.8		1.9	1.4	---	1.21	---
83.74	L_{III}	101.8		---	0.9	---	0.64	---
96.20	M_{II}	101.8		1.2	0.7	---	0.40	---
97.17	M_{III}	101.7		---	---	---	0.36	---
100.3	N_{II}	101.7		---	---	---	---	---
101.4	O	101.7		---	---	---	---	---
			101.7					
96.79	L_{I}	119.9		---	---	---	---	---
113.9	M_{I}	119.8		---	---	---	---	---
118.1	N_{I}	119.7		---	---	---	---	---
			119.8					

Table I (continued)

Electron energy (kev)	Conversion shell	Transition energy[a] (kev)	Selected transition energy[b] (kev)	Abundances per 100 beta disintegrations: Freedman et al.[c]	Slätis et al.[d]	Rasmussen et al.[e]	Relative intensities[g]: Baranov and Shlyagin[f]	This work
99.22	K	221.0	221.0	---	---	---	---	0.09
170.8	K	292.6	292.6	---	---	---	---	(?)
748.8	K	870.6	870.6	---	---	---	---	<0.01
762.8	K	884.6	884.6	---	---	---	---	0.014
803.6	K	925.4	925.4	---	0.05	0.04	---	0.034
818.8	K	940.6		---	0.10	0.07	0.09	0.072
917.9	L_I, L_{II}	940.2		---	0.06	---	---	0.021
934.4	M_I, M_{II}	940.0		---	---	---	---	0.0075
			940.4					
821.3	K	943.1	943.1	---	---	---	---	0.0093
864.0	K	985.8		0.3	0.26	0.20	0.20	0.20
963.1	L_I, L_{II}	985.4		---	0.13	0.06	0.06	0.059
967.8	L_{III}	985.9		---	---	---	---	0.010
980.2	M_I, M_{II}	985.8		---	---	---	---	0.020
985.3	N	~986		---	---	---	---	0.0090
			985.7					
867.3	K	989.1	989.1	---	---	---	---	0.012
905.6	K	1027.4		0.3[i]	0.22[i]	0.20[i]	0.16[i]	0.048
1005.1	L_I, L_{II}	1027.4		---	0.08	0.04	0.03	0.018
1021.7	M	~1027		---	0.06	0.02	---	extremely weak
			1027.4					

Table I (continued)

Electron energy (kev)	Conversion shell	Transition energy[a] (kev)	Selected transition energy[b] (kev)	Abundances per 100 beta disintegrations			Relative intensities[g]	
				Freedman et al.[c]	Slätis et al.[d]	Rasmussen et al.[e]	Baranov and Shlyagin[f]	This work
908.1	K	1029.9		---	---	---	0.08	0.15
1007.3	L_I, L_{II}	1029.6		---	---	---	0.03	0.039
1024.8	M	~1030		---	---	---	---	0.011
			1029.9					
912.1	K	1033.8	1033.8	---	---	---	---	<0.01
973.5	K	1095.3	1095.3	---	---	---	---	?

(a) Electron binding energies were taken from Hill, Church, and Mihelich, Revs. Sci. Instr. 23, 523 (1952).

(b) The selected values are weighted averages of the experimental values.

(c) Reference 23.

(d) Reference 24

(e) Reference 21

(f) Reference 25

(g) For purposes of comparison, the relative intensities from Baranov and Shlyagin and from the work reported here were normalized to Rasmussen's value of 0.20 for the K line of the 985-kev transition. In the last column question marks indicate uncertainty as to the actual existence of the lines.

(h) The weighted average is 44.00. The value 44.11 had been reported previously by Smith and Hollander (Reference 20) and is considered more accurate.

(i) The intensities listed for the 1027-kev transition by Freedman, Slätis, and Rasmussen include those of the unresolved 1030-kev transition. The division of intensities by Baranov and Shlyagin between 1027 and 1030 is reported as only approximate.

exposures. Since no internal standard was used, absolute errors are not given; however, except for very weak lines the relative precision of the energies should be ≈ 0.1%. The value 44.11 kev listed in parentheses has been used in the decay scheme instead of the value 44.00 kev obtained in this experiment, because the former value was obtained[20] with use of several internal standards, and is considered the more accurate.

The more certain features of the decay scheme are shown in Fig. 1a. This scheme is similar to those given by Rasmussen et al.[22] and by Baranov and Shlyagin,[25] with small differences in the energies of some of the states. Figure 1b shows the levels of Pu^{238} populated by the alpha decay of Cm^{242}.[19]

The transition intensities shown in Fig. 1a are those deduced from a consideration of the relative intensities of the conversion electrons together with previous information on the beta-decay branchings; these data are discussed below. The relative conversion-electron intensities listed in Table I are the results of six determinations made by the visual comparison method (Section II.B). For purposes of comparison the intensities are normalized to a value of 0.20 for the K line of the 985.7-kev transition. They are probably accurate to about 25% for the stronger lines and to a factor of 2 for the weaker lines. Intensities reported by the other investigators are also listed for comparison. Note that the relative intensities reported in this work for components of the ≈ 1030-kev doublet, which are completely resolved, disagree with the results of Baranov and Shlyagin.[25] Baranov and Shlyagin report that the lower-energy (1027-kev) component is more intense than the higher-energy (1030-kev) component, whereas this work shows the opposite result. The other investigators reported a composite intensity without attempting to divide it between the two transitions.

4. Branching-Ratio Comparisons

From the experimental K-conversion coefficients measured by Rasmussen et al.[21,22] and by Baranov and Shlyagin,[25] it is fairly certain that the 1030- and 986-kev transitions are predominantly electric quadrupole. It is not unreasonable to assume that the 925-kev transition is

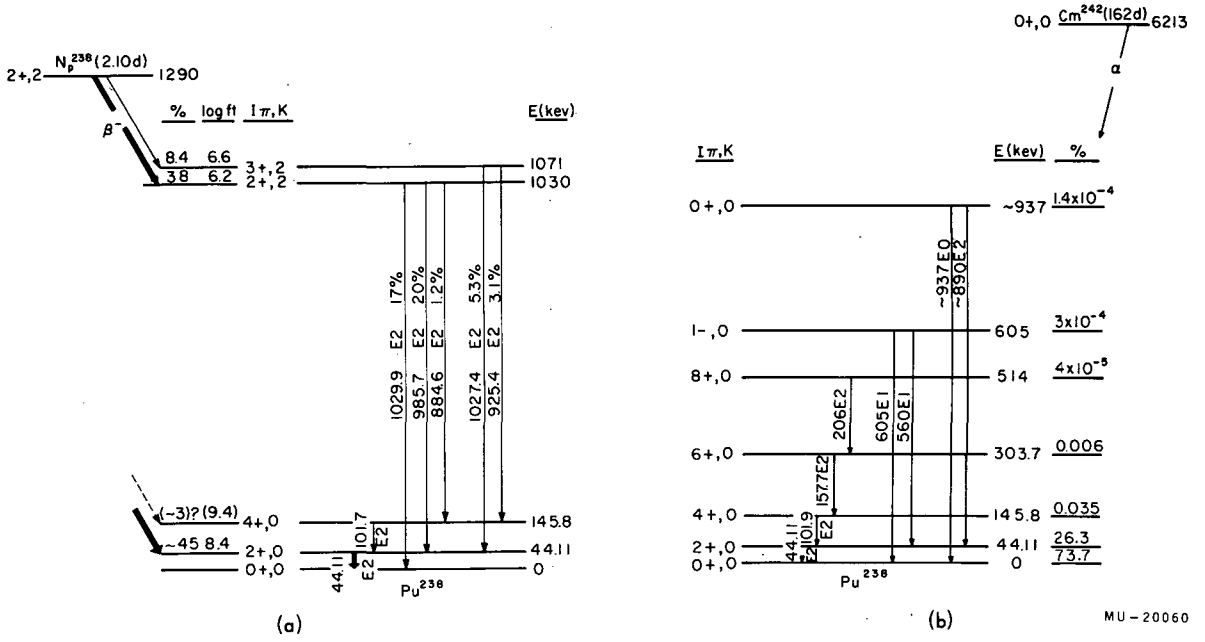

Fig. 1. The energy levels of Pu^{238}.
a. The more certain features of the decay of Np^{238}.
b. Levels populated by the decay of Cm^{242}.

also electric quadrupole, with the possibility of some magnetic dipole admixture.[21,22]

On the assumption that all transitions depopulating the (2+, 2) and (3+, 2) states are electric quadrupole, the experimental relative reduced photon-transition probabilities have been calculated from the observed K-electron intensities by dividing by the theoretical E2 K-conversion coefficients[28] and correcting for the fifth-power energy dependence. The experimental and theoretical intensities are compared in Table II. These data tend to support the assignment made by Rasmussen et al.[22] of K = 2 as the major K value of the upper band, but because of the relatively poor agreement of experimental and theoretical branching ratios, admixtures of other K values cannot be ruled out. It is interesting to note that Nathan reports an experimental value of 1.3 for the ratio $\frac{B\ (3 \rightarrow 2)}{B\ (3 \rightarrow 4)}$ for the depopulation of the (3+, 2) level in Dy^{160}.[29] That this value is nearly the same as our value of 1.0 for the analogous transition in Pu^{238} may be coincidental or may indicate a systematic deviation, perhaps arising from admixtures of M1 radiation. The theoretical value of $\frac{B\ (3 \rightarrow 2)}{B\ (3 \rightarrow 4)}$ for K = 2 is 2.5. If the 1027-kev transition were pure E2 and the 925-kev transition had a 40% admixture of M1 radiation, then the experimental branching ratio $\frac{1027 - E2}{925 - E2}$ would be 2.5, in agreement with the theoretical value. There are no experimental data that rule out the possibility of 40% M1 admixture in the 925-kev transition.

5. Discussion of OtherTransitions

In addition to those considered above, a number of other--mostly much weaker--conversion lines were observed (Table I). If only one conversion line of a transition was seen, it was assigned as a K line. Of the transitions to be discussed here (at 119.8, 221.0, 292.6, 870.6, 940.4, 943.1, 989.1, 1033.8, and 1095.3 kev) only the one of 940 kev has been reported previously. These transitions cannot be fitted uniquely into the level scheme; therefore, the interpretations ventured here are speculative.

Table II

Pu^{238} experimental and theoretical relative reduced E2 photon transition probabilities

(Final states are all in K=0 ground-state band)

E_γ/E'_γ	$\frac{B(I_i \to I_f)}{B(I_i \to I_{f'})}$	Experimental		Theoretical		
		Rasmussen et al.[a]	This work	$K_i=0$	$K_i=1$	$K_i=2$
Initial state 1030 kev						
$\frac{986}{1030}$	$\frac{B(2 \to 2)}{B(2 \to 0)}$	1.3	1.5	1.4	0.36	1.4
$\frac{885}{1030}$	$\frac{B(2 \to 4)}{B(2 \to 0)}$	<0.3	0.15	2.6	1.1	0.071
Initial state 1071 kev						
$\frac{1027}{925}$	$\frac{B(3 \to 2)}{B(3 \to 4)}$	---	1.0	---	0.4	2.5

(a) Reference 22.

Figure 2 is a tentative interpretation of the new data. The two weak transitions of energies 989.1 and 1033.8 kev differ by 44.7 kev, approximately the energy of the first excited state; hence these transitions are used to define a level at 1033.5 kev. The sum 870.6 + 119.8 = 990.4 kev is within approximately 0.13% of the energy 989.1 kev. Although energy differences observed with these instruments between lines lying close in energy are usually much better than 0.13% (see, for example, Fig. 1a), it is possible that the precision of energy measurements of extremely weak lines is no better than this. The above sum may be used, therefore, to assign a level at 914.7 kev. The observation of only L_I, M_I, and N_I lines of the 119.8-kev transition suggests that the multipolarity is M1 and not E1; E2 is certainly ruled out. We know nothing of the multipolarities of the other transitions. It is possible that one, or both, of these levels is associated with an octopole vibrational[30,31] band with the base state (2-, 2) as is postulated, for example, in W^{182},[32] Dy^{160},[29,33] and Th^{228}.[34]

Of the remaining transitions one stands out in intensity, the 940.4-kev transition of which K, L, and M lines are seen. That this transition should occur without a partner of similar strength appears at first strange, for almost any type of state at this excitation is expected to decay by at least two competing transitions to members of the ground rotational band. It is possible to suggest an interpretation within the framework of a beta-vibrational (K = 0) band, following upon earlier work[18,35] that suggested that levels in Pu^{238} at 937 and 988 kev are the first two states of the K = 0 band. One would not expect the first member (0+, 0) of this band to receive direct population by Np^{238} beta decay, because of our assignment of 2+ for the Np^{238} ground state (see Sections 6 and 7); such a beta transition would be second-forbidden. The second member (2+, 0) of the band, however, should be reached by an allowed transition (though K-forbidden), and it is to the de-excitation of this state that we assign the moderately strong 940.4-kev transition. The (2+, 0) state is thus defined as 984.5 kev.

The following considerations explain why there might be observed in the electron spectrum only one transition from the (2+, 0) state.

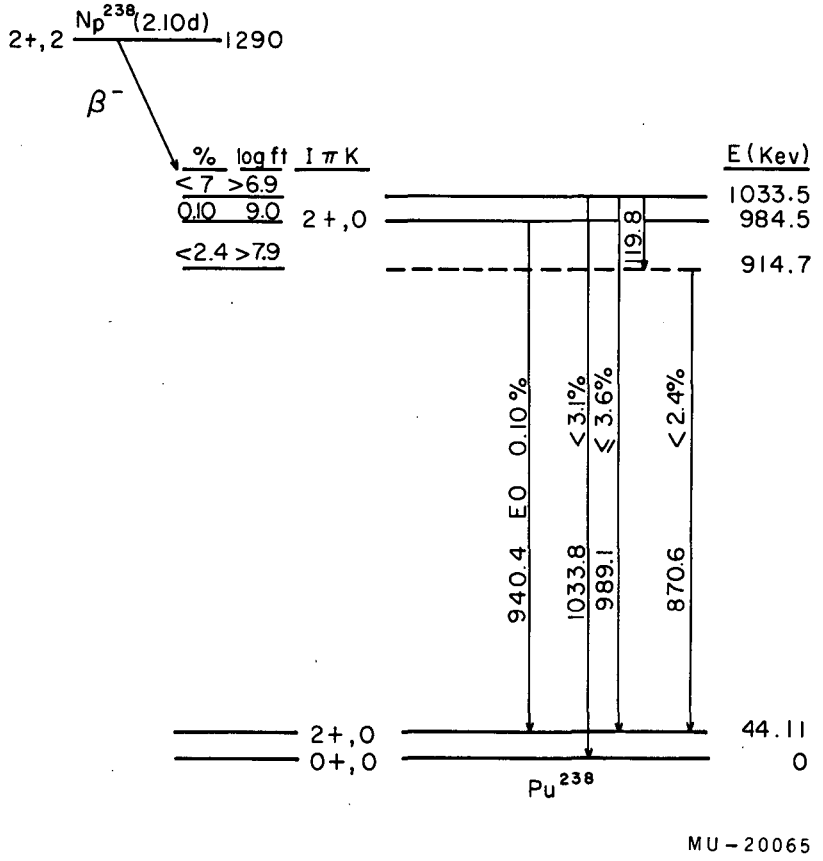

Fig. 2. Tentative assignments of the less prominent transitions in the decay of Np^{238}.

Perlman et al.[36] have found from Cm^{242} alpha decay that the E0 transition from the (0+, 0) level to ground (≈ 940 kev) is about one-half as intense as the E2 transition (≈ 890 kev) from this level to the (2+, 0) state at 44 kev. Because of the great difference in conversion coefficients (e_k/γ (E2) ≈ 1%; e_k/γ (E0) = ∞), the K line of the E0 transition is 50 times as strong as that of the E2 transition. Such a result is consistent with the theoretical studies by Reiner,[37] Peaslee,[38] and Rasmussen[39] concerning E0 transition probabilities. If a similar competition exists between E0 and E2 radiation in the depopulation of the 984.5-kev state, then the much weaker electron lines of the E2 transition (984.5 kev) would not be observable in this work. For example, a line 1/50 as intense as the 940-kev K line would have an intensity of only 0.001.

One expects a weak intraband transition from the (2+, 0) state to populate the (0+, 0) base state of the beta-vibrational band. Such a low-energy transition was not observed in this work, and it is difficult to set an upper limit on its intensity because its conversion lines would fall among those of the very strong 44.11-kev transition. A more sensitive determination of the population of the (0+, 0) state would be the observance of the high-energy E0 transition to ground. We did observe in this work a transition of 943.1 kev which is only 1/10 as strong as the 940.4-kev transition; however, this energy (943 kev) disagrees by 0.7% with the energy (≈ 937 kev) of this E0 transition measured by Perlman et al.[36] and Asaro et al.[19] Because of this energy discrepancy, the 943.1-kev transition cannot be assigned with certainty to the (0+, 0) level; thus we do not know the extent to which this state of the beta-vibrational band arises from Np^{238} decay.

Other possible transitions seen at 221.0, 292.6, and 1095.3 kev have not been placed in the decay scheme. Two weak electron lines observed at ≈ 106 and ≈ 156 kev were without the K lines of the strong 228- and 278-kev transitions in Np^{239} decay, and therefore are not listed in Table I.

6. Spin of Np^{238}

The spin of Np^{238} was determined to be 2 by the atomic-beam magnetic-resonance method. The equipment has been described by Brink et al.[40] and the experiment is fully described by Albridge et al.[41] Transitions were observed corresponding to at least four of the five possible F $(= |\vec{J} + \vec{I}|)$ states for spin I = 2.

7. Beta-Decay Branchings

Information regarding the total intensity of the soft beta component has been obtained by Freedman et al.,[23] Rasmussen et al.,[21] and Baranov and Shlyagin;[25] their respective values, in fairly good agreement, are 53%, 55%, and 59%. In order to obtain intensities of the individual transitions, the measured (relative) electron intensities of this work were converted to transition intensities by use of Rose's theoretical E2 conversion coefficients[28] and placed on an absolute scale by requiring that the total equal 56% (average of above determinations). The values so obtained are compared in Table III with those obtained directly from the absolute electron intensity measurements of Slatis at al.[24] and of Rasmussen et al.[21] The agreement is good.

From the above information, along with the beta populations to the low-lying levels given by Rasmussen et al.[21] and by Baranov and Schlyagin,[25] log ft values of beta decay to the various levels were calculated, and are given in Table IV. It is to be emphasized that these calculations are not independent of the present assignment of the multipole orders of the various transitions; however, the only ft value which is affected strongly is that of the beta decay to the 984-kev level. If the transition which de-excites this state should prove to be MI or E2 instead of E0, then the log ft value would decrease by approximately one unit or two units, respectively.

The log ft for decay to the 146-kev level is also listed as uncertain because of the experimental difficulties involved in determining the beta population of this level (see below). The multipolarities of the transitions that depopulate the 915- and 1034-kev levels are unknown, but some assumption must be made regarding them in order that the

Table III

Intensities of high-energy transitions in Np^{238} decay

E_γ (kev)	K-electron intensities (percent of disintegrations) Slätis[b]	Rasmussen[c]	This work	α_K[d] (Theoretical)	Transition intensity (percent of disintegrations) Slätis[b]	Rasmussen[c]	This work
871	---	---	< 0.01	4.2×10^{-3} (a)	---	---	< 2.4 (a)
885	---	---	0.014	1.2×10^{-2}	---	---	1.2
925	0.05	0.04	0.034	1.1×10^{-2}	5	4	3.1
940	0.10	0.07	0.072	∞	0.10	0.07	0.10
943	---	---	0.009	∞	---	---	0.013
986	0.26	0.20	0.20	1.0×10^{-2}	26	20	20
989	---	---	0.012	3.3×10^{-3} (a)	---	---	≤ 3.6 (a)
1027	0.22	0.20	0.048	0.91×10^{-2}	22	20	5.3
1030			0.15	0.91×10^{-2}			17
1034	---	---	< 0.01	3.2×10^{-3} (a)	---	---	< 3.1 (a)

a. In order to establish the maximum possible transition intensities for the 871-, 989-, and 1034-kev transitions, the theoretical E1 conversion coefficients have been used. Their use is consistent with the postulate made in the text that these transitions may originate from states of odd parity.

b. Reference 24.

c. Reference 21.

d. Reference 28

Table IV

Np^{238} beta-decay branchings and log ft values

Final state (Iπ,K)	Final state (kev)	Percent of beta decay	log ft
2+,0	44.11	~45	8.4
4+,0	145.8	(~3)?	(9.4)
	914.7	<2.4	>7.9
2+,0	984.5	0.10	9.0
2+,2	1030	38	6.2
	1034	<7	>6.9
3+,2	1071	8.4	6.6

transition intensities can be calculated from the electron data. In order to establish the maximum intensities of these transitions (and thus the maximum beta populations of the 915- and 1034-kev levels) we have assumed that these transitions are electric dipoles. This assumption is consistent with the postulate made in the preceding section that these transitions may arise from odd-parity levels.

The log ft values are of importance as an indication of the parity of Np^{238}. The most reasonable choice, based upon the existing data, seems to be even parity. The log ft values of 6.2 and 6.6 to the 1030- and 1071-kev levels, respectively, indicate either slow allowed transitions ($\Delta I = 0$ or 1, no) or rather fast first-forbidden transitions ($\Delta I = 0$ or 1, yes). As pointed out by Rasmussen et al.,[22] the nuclear rearrangement accompanying the decay to the vibrational levels may tend to hinder these transitions; thus the interpretation of the transitions as slow allowed, with even parity for Np^{238}, is chosen.

The reported observance[25] of $\approx$ 3% primary beta decay to the (4+, 0) level at 146 kev (log ft = 9.4) is in contradiction to an assignment of even parity to Np^{238}, because with this assignment the transition should be second-forbidden. However, because of the following theoretical considerations, it would be surprising if as much as 3% primary beta decay occurs, regardless of the parity assignment. The relative reduced beta-decay transition probabilities for decay to the ground-state and 146-kev level can be calculated by means of vector addition coefficients. The result listed in Table V, is $\frac{B\ (2 \rightarrow 0)}{B_{42}(2 \rightarrow 4)} = 14$. The ratio of the ft values for decay to these levels should be just the inverse of this number, or $\frac{ft\ (2 \rightarrow 0)}{ft\ (2 \rightarrow 4)} = 1/14$. Thus, if log ft $(2 \rightarrow 4) = 9.4$, calculated from the 3% beta branching, the value log ft $(2 \rightarrow 0) = 8.3$ is indicated for decay to the ground state, which corresponds to approximately 60% beta population. The prediction of such a large percentage of decay to the ground state is inconsistent with the conclusion of Rasmussen et al.[22] that approximately 100% of the hard betas go directly to the 44-kev level. In consideration, also, of the fact that the experimental difficulties of measuring a small percentage of beta decay to the 146-kev level are large, we seriously doubt the measurement of direct beta decay to this level.[25]

Table V

Np^{238} experimental and theoretical relative reduced beta-decay transition probabilities (initial state is the (2,2) ground state of Np^{238})

$\frac{B(I_i \to I_f)}{B(I_i \to I_{f'})}$	Experimental[a]	Theoretical
Ground-state rotational band	L = 2	
$\frac{B(2 \to 0)}{B(2 \to 4)}$	?	14
Gamma vibrational band	L = 1	
$\frac{B(2 \to 2)}{B(2 \to 3)}$	2.5	2.0

a. The experimental values are the inverse of the ratio of the experimental ft values for decay to the states.

The predicted and observed reduced transition-probability ratios for beta decay to the gamma vibrational band, also listed in Table V, are in reasonably close agreement, which is an indication of the K purity of these states. The beta decay to the 2+, 2 level can proceed by either L = 1 or L = 0 decay. Since the theoretical branching ratio was calculated for L = 1 decay, the agreement between the theoretical and experimental ratios is also an indication that the 2+ → 2+ beta transition is predominantly L = 1.

The log ft value of 9.0 for decay to the (2+, 0) level at 984 kev is consistent with an interpretation of a K-forbidden allowed transition as required by the level assignments. The log ft values for decay to the levels at 1034 and 915 kev are not in disagreement with the suggestion that these levels may be associated with an octopole vibrational band.

8. Proton and Neutron States in Np^{238}

The measured spin of Np^{238} is 2 (Section III.A.6). Knowledge of the parity of Np^{238} is of interest because it can shed light on the nature of the single-particle states that comprise the ground state of this nucleus.

The coupling rules for the angular momentum of individual particle states in odd-odd nuclei, originally presented by Nordheim,[43] have recently been modified by Gallagher and Moszkowski[44] to apply to the particle states of deformed nuclei. Within the asymptotic quantum description of these states $[Nn_z \Lambda \pm] \Omega \pi$, where the ± in the brackets indicates $\Omega = \Lambda \pm 1/2$,[45] the rules predict which of the two possibilities $I = |\Omega_p \pm \Omega_n|$ lies lower, as follows:

$$I = \Omega_p + \Omega_n \text{ for } \Omega_p = \Lambda_p \pm 1/2 \text{ and } \Omega_n = \Lambda_n \pm 1/2,$$

$$I = |\Omega_p - \Omega_n| \text{ for } \Omega_p = \Lambda_p \pm 1/2 \text{ and } \Omega_n = \Lambda_n \mp 1/2.$$

Here N is the principal quantum number (total number of nodes in the wave function); n_z is the number of planar nodes perpendicular to the nuclear symmetry axis; Λ is the projection of orbital angular momentum on the symmetry axis; Σ is the projection of the intrinsic spin on the symmetry

axis; Ω is the projection of the total spin on the symmetry axis; and π is the parity.

It is simplest to assume at first that the ground states of the odd proton and neutron in Np^{238} are the same as in the nearest isotopes and isotones; that is, that the 93rd proton is in the [642+] 5/2+ state as in the Np^{239} and Np^{237} ground states,[46] and that the 145th neutron is in the [631-] 1/2+ state, as in the Pu^{239} ground state.[46] It is also possible that the proton is in the [523-] 5/2- state, found in Np^{237} at 60 kev[47] and in Np^{239} at 75 kev. Although the (1/2-) spin assingment of U^{237} is less certain,[48] we must consider also the neutron state [501-] 1/2- . According to the above coupling rules the possible combinations of these states that give a ground-state of spin 2 are as shown below.

Proton	Neutron	Final state
[642+] 5/2+	[631-] 1/2+	2+
[642+] 5/2+	[501-] 1/2-	2-

Thus, the coupling rules predict for the proton state in Np^{238} the unique assignment [642+] 5/2+. With the selection of even parity for Np^{238} the choice of the neutron state is [631-] 1/2+.

B. Protactinium-233

1. Introduction

Although the nuclear energy levels of U^{233} populated by the decay of Pa^{233} had been studied previously by a number of workers,[16,49-54] and the general features of the decay scheme were well known, a large amount of information had yet to be obtained before a detailed discussion of the scheme could be attempted with confidence. Newton has analyzed the scheme in light of the previously known data and has mentioned the need for further experimental work.[55]

It was thought that the Berkeley permanent-magnet spectrographs and the bent-crystal spectrometer at the California Institute of Technology, Pasadena, could be used to obtain additional information on the transition

intensities and multipolarities. Correlation of these data with the transition intensities predicted by the theory of Bohr and Mottelson[3,4,42] would serve as a test for the quantum assignments of the nuclear energy states of U^{233}.

In addition, the ability to produce very intense sources of Pa^{233} by the neutron irradiation of Th^{232} and to study these sources on high resolution equipment offered the hope of discovering weak transitions that had not previously been observed.

2. Source Preparation

Sources used in the permanent-magnet spectrographs and in the double-focusing spectrometer were prepared by electrodeposition onto 0.010-in.-diameter platinum wires. An ammonium fluoride electrolyte (pH 6.3) was used with a plating current of 100 to 150 ma. These sources varied in strength from 0.02 to 50 r/hr as measured by a beta-gamma survey meter at a distance of approximately 3 inches.

Two sources were prepared for the bent-crystal spectrometer. The first was electroplated onto a 0.005-in.-diameter platinum wire in the manner described above. This wire was threaded into a 0.008-in. i.d. quartz capillary which was then sealed with a torch. The source was measured as greater than 100 r/hr of gamma activity at a distance of approximately 4 inches.

Because x-ray emission of the platinum wire (induced by the intense beta source) proved troublesome, a second source was prepared without the wire. Approximately 3.5 mg of ThO_2 in a 0.008-in.-diameter quartz capillary was neutron-irradiated for two months in the Materials Testing Reactor. The irradiated ThO_2 in the capillary was itself used as the spectrometer source without further treatment.

3. Conversion-Electron Data

The Pa^{233} conversion-electron data, taken on the permanent-magnet spectrographs, are summarized in Table VI. Reproductions of several representative photographic plates are shown in Fig. 3. The unassigned lines, listed in Table XIV, are discussed below. Most of the electron

Table VI

Pa^{233} conversion-electron data

Electron energy (kev)	Conversion shell	Transition energy[a] (kev)	Selected transition energy[b] (kev)	Conversion-electron intensities[c] (percent beta decay) This work	Hollander and Hamilton[d]	Selected value	Remarks
11.72	M_I	17.27					
12.07	M_{II}	17.25					
12.96	M_{III}	17.26					
15.78	N_I	17.22					
15.97	N_{II}	17.24					
			17.26				
6.76	L_I	28.52					
7.57	L_{II}	28.51					
11.37	L_{III}	28.53					
23.01	M_I	23.56		1.9	1.7	1.7	
23.37	M_{II}	28.55		0.94	0.47	0.47	
24.26	M_{III}	28.56		1.0	--	0.52	
27.06	N_I	28.50					
27.22	N_{II}	28.49					
27.50	N_{III}	28.54					
28.25	O_I	28.57					
			28.54				
18.62	L_I	40.38		1.1	--	0.96	
19.42	L_{II}	40.36		4.2	--	3.7	
23.15	L_{III}	40.31		3.1	2.7	2.7	
34.73	M_I	40.28					
35.10	M_{II}	40.28		0.70	--	0.70	
35.96	M_{III}	40.26		0.78	--	0.78	Masks 58-L_I
38.99	N_{II}	40.26					
39.24	N_{III}	40.28					
40.06	O_{II}	40.31					
			40.29				

Table VI (continued)

Electron energy (kev)	Conversion shell	Transition energy[a] (kev)	Selected transition energy[b] (kev)	Conversion-electron intensities[c] (percent beta decay) This work	Hollander and Hamilton[d]	Selected value	Remarks
36.92	L_{II}	57.86					L_I line masked by 40-M_{III}
40.74	L_{III}	57.90					M_{III} line masked by 75-L_I
			57.90				
53.37	L_I	75.13		8.2	8.6	8.6	Masks 58-M_{III}
54.14	L_{II}	75.08		1.1	1.2	1.2	
58.01	L_{III}	75.17		0.12	--	0.13	
69.57	M_I	75.12		2.5	2.1	2.1	Masks 87-L_{III}
69.90	M_{II}	75.08					
70.81	M_{III}	75.11					
73.65	N_I	75.09		0.78	--	0.78	
73.82	N_{II}	75.09					
74.77	O_I	75.09		0.31	--	0.31	
75.06	P_I	~75.1					
			75.13				
64.75	L_I	86.51		9.6	9.4	9.4	
65.50	L_{II}	86.44		1.2	1.3	1.3	
	L_{III}			--	0.26	0.26	Masked by 75-M_I
80.85	M_I	86.40		2.8	2.6	2.6	
81.14	M_{II}	86.32		0.47	0.58	0.58	
	M_{III}			--	0.13	0.13	Masked by 103-L_I
84.93	N_I	86.37		0.73	--	0.73	
86.05	O_I	86.37		0.18	--	0.18	
			86.45				
81.91	L_I	103.7		2.7	2.6	2.6	Masks 86-M_{III}
82.68	L_{II}	103.6		0.39	0.47	0.47	

Table VI (continued)

Electron energy (kev)	Conversion shell	Transition energy[a] (kev)	Selected transition energy[b] (kev)	Conversion-electron intensities[c] (percent beta decay) This work	Hollander and Hamilton[d]	Selected value	Remarks
86.37	L_{III}	103.5		0.11	0.10	0.10	
98.11	M_I	103.7		0.81	--	0.81	
98.39	M_{II}	103.6					
99.36	M_{III}	103.7					
102.2	N_I	103.7		0.36	--	0.36	
103.3	O_I	103.7					
			103.6				
155.8	K	271.4		0.057	--	0.057	
250.6	L_I, L_{II}	271.5		0.055	--	0.055	
254.4	L_{III}	271.5		$\leq$0.042	--	$\leq$0.042	
266.0	M_I, M_{II}	271.6					
269.9	N_I, N_{II}	271.3					
			271.5				
184.4	K	300.0		5.5	5.2	5.2	
278.1	L_I	299.9		1.3	1.1	1.1	
278.5	L_{II}	299.4		0.14	0.16	0.16	
	L_{III}		(estimated as 0.014)		--	--	Masked by 398-K
294.4	M_I	299.9		0.31	0.32	0.32	Masks 311-L_{III}
298.3	N_I	299.7		0.083	--	0.083	
300.0	O_I	300.3	(estimated as 0.024)		--	--	Masked by 416-K
			299.8				
196.2	K	311.8		22	27	27	
289.7	L_I	311.4		4.8	6.3	6.33	
290.7	L_{II}	311.6		0.57	0.59	0.59	
	L_{III}		(estimated as 0.021		--	--	Masked by 300-M_I
306.3	M_I	311.9		1.5	1.5	1.5	
306.9	M_{II}	312.1		--	--	--	
310.0	N_I	311.4		0.52	--	0.52	

Table VI (continued)

Electron energy (kev)	Conversion shell	Transition energy[a] (kev)	Selected transition energy[b] (kev)	Conversion-electron intensities[c] (percent beta decay) This work	Hollander and Hamilton[d]	Selected value	Remarks
311.4	O_I	311.8		0.13	--	0.13	
			311.7				
224.9	K	340.5		2.6	2.6	2.6	
318.5	L_I	340.3		0.57	--	0.57	
319.5	L_{II}	340.5		0.073	--	0.073	
323.0	L_{III}	340.1		--	--	--	
334.8	M_I	340.3		0.18	--	0.18	
339.5	N_I	340.9		0.073	--	0.073	
340.1	O_I	340.4					
			340.3				
259.9	K	375.5		0.078(0.055)[e]	0.043	0.043	
353.6	L_I	375.3		[0.023][f]	--	0.012	
354.2	L_{II}	375.2		[0.047]	--	0.025	
358.4	L_{III}	375.5		[0.023]	--	0.012	
369.8	M_I	375.4					
			375.5				
282.7	K	398.3		0.10(0.073)[e]	--	0.073	Masks 300-L_{III}
376.6	L_I	398.3		[0.044][f]	--	0.022	M_{III} line masked by 416-L_I,L_{II}
377.3	L_{II}	398.3		[0.075]	--	0.039	
381.3	L_{III}	398.4		[0.024]	--	0.012	
			398.3				
300.0	K	415.6		0.26(0.18)[e]	0.18	0.18	Masks 300-O_I
393.7	L_I	415.5		[0.078][f]	--	0.036	Masks 398-M_{III}
394.4	L_{II}	415.3		[0.055]	--	0.025	Masks 398-M_{III}
398.3	L_{III}	415.4		[0.015]	--	0.0068	
410.0	M_I	415.5					
413.8	N_I	415.3					
			415.6				

Table VI (continued)

a. Electron binding energies were taken from Hill et al., Rev. Sci. Instr. 23, 523 (1952).

b. The selected values are weighted averages of the experimental values.

c. The measured relative intensities have been converted to absolute values by a method described in the text.

d. Reference 57.

e. The values in parenthesis have been renormalized by a method described in the text.

f. The square brackets indicate an uncertainty in the normalization factor used for these values. See text.

lines listed in Table VI were detected by means of the conventional permanent-magnet spectrographs; however, the lines of the 17-kev transition and the L lines of the 28-kev transition were detected with the pre-accelerator camera described in Part Two of this dissertation.

It was possible to observe most of the electron lines in from two to four different spectrographs (i.e., at two to four different field strengths) so that a cross check on the measured energies was possible. The maximum difference observed in the energies of lines measured on more than one spectrograph was ≈ 0.6%; these differences appear to be systematic, probable arising from errors in the calibration of the individual spectrographs. The relative precision of measurement of the energies of lines taken on a single spectrograph is within 0.1% except for extremely weak or extremely strong lines.

The selected transition energies listed in Table VI were chosen as most representative of the data; they are weighted averages of several determinations.

Only relative conversion-electron intensities were determined directly in this work. The absolute intensities listed in Table VI are the relative intensities normalized by a means described in Section III.B.7. The intensities listed for this work are averages of from two to seven visual estimates (see Section II.B) and, when possible, two or three densitometer traces. Densitometry could not be used for very weak lines or lines in regions of strong background. When the visual estimates were being made, comparisons were made among the lines until a self-consistent set of values was obtained. If later the assigned intensities seemed questionable for any reason, more estimates were made and a new average computed.

In a few cases two different conversion lines arising from different transitions overlap. In these cases the intensities of the two lines were estimated from the assigned multipolarities of the transitions. The estimated intensity of the weaker component was then subtracted from the total measured intensity to give the final intensity for the stronger component. The estimated value of the weaker line is listed in Table VI.

It is estimated that the electron intensities of this work are accurate within ~ 25% for the strong and medium lines and within a factor of two for the weak lines.

Relative conversion-electron intensities were also obtained with the Berkeley double-focusing spectrometer. These data are listed in Table VII along with the data of other workers for comparison. The relative intensities in Table VII have been normalized to absolute intensities by the method described in Section III.B.7. Column 1 lists the energies of the peaks recorded by the double-focusing spectrometer and column 2 the conversion lines which, on the basis of energy considerations, are included in the peak. The relative intensities of the peaks were determined by integrating each peak with a planimeter and dividing the result by the $\mathcal{H}_\rho$ value of the peak. For the low-energy electron lines window-absorption corrections were made by use of the curves of Saxon for nylon films.[56] No corrections were made for source absorption which, for the low-energy lines, might have been appreciable, since the source used in the spectrometer was not mass-free.

Most values in column 6 are the averages of from one to four separate determinations; parentheses indicate the value is that of a single determination only or that the value is uncertain for some reason. The intensity values listed in columns 7 and 8 were obtained by summing the intensities obtained by means of the high-resolution instruments (Table VI, columns 5 and 6) for the conversion lines comprising the peaks. (The data of Hollander and Hamilton are discussed below.) Columns 3, 4, and 5 are normalized relative intensities reported previously by other investigators. Columns 3, 4, and 5 are normalized to a value of 26 for the K line of the 312-kev transition. The intensity of the K line of the strong 312-kev transition was difficult to determine in this work because of the intense sources used; therefore columns 6, 7, and 8 are normalized to a value of 2.6 for the K line of the 340-kev transition. In most cases the agreement between the intensity values obtained in this work by spectrometer and spectrograph is within 30%; however, the agreement between these values and those in columns 3, 4 and 5 is in general poor. There is good agreement between the data of this work and those of Hollander and Hamilton,[57] (see below).

Table VII

The decay of Pa^{233} – comparison of conversion line

Intensities measured by several workers

Ee^{-} [a] (kev)	Conversion lines[b]	Intensities (normalized to percent beta decay)[c]					
		Elliott and Underhill[d]	Brodie[e]	Hok and Kramer[f]	This work (double-focusing spectrometer)[g]	This work (spectrograph)[h]	Hollander and Hamilton[h,i]
18.3	40-L_I,L_{II}	--	1.3	--	1.9	5.3	--
21.5	40-L_{III}; 28-M	--	2.6	--	4.2	6.9	4.9
25.9	28-N	--	0.39	--	0.79	--	--
34.8	40-M	--	--	--	2.5	1.5	--
39.2	40-N,O; (58-L_{III}?)	--	--	--	0.89	--	--
53.3	75-L_I,L_{II}	5.2	5.5	5.2	12	9.3	9.8
64.7	86-L_I,L_{II}	6.2	4.6	(7.5)	(15)	11	11
69.7	75-M	1.3	0.26	(1.8)	2.4	2.5	2.1
74.0	75-N, O	--	--	0.078	(1.2)	1.1	--
81.9	86-M; 103-L_I,L_{II}	--	--	3.5	6.3	6.4	6.4
84.5	86-N, O; 103-L_{III}	--	--	0.78	0.78	1.0	--
98.8	103-M	0.78	0.52	0.78	0.86	0.81	--
102	103-N, O	--	--	0.21	0.36	0.36	--
186	300-K	2.6	1.0	5.7±0.52	(6.0)	5.5	5.2
197	312-K	[26]	[26]	[26]	--	22	27
225	340-K	2.6	2.1	2.6	[2.6]	[2.6]	[2.6]
260	375-K	--	--	--	(0.039)	0.078	0.043

Table VII (continued)

Ee^- [a] (kev)	Conversion lines[b]	Intensities (normalized to percent beta decay)[c]					
		Elliott and Underhill[d]	Brodie[e]	Hok and Kramer[f]	This work (double-focusing spectrometer)[g]	This work (spectrograph)[h]	Hollander and Hamilton[h,i]
278	300-L_I,L_{II}	--	--	0.91	1.1	1.4	1.3
281	300-L_{III}; 398-K	--	--	--	(0.31)	0.10	--
291	312-L_I,L_{II}	6.5	6.5	5.2	(6.0)	5.4	6.9
293	300-M; 312-L_{III}	--	--	--	0.29	0.33	0.32
300	415-K; 300-N, O	--	--	--	0.29	0.37	--
306	312-M	--	--	1.2	1.2	1.5	1.5
310	312-N, O	0.65	< 1.0	0.39	0.44	0.65	--
320	340-L_I,L_{II}			0.47	0.49	0.64	--
335	340-M	--	--	0.13	0.12	0.18	--
342	340-N, O	--	--	--	0.065	0.073	--
357	375-L	--	--	0.026	0.049	0.093	--
378	398-L	--	--	0.039	(0.034)	0.14	--
399	416-L	--	--	0.065	0.065	0.15	--
411	416-M	--	--	0.026	(0.020)	--	--

a. Ee^- is the approximate energy of the peak shown in the double-focusing-spectrometer spectrum. Only peaks whose intensities were measured by the spectrometer of this work have been listed for comparison.

Table VII (continued)

b. The conversion lines listed are those whose energies (as determined by the permanent-magnet spectrographs) fall within the limits of the spectrometer peak.

c. The intensities are normalized to a value of 26 for the K line of the 312-kev transition with the exception of the Berkeley and Uppsala work, which are normalized to a value of 2.6 for the K line of the 340-kev transition. This normalization converts the relative intensities to percent beta decay, as discussed in the text.

d. Reference 50.

e. Reference 51.

f. Reference 49.

g. These values are the averages of from one to four determinations with the double-focusing spectrometer. Lines for which only one determination was made or which are uncertain for some other reason are enclosed in parentheses.

h. These values are the intensities determined from the higher-resolution equipment. They are the sums of the intensities of the individual conversion lines appearing in the peak.

i. Reference 57.

In general, the intensity data of the double-focusing spectrometer have been used only as an indication of the precision of the spectrographically determined intensities. The latter values are selected as the experimental intensities of this work because the high resolving power of the spectrographs makes possible the individual determination of the intensities of many lines that are unresolved by the double-docusing spectrometer. In some cases, however, the spectrometer values have been used to unravel problems created by ambiguous spectrographic data. These cases are explained below.

After this work had been completed, Hollander and Hamilton[57] measured the intensities of some of the stronger conversion lines with an iron-free double-focusing spectrometer[58] at the University of Uppsala, Sweden. These intensities, normalized to a value of 2.6 for the K-line of the 340-kev transition, are listed in Tables VI and VII for comparison. It is seen that the agreement with the spectrographic data of this work (Table VI)is quite good; the two sets of data agree within 10% in the majority of cases. Poor agreement occurs only for a few of the weak lines; these cases are discussed below. The agreement between the two sets of data speaks well for the method of intensity measurements used in this work, and lends a large degree of confidence to those intensities reported here but not measured by Hollander and Hamilton.

In those cases in which an intensity was measured at Uppsala this value has usually been chosen as the final value because a high-resolution counter spectrometer is inherently a better instrument for determining intensities than is a photographic recording spectrograph. It should be noted, however, that there would be no appreciable difference in the interpretation of the decay scheme were the intensity data of this work used exclusively.

More than half of the intensities reported in this work were not measured at Uppsala. In these cases the final values were taken as the data of this work which, in come cases, were slightly adjusted. These adjustments were made in the cases where Hollander and Hamilton had measured only one line of a given conversion shell. The adjustment

consisted of multiplying this author's intensity values for that shell by a factor which brought about agreement with the one Uppsala intensity value. In this manner the relative subshell ratios of this work were maintained.

The interpretation of the two highest energy levels in U^{233} depends strongly on the assignments of multipolarities to the 375-, 398-, and 415-kev transitions. These multipole assignments in turn depend upon the measured intensities of the conversion lines of these transitions. Because of the importance of these intensity values and of the difficulty in obtaining them, it is thought that special comment is warranted.

The Uppsala group[57] measured the intensities of the K lines of the 375- and 415-kev transitions, and those values do not agree well with the values of this work. Because of this disagreement, several more visual estimates were made by this author of the intensities of these lines and of the K lines of the 398-kev transition. The new determinations did not differ appreciably from the original ones.

The intensity of the 415-kev K line has been well established by the Uppsala iron-free spectrometer and the Berkeley double-focusing spectrometer. In the Berkeley double-focusing spectrum this line is not resolved from the N and O lines of the 300-kev transition; however, corrections were made for the intensity of these interfering lines by means of the spectrographic data. A corrected average of 0.18 was obtained from four spectrometer measurements. The value is probably accurate to within 16%, and agrees well with the iron-free value of 0.18.

In obtaining the intensities of the three high-energy K lines by means of the permanent-magnet spectrum, a special effort was made to insure that the measured intensities of the lines relative to one another were as precise as possible so that a normalization of these intensities to a value of 0.18 for the 415-kev K line would be justified. The values so normalized are given in parentheses in Table VI next to the measured values. It is seen that for the K line of the 375-kev transition there is reasonable agreement between the normalized value and the value reported by Hollander and Hamilton.[57] For this reason, the normalized

intensity value for the K line of the 398-kev transition (not measured at Uppsala) is taken as the final value. The intensity of this line as measured by the Berkeley spectrometer is highly uncertain because in the lower-resolution spectrum the line lies between two fairly intense conversion lines.

The intensities of the L lines of the 375-, 398-, and 415-kev transitions were determined in this work but not at Uppsala. The photographic plate by means of which these intensities were determined is shown in Fig. 3. The intensities of these nine lines relative to one another are probably fairly precise; however, there was difficulty in normalizing these values to the intensity scale used for reporting the data (i.e., to a value of 2.6 for the 340-kev K line). This difficulty arises from the fact that the lines in question are quite weak, so that the lower-energy portion of the photographic plate on which the lines are seen is extremely dark, hence it was difficult to observe a line of known intensity so that the normalization could be effected. Because of these uncertainties the intensities of these lines listed in Table VI are enclosed in square brackets. The L-subshell ratios of these lines are not affected by this normalization uncertainty.

Fortunately, it was possible to bring about a normalization of these lines in an indirect manner. The values of the total intensities of the L lines of the 375- and 415-kev transitions measured by the Berkeley double-focusing spectrometer (Table VII) are fairly precise (i.e., in each case three individual measurements agree with their average to within 20%). The values (0.049 and 0.065, respectively) indicate that the spectrographically determined values are too large by a factor of approximately two; hence the spectrographically determined intensity values for the 375- and 416-kev L lines have been normalized to bring about agreement with the total L values measured by means of the Berkeley double-focusing spectrometer. The spectrographically measured intensities of the 398- kev L lines have likewise been corrected by dividing by a factor of two. (The value of 0.034 for the intensity of the 398-kev L line, as measured by the Berkeley spectrometer, is uncertain.) These corrected values are listed as the selected values in Table VI.

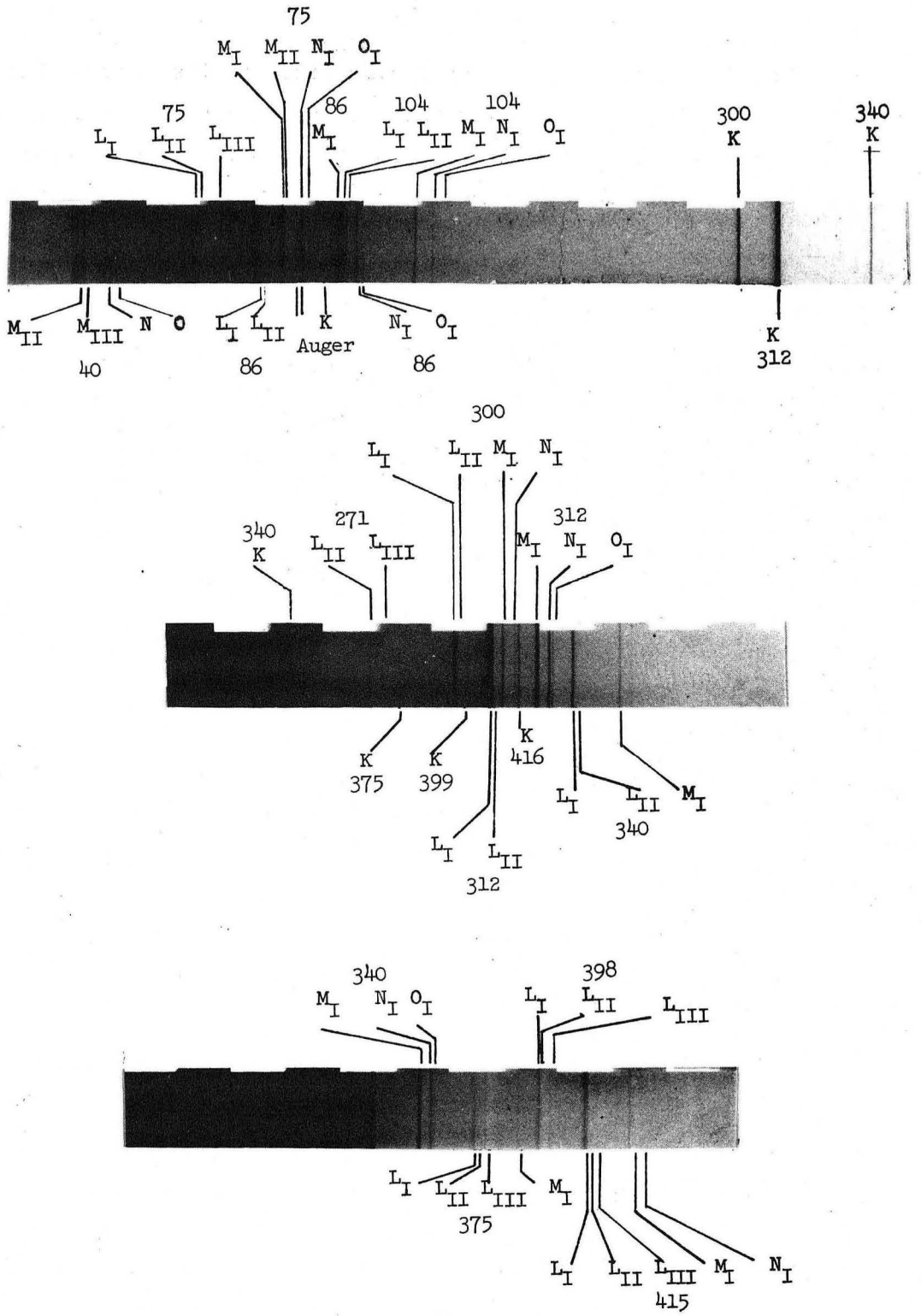

Fig. 3. The conversion spectrum of Pa^{233} -- portions of plates exposed in the 160 gauss spectrograph.

The intensities of the conversion lines of the 40-kev transition are also of special importance in the interpretation of the decay scheme (see Section III.B.8). For this reason it is worth while to discuss here the accuracy with which the intensities of the low-energy electron lines have been determined. For the intensities of the conversion lines of the 28- and 40-kev transitions the spectrographically determined values of this work are subject to large errors due to film efficiency correlations and to line broadening which makes visual estimates difficult; hence these values are probably not accurate to any better than a factor of two. The values obtained with the Berkeley double-focusing spectrometer could also be in error by a factor of two.

The intensities of the low-energy electron lines as measured by the Uppsala group from the peak heights of the lines are probably the most accurate; however, these values, too, are subject to large uncertainties. These uncertainties are evidenced by the fact that the resolutions obtained for the 40-kev L_{II} and L_{III} lines were 0.42% and 0.24%, respectively, as compared with a typical 0.1% for lines of higher energy. Such line broadening at low energies was undoubtedly due to absorption effects. For these reasons it is felt that the selected values of the intensities of the conversion lines with energies less than approximately 50 kev may be too small by as much as a factor of two.

4. Photon Data

The gamma-ray and x-ray data taken on the Pasadena bent-crystal spectrometer are listed in Table VIII. The method of determining the energy of an observed photon is described fully by DuMond.[8] Briefly, this method consists of taking two profiles of each photon--one on each side of the zero-angle position of the source. Several of the profiles are combined to give a "composite profile" which represents an average shape of the observed profiles. This composite profile is normalized to the height of each individual profile and superimposed in such a way as to give the best fit between the composite and individual profiles. The centerline of the composite profile is then taken as the position of the photon profile, and the average of the values for the right hand and the

Table VIII

The decay of Pa^{233} – photons detected with the Pasadena bent-crystal spectrometer

Gamma rays

Energy (kev)		Intensity (percent beta decay)			
This work	Browne[a]	Pt wire source	ThO_2 source	Average	Browne[a]
	28.67 ± 0.02				0.060
40.35 ± 0.01	40.47 ± 0.1	0.015		0.015	0.048
41.65 ± 0.02		(weak)			
75.28 ± 0.01	75.4 ± 0.2		0.82	0.82	1.3
86.59 ± 0.01	87.0 ± 0.3	2.0	1.5	1.7	[1.7]
103.86 ± 0.02		0.62	0.70	0.66	
145.42 ± 0.05			0.44	0.44	
271.62 ± 0.23		0.33	0.25	0.29	
300.20 ± 0.24		6.0	6.5	6.3	
311.91 ± 0.13		[34]	[34]	[34]	
340.51 ± 0.18		3.9	3.8	3.9	
375.35 ± 0.32		0.51	0.61	0.56	
398.57 ± 0.40		1.1	1.0	1.1	
415.87 ± 0.42		1.4	1.6	1.5	

X-rays

Energy (kev)		Intensity (percent beta decay)					Transition	
This work	Accepted[b]	Pt wire source	ThO_2 source	Average	Browne[a]	Beckman[c]		
Uranium								
94.655	94.664	8.3	7.2	7.7	[7.7]	[7.7]	$K\text{-}L_{II}$	$K\alpha_2$
98.441	98.442	16	12	14	15	14	$K\text{-}L_{III}$	$K\alpha_1$
110.421	110.428	2.0	0.95	1.5		2.0	$K\text{-}M_{II}$	$K\beta_3$
111.297	111.307	3.6	3.0	3.3		3.8	$K\text{-}M_{III}$	$K\beta_1$
114.502	114.568	1.3	1.7	1.5		1.7	$K\text{-}N_{II}$, N_{III}	$K\beta_4$, $K\beta_2$
115.405	115.412	0.37	0.37	0.37		0.42	$K\text{-}O_{II}$, O_{III}	--

Table VIII (continued)

X-rays

Energy (kev)		Intensity (percent beta decay)					Transition
This work	Accepted[b]	Pt wire source	ThO_2 source	Average	Browne[a]	Beckman[c]	
Platinum							
65.127	65.122						$K\text{-}L_{II}$ $K\alpha_2$
66.861	66.831						$K\text{-}L_{III}$ $K\alpha_1$
75.292							75-kevγ+ $K\beta_3$
75.754	75.749						$K\text{-}M_{III}$ $K\beta_1$

a. Reference 64.

b. The accepted energies were deduced from electron binding energies listed in the tables of Nijgh, et al., (Reference 69).

c. Reference 65.

left-hand profiles is used for the purpose of energy determinations. Corrections are made for--among other things--the nonlinearity of the screw that drives the source. This method eliminates the need for determining the exact zero-angle position of the instrument.

A second method of determining the center position of a recorded photon was also employed. In this method the center of the peak was found by superimposing the two photon profiles back to face. After the profiles were carefully aligned to give a best fit, a pin was pushed through the profiles to produce a mark on each. The average value of the positions of the pin marks is the center position of the photon peak regardless of where the pin is inserted. Once the center position was determined the photon energy was calculated in the same manner as outlined above. The energies determined by these two different methods were in excellent agreement. The limits of error quoted are based upon estimates of the precision with which the center positions of the profiles were determined. The agreement between the measured and accepted energies of the uranium and platinum K x-rays[59] indicates that the accuracy of the energy measurements is good.

The photon relative-intensity values listed were obtained by positioning the source at the angular position determined during the energy measurements as the profile center, and recording the photon peak with the pulse-height analyzer. The pulse-height analyzer is used in order to reduce the background counting rate. The values obtained by means of the wire source and the single-channel analyzer, and those obtained by C. J. Gallagher with the ThO_2 source[60] and the 100-channel analyzer are listed in Table VIII.

These intensities have been corrected for detector efficiency and the photopeak-to-total ratio.[61] Corrections were made for absorption in the source, SiO_2 capsule, air between source and detector, and the aluminum cover of the detector crystal. With the exception of the source absorption these corrections were made by the direct use of the exponential attenuation equation and the attenuation coefficients of Grodstein.[62] A graphical integration method was used to calculate the source absorption. This method as applied to each source is described in detail in the Appendix.

The largest correction applied to the gamma-intensity data arises from the energy dependence of the reflectivity of the quartz crystal. When the spectrometer is adjusted to accept photons of a given energy, not all the photons of this energy that strike the bent crystal are diffracted toward the detector. Lind et al. have reported that for a bent quartz crystal the ratio of the diffracted beam to the incident beam (the reflection coefficient) is proportional to $1/E^2$.[63] This energy-dependent correction was applied to the data in Table VIII by multiplying each photon intensity by $(E_\gamma/E_{340})^2$ in order to normalize the intensity to that of the 340-kev transition. The 340-kev transition was chosen as the norm because it is near the middle of the energy range investigated and because the majority of the gamma rays observed were of energies close to 340 kev. The magnitude of the correction factor varies from 0.014 for the 40-kev transition to 1.49 for the 415-kev transition.

In selecting the final intensity values from the bent-crystal data there was some question which set of data (that of the platinum wire source or that of the ThO_2 source) was the more reliable. The data of the ThO_2 source have the advantage of being obtained by means of a 100-channel analyzer which permitted a simultaneous sweep of the energy spectrum, whereas the intensity data of the platinum wire source were obtained point by point with the single-channel analyzer. On the other hand, the platinum source was many times as intense as the ThO_2 source. When the averages of the two sets of data were taken it was seen that individual values agreed with the averages to within 10% in all but two cases and that the maximum deviation was 16%; hence the averages (listed in Table VIII) have been chosen as the final values. All the intensity data listed in Table VIII have been normalized to the conversion-electron relative-intensity data by means of the theoretical K-conversion coefficient of the 312-kev transition (see Section III.B.6). The photon intensities have also been placed on an absolute basis of percent beta decay by a means described in Section III.B.7.

Gamma-ray data published by Browne[64] are also presented in Table VIII. The energy data of Browne are in reasonably good agreement with the data of this work; however, the relative intensities of the low-energy

gamma rays are not in agreement. For the purpose of comparison the intensity data of Browne were normalized by means of the 87-kev photon intensity. The values of this work and of Browne, so normalized, deviate considerably at lower energies. This deviation is such that the ratio of Browne's intensities to those of this work, for photons of lower energy than 87 kev, varies linearly with energy. The deviation therefore suggests a systematic error in one of the sets of data. The cause of the deviation is unknown.

In Table VIII uranium K-x-ray relative-intensity data of Beckman[65] and of Browne[64] are listed, normalized to a value of 7.7 for the K α_2 line. The relative intensities of this work are seen to be in close agreement with those of the previous workers. The absolute values of the uranium x-ray intensities determined in this work require discussion.

Because of the short lifetimes of vacancies in the atomic K shell,[66] K x-rays have large intrinsic line widths. These line widths are, in fact, larger than the instrumental spectral window of the Pasadena bent-crystal spectrometer;[67] hence when the x-ray intensities are measured by focusing on the center of the peak, the spectrometer does not "see" all the line. Nuclear gamma rays, however, arise from nuclear states whose lifetimes are of sufficient length that the natural line widths of the gamma rays are smaller than the spectral window of the spectrometer.

It is true, therefore, that the technique of intensity measurements employed here decreases the measured intensities of the x-rays relative to those of the gamma rays. Gallagher, who pointed out this fact to the author, has observed in the decay of W^{187} that the rhenium x-ray intensities as measured by the Pasadena bent-crystal spectrometer are reduced by a factor of 1.6 relative to the gamma intensities.[68] In this work it was possible to determine the total K-x-ray intensity by means other than the bent-crystal spectrometer, and hence to determine the factor by which the relative K-x-ray intensities are too small in the bent-crystal measurements. This determination (explained in detail below) gave a factor of 2.0.

The total measured K-x-ray intensity (i.e., the sum of the individual x-ray intensities in Table VIII) is 17. The total K-x-ray intensity was also determined from the K-conversion electron intensity data, from the

K-Auger electron intensity data, and from the photon spectrum recorded on the Penco scintillation spectrometer. The values obtained by these three methods were 34, 31, and 44, respectively. The first determination was made by summing the K-conversion electron intensities listed in Table VI and multiplying this sum by the fluorescent yield (0.963) as given by Nijgh et al.[69]

The second determination involves the K-Auger electron intensities given in Table XV. The total intensity of the KL_pL_q lines is 0.68. Included in this sum are estimates of 0.02 and 0.08 for the intensities of the $KL_{II}L_{II}$ and $KL_{III}L_{III}$ lines which are not observed in this work. These estimates were obtained from the data of other workers (listed in Table XV) for Auger lines in the region of Z = 80 (see Section III.B.9 for details). Although intensities were not obtained for Auger lines of the type KLY and KXY, where X and Y indicate shells higher than L, it is possible to estimate these intensities by means of the tables of Nijgh et al.[69] This publication gives values of 0.7 and 0.05 for the ratios of $\frac{KLY}{KLL}$ and $\frac{KXY}{KLL}$, respectively, for Z = 90. For this work, therefore, the estimated intensities of the KLY and KXY lines are 0.48 and 0.034, respectively; and the total K Auger intensity (KLL+KLY+KXY) is 1.2. Using the fluorescent yield of 0.963 leads to a calculated K-x-ray intensity of 31.

The third x-ray intensity determined was made by using the gamma-ray spectrum taken on the Penco scintillation spectrometer; this is a much less accurate method. The spectrum shown in Fig. 4 was obtained with a mass-free Pa^{233} source evaporated on Mylar film. The source was approximately 20 cm from the sodium iodide crystal. The relative intensities of the peaks at 100 and 312 kev were determined and normalized to the intensity data of Table VIII by means of the 312-kev peak, which is a composite of all gamma rays between 270 and 340 kev. The intensities from the Penco spectrum were corrected for photoefficiencies by means of the curves of Heath.[70] The K-x-ray intensity contribution to the 100-kev peak was then determined by subtracting the gamma intensities listed in Table VIII for the 75-, 87-, and 104-kev gamma rays. The K-x-ray intensity determined in this manner is 44. That this value is larger than those determined by the other two means is probably due to the Compton

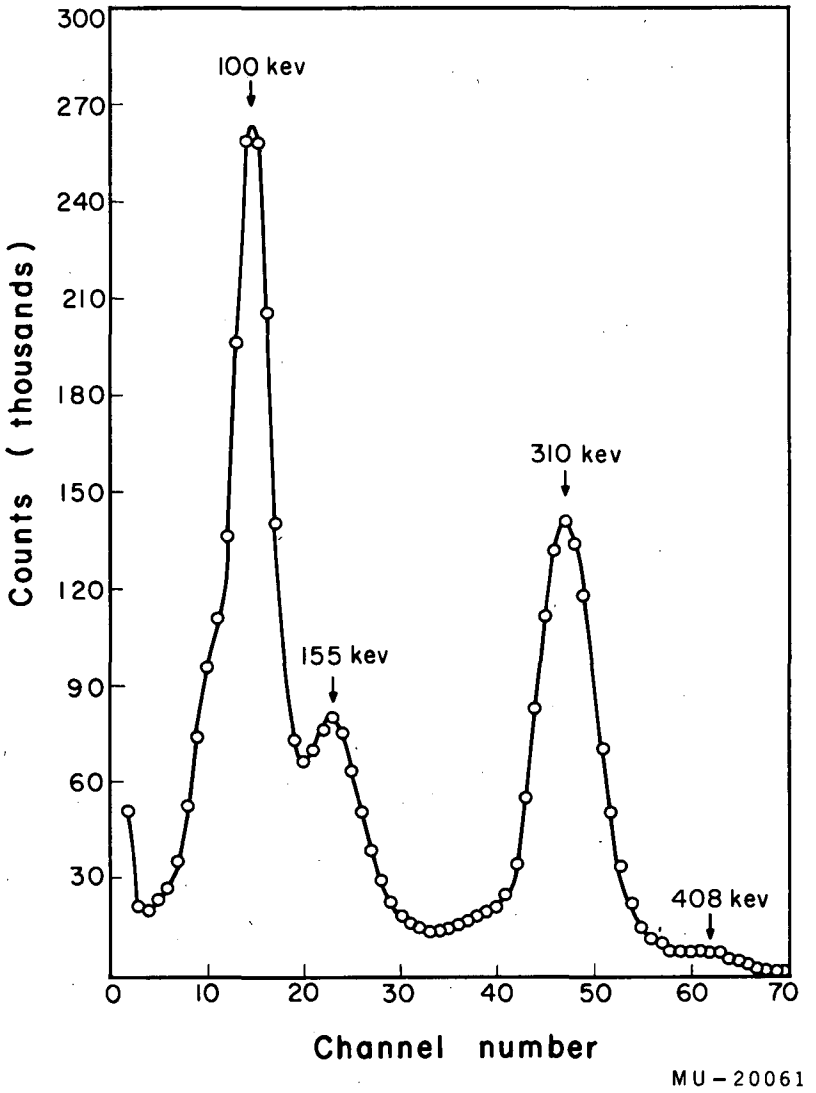

Fig. 4. Gamma-ray spectrum of Pa^{233}.

tail of the higher-energy gamma rays in the 100-kev peak. It was difficult to estimate this contribution to the lower-energy peak, hence the value 44 is only approximate.

The most accurate of these three determinations is undoubtedly the value 34 obtained from the K-conversion electron intensities. This value is exactly twice the directly measured value Σ K-x-ray = 17, hence the x-ray intensity correction factor we obtain is 2.0, somewhat higher than the factor 1.6 determined by Gallagher.[68] Presumably this correction factor would be unity if the intensity measurements were made by recording the entire photon and x-ray lines (by sweeping in energy) rather than by focusing only on the line peaks.

5. Multipolarity of the 312-kev Transition

The multipolarity of the 312-kev transition was determined from its L-subshell ratios and measured K-conversion coefficient. These data show the transition to be approximately pure M1. The K/L ratio is discussed in the next section.

From Table VI it is seen that the L_I/L_{II} ratio of the 312-kev transition measured by the Uppsala group[57] is 11. The theoretical value[28] (Table IX) for M1 radiation is 10; hence the measured L_I/L_{II} ratio is consistent with an assignment of pure M1. The 312-kev L_{III} line is masked by the 300-kev M_I line; however, it is possible to set an upper limit on the intensity of the L_{III} line in the following manner: The L-subshell ratio of the 300-kev transition indicates that this transition is predominantly M1. The other predominantly M1 transitions seen in this work have L_I/M_I ratios of about 3.6, none exceeding a value of 4.2. If we assume that the upper limit of this ratio for the 300-kev transition is 4.5, then from the measured intensity of the 300-kev L_I line (1.1) we can set a lower limit of 0.25 on the intensity of the 300-kev M_I line. Subtracting this value from the total measured intensity of the composite line (0.33) gives a maximum value of 0.07 for the intensity of the 312-kev L_{III} line. An L_{III} line of this intensity would indicate a 9% E2 admixture in the 312-kev transition; thus the E2 admixture does not exceed 9% and is most likely much less than this value.

Table IX

Experimentally determined conversion coefficients of transitions in U^{233}

Experimental values													Theoretical values[c]											
													M_I						E_2					
ENERGY (kev)	α_K	α_{L_I}	$\alpha_{L_{II}}$	$\alpha_{L_{III}}$	α_{M_I}	$\alpha_{M_{II}}$	$\alpha_{M_{III}}$	α_{N_I}	α_{O_I}	$\alpha_{\Sigma L_1}$[a]	$\frac{\alpha_K}{\alpha_{\Sigma L_1}}$[a]	Multipole assignment	α_K	α_{L_I}	$\alpha_{L_{II}}$	$\alpha_{L_{III}}$	$\alpha_{\Sigma L_I}$[a]	$\frac{\alpha_K}{\alpha_{\Sigma L_1}}$[a]	α_K	α_{L_I}	$\alpha_{L_{II}}$	$\alpha_{L_{III}}$	$\alpha_{\Sigma L_1}$[a]	$\frac{\alpha_K}{\alpha_{\Sigma L_1}}$[a]
28	--	--	--	--	$M_I/M_{II}/M_{III}$=1.0/0.27/0.30			--	--	--	--	98% M1 2% E2	--	$M_I/M_{II}/M_{III}$ = 1.0/0.1/0.0047				--	--	$M_I/M_{II}/M_{III}$ = 1.0/28/28				--
40	--	64	230	180	--	47	52	--	--	470	--	70% M1 30% E2	--	50	4.2	0.29	54	--	--	16	400	390	806	--
75	--	11	1.5	0.16	2.6	--	--	0.95	0.38	13	--	98% M1 2% E2	--	8.9	0.75	0.043	9.7	--	--	1.2	23	17	41	--
87	--	5.5	0.76	0.15	1.5	0.34	0.076	0.43	0.11	6.4	--	97% M1 3% E2	--	5.8	0.49	0.027	6.3	--	--	0.60	11	8.0	20	--
104	--	3.9	0.71	0.15	1.2	--	--	0.55	--	4.8	--	95% M1 5% E2	--	3.5	0.30	0.016	3.8	--	--	0.30	4.9	3.2	8.0	--
272	0.20	0.19	$\leq$0.14		--	--	--	--	--	$\leq$0.33	$\geq$0.59	E2	1.2	0.23	0.023	0.00093	0.25	4.7	0.089	0.023	0.082	0.033	0.138	0.65
300	0.83	0.17	0.025	--	0.051	--	--	0.013	--	0.20	4.1	90% M1 10% E2	0.86	0.17	0.017	0.00068	0.19	4.6	0.075	0.018	0.055	0.020	0.073	1.0
312	[0.79][b]	0.19	0.017	--	0.044	--	--	0.015	0.0038	0.21	3.9	M1	0.79	0.16	0.016	0.00062	0.18	4.5	0.070	0.017	0.048	0.017	0.065	1.1
341	0.67	0.15	0.019	--	0.046	--	--	0.019	--	0.17	4.0	95% M1 5% E2	0.60	0.12	0.012	0.00046	0.13	4.5	0.059	0.014	0.033	0.011	0.047	1.3
375	0.077	0.021	0.045	0.021	--	--	--	--	--	0.087	0.90	E2	0.48	0.098	0.0099	0.00036	0.11	4.4	0.051	0.012	0.024	0.0076	0.044	1.2
399	0.066	0.020	0.035	0.011	--	--	--	--	--	0.066	1.0	E2	0.40	0.081	0.0082	0.00030	0.089	4.5	0.045	0.010	0.018	0.0055	0.034	1.3
416	0.12	0.024	0.017	0.0045	--	--	--	--	--	0.046	2.7	12% M1 78% E2	0.36	0.074	0.0076	0.00027	0.082	4.4	0.043	0.0094	0.016	0.0047	0.030	1.4

a. $\alpha_{\Sigma L_1}$ refers to the sum of the L-conversion coefficients determined in this work. $\alpha_{\Sigma L_1}$ differs from α_L (total L-conversion coefficient) in those cases in which not all of the L-subshell electron intensities were measured.

b. The relative photon intensities were normalized to the relative electron intensities by means of the theoretical α_K^{312}, which is 0.79 (see text).

c. Reference 28.

The K-conversion coefficient of the 312-kev transition was measured by use of the thick-lens spectrometer and 100-channel scintillation spectrometer. Four sources were prepared by evaporating a solution of Pa^{233} onto Mylar films which were mounted on brass rings. A 1/4-inch margin on the source side and the entire back side of the Mylar was coated with Aquadag to minimize source charging. These sources were used to measure the intensity of the gamma-ray and K-conversion electrons of the 312-kev transition in the scintillation spectrometer and thick-lens beta spectrometer, respectively. The peaks of the 312-kev transition were not resolved in either the gamma spectrum or electron spectrum, however, the relative-intensity data obtained from the permanent-magnet spectrographs and bent-crystal spectrometer were used to determine the extent to which the 312-kev transition contributed to the composite peaks. Since these fractions were large in both cases, the errors associated with these quantities led to small percentage errors in the final value of α_k^{312}.

A Bi^{207} source was used to determine the normalization factor for converting the observed ratio of electron intensity/gamma intensity to an absolute conversion coefficient. Used for this purpose was the Bi^{207} 570-kev transition whose conversion coefficient is known ($\alpha_K = 0.017$).[71,72] Measurements of the Bi^{207} source were taken in the same manner as with the Pa^{233} and the known conversion coefficients used to determine the normalization factor. The photon intensities were corrected for photoefficiencies by means of the curves of Heath.[70]

Four separate Pa^{233} sources were used in the determination of the conversion coefficient. The relative activities of these sources were 1/3/5/7, and the values of α_k^{312} obtained were 0.86, 0.89, 0.62, and 0.54, respectively. For the most active source the electron counts were of the order of 10^5/min at the peak of the 312-kev conversion line, and it is almost certain that the use of the two most active sources resulted in low values for α_k^{312} because of coincidence losses in the scaler unit of the beta spectrometer. No correction was made for such coincidence losses because it was easier to use the less intense sources in order to eliminate the coincidence losses than it was to determine the correction factors. Corrections in the gamma-counting rate were made through use of a "dead time" meter on the gamma spectrometer.

The theoretical value for the conversion coefficient of a 312-kev magnetic dipole transition is given as 0.79 by Rose[28] and as 0.72 by Sliv and Band.[73] The value 0.86 has been selected as the experimental value of α_k^{312}, and the limits of error are estimated as ± 30%; hence the experimental value is not inconsistent with an interpretation of pure M1 for the 312-kev transition.

6. Conversion Coefficients and Multipole Assignments

In order to calculate from the electron and gamma relative intensities the conversion coefficients of the observed transitions, the gamma intensities were normalized to the electron intensities by means of Rose's theoretical K-conversion coefficient for a 312-kev M1 transition.[28] (Subsequently both the electron and photon intensities were normalized to "percent beta decay" as explained in Section III.B.7.) This means of normalization was chosen because the large limits of error on the experimental value of α_k^{312} made this value undesirable as a normalization factor. If the 312-kev transition had the 9% E2 admixture set as an upper limit, then the use of the theoretical α_k^{312} for a pure M1 transition would introduce an approximate 8% error in the normalization and in the calculated conversion coefficients.

The conversion coefficients calculated are listed in Table IX. From the limits of error placed on the electron and gamma intensities, one can estimate limits of error of about 35% for most of the experimental conversion coefficients listed in Table IX. The values for the weak transitions may be in error by as much as a factor of two.

The experimental L-subshell ratios, $\alpha_k/\alpha_{\Sigma L_i}$ ratios,[74] and absolute conversion coefficients were compared to the theoretical values of Rose[28] in order to assign transition multipolarities. Rose's theoretical values for M1 and E2 transitions are listed in Table IX along with the experimental values and the assigned multipolarities.

Some general observations can be made about the data and assignments presented in Table IX. First, it is true that in most cases the major multipole component of each transition is clearly indicated. The percentages of admixed multipoles were calculated from the conversion

coefficient data; and although the listed percentages of the less intense multipole components are approximate, they are quantitative.

In making these quantitative estimates of multipole admixtures most weight was given to the L-subshell ratio data. In most cases the experimental absolute conversion coefficients are larger than expected from these assignments and the theoretical conversion coefficients. This is especially evident in the pure E2 assignments. These differences are probably due to experimental errors in the electron- and photon-intensity data and to the means of normalizing the photon intensities to the electron intensities. If it were assumed that the K-conversion coefficient of the 312-kev transition were less than 0.79 because of a few percent of E2 admixture, then the photon-intensity normalization would make all calculated conversion coefficients several percent lower. Not all the discrepancies can be eliminated by an adjustment of the normalization factor, however.

Finally, it is noted that the experimental $\alpha_k/\alpha_{\Sigma L_i}$ values of the 300-, 312-, and 340-kev transitions are approximately 10% smaller than would be predicted by the assigned multipolarities and theoretical values. It has been mentioned that the electron intensities from Hollander and Hamilton[57] are the measured peak heights of the conversion lines. These workers also measured the intensities of the 312-kev K and L_I lines by integrating the area under the peaks. The K/L ratio of the 312-kev transition obtained in this manner is 4.2 ± 0.4 and is more accurate than the value of 3.9 obtained from the peak heights; thus unless the error limits have been chosen too conservatively, there is no discrepancy between the experimental and theoretical K/L ratios for this transition. It would be of interest to perform a more accurate experimental measurement of this quantity.

The K/L ratios of the 300-kev transition (measured by the Uppsala group from peak heights) and the 340-kev transition (measured in this work by means of photographic film) are known less accurately than that of the 312-kev transition. Furthermore, it is reasonable to assume that the former quantity would be approximately 6% larger if it were measured from integrated areas rather than from peak heights. The experimental K/L

ratios of the 300- and 340-kev transitions, therefore, most likely agree with the theoretical values within the experimental errors. It should be noted that Bisgard et al. report values of approximately 5 for the K/L ratios of the 300-, and 312-, and 340-kev transitions.[53]

Table X is a reproduction of a table from Bisgard et al.,[53] who have assigned multipolarities to the transitions in U^{233} on the basis of relative conversion-electron intensities measured with a six-gap beta spectrometer. For comparison the corresponding experimental values used for the interpretation in this work have been included. (Also included in the table are the multipole assignments of Albouy and Valadares[54] and those of this work.)

The theoretical values listed by Bisgard et al. were reported to be taken from the tables of Rose.[28] In some cases the theoretical values used in this work (also from Rose's tables but not listed) do not agree exactly with those of Table X. These differences are probably due to differences in the assigned transition energies and are not large enough to greatly affect the interpretation of the data.

The agreement between the data of Bisgard et al.[53] and this work is not good, the differences being by a factor of two in many cases. The multipole assignments made by the Danish group are, however, essentially the same as those of this work, the assignments of this work being more quantitative. One exception is present. Bisgard et al. assign the 416-kev transition as magnetic dipole, whereas we interpret the transition as an M1-E2 mixture, predominantly E2. We do not understand why Bisgard et al. make this assignment, since their experimental values do fall between the theoretical M1 and E2 values.

It is encouraging that the data of the Danish group[53] and of this work for the 375- and 399-kev transitions are in reasonably close agreement. The multipole assignments of these transitions are quite important in the interpretation of the decay scheme, and this agreement supports the assignments of these transitions as electric quadrupole.

The multipole assignments by Albouy and Valadares[54] are also in essential agreement with those of this work, with the exception of the 40-kev transition. The French authors report this transition as an M1-E2

Table X

The decay of Pa^{233} – multipolarity assignments of various workers

E_γ (kev)	Conversion ratio	Experimental values Bisgard et al.[b]	This work	Theoretical values[a] E_1	E_2	M_1	Multipolarity Bisgard et al.[a]	Albouy and Valadares[c]	This work
28	$\frac{M_I + M_{II}}{M_{III}}$	~9	4.3	2.2	0.7	170	M1 + E2	M1 + E2	98% M1 2% E2
	$\frac{M_{III}}{M_{IV}}$	>20	--	1.9	62	7.6			
40	$\frac{L_I + L_{II}}{L_{III}}$	1.0	1.7	1.1	1.1	230	M1 + E2	20% M1 80% E2	70% M1 30% E2
	$\frac{L_I}{L_{II}}$	~0.4	0.27	0.7	0.03	13			
	$\frac{M_I + M_{II}}{M_{III}}$	1.7	--	2.0	1.1	200			
	$\frac{M_{III}}{M_{IV}}$	$\gtrsim$50	--	2.8	46	7.3			
76	$\frac{L_I + L_{II}}{L_{III}}$	>130	74	2.2	1.3	223	M1	M1 (<1% E2)	98% M1 2% E2
	$\frac{L_I}{L_{II}}$	~13	7.1	1.4	0.06	12			
87	$\frac{L_I + L_{II}}{L_{III}}$	>20	40	2.4	1.3	207	M1	M1 (<1% E2)	97% M1 3% E2
	$\frac{L_I}{L_{II}}$	~9	7.4	1.5	0.06	11			
104	$\frac{L_I + L_{II}}{L_{III}}$	>30	30	1.9	1.6	229	M1	M1 (<1% E2)	95% M1 5% E2
	$\frac{L_I}{L_{II}}$	~9	5.6	0.9	0.06	11			
273	K/L	0.55	$\gtrsim$0.59	5.2	0.67	4.6	E2	E3, E4, or E5 or M1 + E2	E2
	$\frac{L_I + L_{II}}{L_{III}}$	2.8	$\gtrsim$1.3	6.7	3.3	274			
301	K/L	5.0	4.1	5.2	0.84	4.5	M1	M1	90% M1 10% E2
313	K/L	5.1	3.9	5.1	0.9	4.5	M1	M1	M1
341	K/L	5.0	4.0	5.2	1.1	4.5	M1	M1	95% M1 5% E2
	$\frac{L_I + L_{II}}{L_{III}}$	>100	--	8.2	4.2	277			
377	K/L	1.2	0.90	5.1	1.2	4.6	E2	--	E2
	$\frac{L_I + L_{II}}{L_{III}}$	3.1	3.0	9.0	4.9	287			
400	K/L	~2.4	1.0	5.2	1.3	4.5	E2	--	E2
	$\frac{L_I + L_{II}}{L_{III}}$	4.0	5.1	9.2	5.1	294			
417	K/L	3.9	2.8	5.1	1.5	4.4	M1	--	22% M1 78% E2
	$\frac{L_I + L_{II}}{L_{III}}$	>20	9.0	9.9	5.5	297			

a. Reference 53.

b. Reference 54.

c. This table is a copy of one presented by Bisgard et al., with the data of this work and of Albouy and Valadares included for comparison. The theoretical values listed are those in the original table and in some cases are not exactly the same as those used for the interpretation herein (see text).

admixture with approximately 20% M1, whereas we interpret the transition as M1-E2 with approximately 70% M1.

7. Absolute Transition Intensities and Log ft Values

From the data of previous investigators,[49,50,51] it is apparent that approximately 95% of the beta decay populates the upper four levels in U^{233}. (Beta intensities measured in this work with the Berkeley double-focusing spectrometer showed approximately 90% of the beta decay populating the upper four levels; however, the intensities of the previous workers are considered more accurate because the emphasis in this work was placed upon conversion-electron intensities, not on beta intensities.) The measured relative intensities in Tables VI, VII, and VIII have been placed on an absolute basis of percent beta decay by requiring that the sum of the intensities of the transitions depopulating the upper four levels be 95% of the total beta decay. The transition intensities (the sums of the electron and gamma-ray intensities) are listed in Table XI.

Since no gamma-ray data and only limited electron-intensity data are available for the 28-kev transition, its intensity was estimated in the following manner. The multipolarity of the 28-kev transition was deduced from the relative M-subshell ratios by comparing the experimental values to Rose's theoretical values.[28] The transition was found to be M1 with approximately 2% E2 admixture. The theoretical M-conversion coefficients for a gamma ray of this multipole admixture were deduced from Rose's M1 and E2 conversion coefficients. The measured M electron intensities and the deduced conversion coefficients were used to estimate the 28-kev gamma-ray intensity. Since the conversion coefficients are large, this estimated gamma intensity is a small fraction (0.2%) of the total intensity.

The total L-electron intensity was approximated as 3.6 times the total M electron intensity. The factor 3.6 is an average of the ratio of total L to total M intensities for other M1 transitions observed in this work. This empirical factor was used in preference to a theoretical factor deduced from Rose's tables,[28] because the M conversion coefficients of Rose have not been corrected for screening or for finite nuclear size.

Table XI

The decay of Pa^{233} –
Total absolute transition intensities

Transition energy (kev)	Transition intensity (percent beta decay)
17	--
28	~12
40	9.4
75	14
86	17
104	5.1
272	0.48
300	13
312	70
340	7.3
375	0.66
398	1.3
415	1.7

Finally, the N and O electron intensities were assumed to be smaller than the M-electron intensity by factors 3 and 9, respectively. (This latter assumption was made also in estimating the total intensities of other transitions whose N and O intensities had not been measured.)

The percent beta population to each level in U^{233} was deduced from the absolute transition intensities; these are listed in Table XII. Hok's measured intensity values for the low- and medium-energy beta components are 37% and 58%, respectively.[49] The corresponding values deduced from the values in Table XII are 40% and 54%; thus there is close agreement in the values of these beta-decay groups determined in independent ways.

The value of 5% decay to the ground state listed in Table XII is the value measured by previous workers[49,50,51] The log ft values in Table XII were calculated by the method of Moszkowski[75] by using the beta intensities listed.

8. Discussion of Decay Scheme

The above data have been used to construct the decay scheme shown in Fig. 5. The general features of the scheme are the same as proposed by Brodie[51] and supported by Hok and Kramer.[49] The quantum assignments of the U^{233} levels suggested by Newton[55] are confirmed. Some Coulomb-excitation data of Newton are included in the scheme for completeness. The energies of the levels have been assigned so as to give good agreement between the sums and differences of the energies of the gamma rays connecting the levels. In all cases the different possible energy values of a level as computed by different sums and differences agree within 0.04%.

The ground-state spin of U^{233} has been measured as 5/2 by a number of investigators.[76-80] As pointed out by Newton,[55] the ground state is most probably the 5/2+ [633] Nilsson level. The ground state of Pa^{233} was measured as 3/2 by Hubbs and Winocur.[81] Evidence that the ground state of Pa^{233} has odd parity was obtained by a beta-gamma angular correlation experiment performed at Uppsala by Hamilton, Hollander, and Pettersson.[82] An anisotropy observed between the 250-kev beta group and the 312-kev photon establishes that the beta transition to the 312-kev

Table XII

Beta-component intensities and log ft values in the decay of Pa^{233}

Final state (kev)	Intensity (percent)	log ft
415.80	$\gtrsim$ 22	$\lesssim$ 6.72
398.55	$\lesssim$ 18	$\gtrsim$ 6.93
340.52	18	7.32
311.93	36	7.20
40.35 } 0.00 }	5	} 9.16

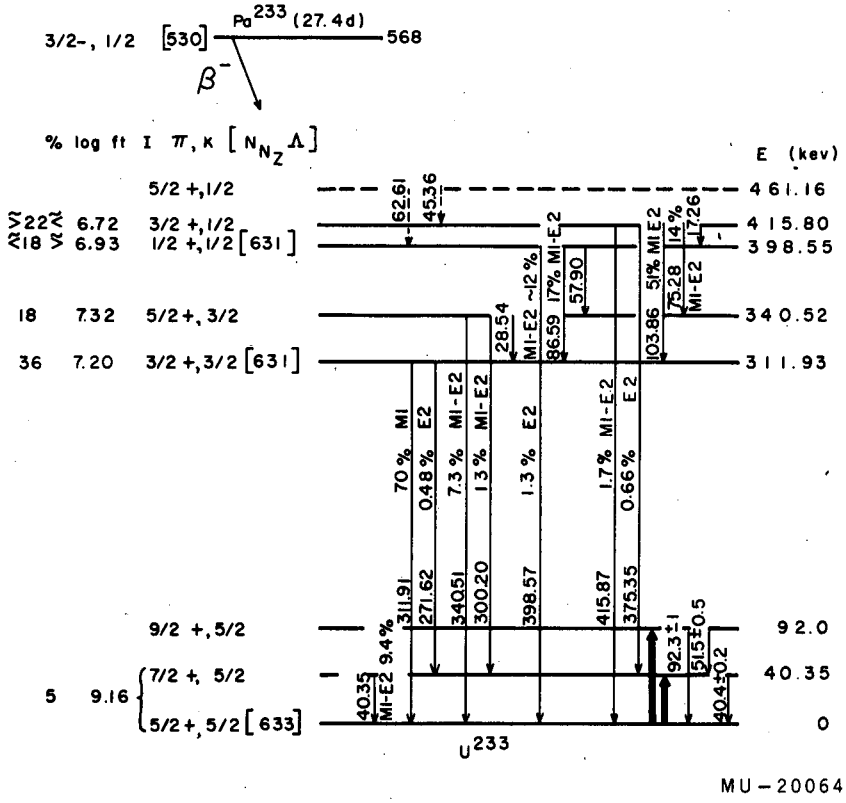

Fig. 5. The energy levels of U^{233}.

level cannot be purely allowed. Thus, the parity of Pa^{233} is odd if that of the 312-kev level is even. The Pa^{233} ground state has been interpreted[83] as the 3/2 member of a K = 1/2 band based on the Nilsson level 1/2 - [530]. With this basic information and the data at hand it is possible to analyze the scheme with respect to beta branchings, photon branchings, and log ft values. It will be convenient to discuss each of the rotational bands separately.

a. Ground-State Band

The assigned quantum states indicate that the ground-state beta transition proceeds largely by the "unique" $\Delta I = 2$, yes type of decay, since $\Delta I = 1$ transitions are K-forbidden ($\Delta K = 2$). In addition, the first-forbidden transition to the ground state is "hindered," in the notation of Alaga,[84] since a selection rule on the asymptotic quantum number Λ is violated. Thus, the calculated log ft of 9.16 for the ground-state transition is consistent with the assigned quantum states.[85]

It is possible to estimate from theory the beta branchings to the ground and first excited states in the following manner: From Hok's work it is known that the total beta population of these two levels is approximately 5%.[49] The relative amounts of beta decay to the ground and first excited states may be estimated from vector-addition coefficients if it is assumed that the decay to both states is L = 2 radiation. This assumption is justified since L = 1 radiation is, according to the quantum assignments made, K-forbidden. The ratio of the ft value for decay to the ground and first excited states is thus predicted as 0.75, and this ratio is realized if the beta populations of the ground and 40-kev levels are 3% and 2% respectively. In this case the log ft values are 9.38 and 9.48, respectively.

The rotational constant ($\hbar^2/2\mathfrak{J}$) for the ground-state band was calculated from the energy of the first excited state (40.35 kev) by means of the equation[3,4]

$$E_{rot} = \hbar^2/2\mathfrak{J} \; [I\,(I + 1) - I_o\,(I_o + 1)] \; .$$

The result is $\hbar^2/2\mathfrak{J} = 5.764$ kev. With this constant the energy of the second excited state is calculated to be 92.22 kev, in reasonable agreement with Newton's measured value of 92.0 kev.

One apparent discrepancy has been pointed out by Albouy and Valadares.[54] The total estimated population of the 40-kev level is larger than the measured intensity of the 40-kev transition. The French workers reported this difference to be a factor of 3 to 4. In this work the difference is by a factor of 1.7 if the assignment of 2% beta decay to the 40-kev level is correct and by a factor of 1.5 is no beta decay proceeds to the first excited state.

It is of interest to determine if the errors associated with our measured transition intensities are large enough to explain this inconsistency. The predominant decay to the first excited state is the 300-kev transition (13%); the measured intensity of the 40-kev transition is 9.4%. The values of the gamma-ray intensity of the 300-kev transition measured from the wire and ThO_2 sources agree exceptionally well. Likewise, the intensity measurements of the conversion electrons of this transition by the Uppsala group[57] and by this author are in excellent agreement. It is therefore probably reasonable to assing an error of about 15% to the measured relative gamma and electron intensities of the 300-kev transition.

Errors in the normalization of the relative gamma intensities to the relative electron intensities result in errors in the absolute transition intensities. If the possible error in the normalization is ± 10% and the error limits of the relative gamma and electron intensities are ± 15%, then the over-all error limits of the 300-kev transition intensity are about ± 20%.

If the measured intensity of the 300-kev transition is 20% too large and the population of the 40-kev state by modes other than the 300-kev transition is approximately 3, then the measured intensity of the 40-kev transition is about 32% too small. If no beta decay proceeds to the 40-kev level and if the intensities of the 375- and 271-kev transitions have been slightly overestimated, then the measured intensity of the 40-kev transition is approximately 20% too small.

The discussion in Section III.B.3 shows that the electron-line peak heights of the 40-kev transition may have been substantially attenuated by source absorption effects. For this reason, it is believed

that the discrepancy of 20 to 30% in the intensity balance which we note for the 300-kev—40-kev cascade is not only within the experimental uncertainty but also actually in the direction that should be expected. Thus we do not confirm the observation of Albouy and Valadares that there is an intensity discrepancy here of a factor of three to four.[54]

b. K = 3/2 Band

The levels at 311 kev and 340 kev have been interpreted as the 3/2 and 5/2 members of a rotational band based on the Nilsson level 3/2 + [631].[55] The calculated log ft values listed in Table XII for beta decay to these levels are in agreement[85] with first-forbidden nonunique decay (Δ I = 0 or 1, yes) and hence in agreement with the assigned spins and parities. The experimental beta branching to these two levels differs by a factor of two from the theoretical value predicted from vector-addition coefficients. The theoretical value for L = 1 decay is $\frac{B\ (3/2 \rightarrow 5/2)}{B\ (3/2 \rightarrow 3/2)} = 1.5$, whereas the experimental value (inverse ratio of ft values) is 0.76. It is permissible to compare only L = 1 radiation because L = 0 decay to the 3/2 level is K forbidden. It is possible to explain this disagreement by assuming an error of about 75% in the estimated intensity of the 28-kev transition. To bring about agreement the intensity would have to be about 21 instead of the assigned value of 12, which is quite possible in view of the absorption effects on these low-energy conversion line (as discussed earlier) and because the intensities of the L lines of the 28-kev transition were not measured but only estimated from the measured M-electron intensities. It is possible, too, that some decay to the 312-kev state takes place by L = 0 radiation due to admixtures of K values other than the principal ones in the initial or final states (or both).

It is possible to test by photon branching the quantum assignments of only the 340-kev level and this by only one ratio, $\frac{300\text{-M1}}{340\text{-M1}}$. Other comparisons for transitions depopulating the K = 3/2 band involve small admixtures of electric quadrupole radiation whose intensities are not known accurately enough to justify quantitative evaluation. The experimental and theoretical relative reduced photon transition probabilities are listed in Table XIII. The theoretical values are the ratios of the squares

Table XIII

The decay of Pa^{233} – experimental and theoretical relative reduced photon transition probabilities

E_γ/E'_γ	K_i/K_f	$\frac{L: B(I_i \rightarrow I_f)}{L: B(I_i \rightarrow I'_f)}$	Theoretical values	Experimental values: From photon intensities	Experimental values: From electron intensities
75/103	1/2/3/2	$\frac{M1: B(3/2 \rightarrow 5/2)}{M1: B(3/2 \rightarrow 3/2)}$	1.5	3.3	3.2
416/375	1/2/5/2	$\frac{E2: B(3/2 \rightarrow 5/2)}{E2: B(3/2 \rightarrow 7/2)}$	1.3	1.2	1.2
300/340	3/2/5/2	$\frac{M1: B(5/2 \rightarrow 7/2)}{M1: B(5/2 \rightarrow 5/2)}$	2.5	2.3	2.1

of vector-addition coefficients; the experimental ones were calculated by two nearly independent means. The experimental values in the first set are the ratios of the measured gamma-ray relative intensities corrected for the $E^{2\ell+1}$ energy dependence and for multipole admixtures. Those in the second set were determined in a like manner except that the relative photon intensities used were deduced from the measured conversion-electron intensities and the theoretical conversion coefficients. The values calculated by these two means are nearly the same. It is seen that there is good agreement between the experimental and theoretical values for the 300- and 340-kev transitions.

The assigned transition multipolarities (Table IX) allow no other spin assignments to the 312-kev and 340-kev levels. The only K values consistent with these spins are K = 1/2 or 3/2 for the 312-kev state and K = 1/2, 3/2, or 5/2 for the 340-kev state. In both cases the value of 1/2 is ruled out by the character of the radiation depopulating the two levels since, with K = 1/2, dipole radiation would be K-forbidden. The value K = 5/2 for the 340-kev state is not in agreement with the experimental data since this assignment leads to a theoretical value of 0.40 for the photon relative reduced transition probability. (The experimental value is 2.3.) Therefore the agreement between the experimental and theoretical ratios in Table XIII for the 300- and 340-kev transitions supports the assignment of K = 3/2 for the 340- kev level and thus makes reasonable the interpretation of this level as a rotational level based on the state at 312 kev.

From the energy difference between 3/2+ and 5/2+ members of this band (28.59 kev) one calculates a rotational constant of 5.718 kev. The calculated energy of the 7/2+ members is, then, 380.6 kev. No evidence for a state of this energy was found in this work.

c. <u>K = 1/2 Band</u>

According to the multipole assignments listed in Table IX the levels at 398 and 415 kev must have spins and parities of 1/2+ and 3/2+, respectively. These assignments are in agreement with the interpretation by Newton, who postulated that these levels are the first two members of a K = 1/2 rotational band with the Nilsson level 1/2 + [631] as the base state.[55]

The division of the primary beta population between these two levels cannot be estimated accurately because the intensity of the 17-kev transition is not known. In Table XII the log ft values listed for these two levels were calculated for the intensity of 0% for the 17-kev transition, and the uncertainties indicated by (<) and (>) signs. These approximate log ft values are in agreement with the postulated spin and parity assignments.

The theoretical branching ratio for beta decay to these levels cannot be calculated from vector-addition coefficients without knowledge of the relative amounts of L = 0 and L = 1 types of decay to the 416-kev level; however, if the quantum assignments of the 399- and 416-kev levels are assumed to be correct it is possible to make an indirect test of the assignment K = 1/2 to the ground state of Pa^{233}. The only other K value consistent with the measured spin for Pa^{233} is K = 3/2. If this value is assumed, it is possible to make branching-ratio comparisons for decay to the 415- and 398-kev levels because L = 0 transitions are then K-forbidden. With this assumption the theoretical ratio for L = 1 decay to the two highest levels is $\frac{B\ (3/2 \rightarrow 1/2)}{B\ (3/2 \rightarrow 3/2)} = 1.25$; the experimental value is 0.62. The value 0.62 was calculated by assuming the intensity of the 17-kev transition to be negligible. The calculated ratio would be smaller if a larger value were assumed for the intensity of the 17-kev transition. Thus, the theoretical and experimental values differ by at least a factor of two; however, this is not conclusive evidence against an assignment of K = 3/2 for the ground state of Pa^{233} because such deviations can be caused by admixtures of K values in the initial or final states. Much stronger evidence that the ground state of Pa^{233} has K = 1/2 comes from the work of Stephens, Asaro, and Perlman[86] on the alpha decay of Np^{237}, which populates several excited states in Pa^{233} whose spacings appear to be characteristic of a K = 1/2 band.

The theoretical and experimental values of the reduced photon branching ratio $\frac{416\text{-E2}}{375\text{-E2}}$ are compared in Table XIII. The agreement is quite good and supports the quantum assignment of (3/2+, 1/2) for the 416-kev level. Note that M1 transitions from the K = 1/2 band to the ground-state band are K-forbidden. This accounts for the predominantly E2 character

of the 416-kev transition. The theoretical and experimental reduced photon branching ratios $\frac{76\text{-M1}}{103\text{-M1}}$ also are compared in Table XIII. The values are seen to disagree by a factor of two. This disagreement is certainly outside the limits of error of the experimental intensities of these photons. If the multipolarities of the gamma rays depopulating the 416-kev level have been correctly deduced, the only choice of spin for this level is 3/2; and thus the only possible K values are 1/2 and 3/2. The choice of K = 3/2 leads to a theoretical value of $\frac{\text{M1: B } (3/2 \rightarrow 5/2)}{\text{M1: B } (3/2 \rightarrow 3/2)} = 0.67$, which differs from the experimental value by a factor of 4.5, in worse disagreement than the theoretical branching ratio for K = 1/2.

The difference of a factor of two between the experimental and theoretical values can most easily be explained as being due to admixtures of K values other than the principal one in the initial or final states; however, if such admixtures are present, it is surprising that the experimental branching ratios $\frac{416\text{-E2}}{375\text{-E2}}$ and $\frac{300\text{-M1}}{340\text{-M1}}$ agree so well with the theoretical values. Despite these difficulties we believe that the quantitative evidence obtained in this study indicates that the major component of the 399- and 416-kev state is K = 1/2.

It is possible that transitions from the 5/2 member of this K = 1/2 band were observed in this study. These transitions, of 62.61 and 45.36 kev, are shown in Fig. 5 depopulating a level at 461.16 kev. The evidence for these transitions is two weak electron lines of energies 41.67 and 23.60 kev listed in Table XIV. It was assumed that the first of these lines is the L_{II} line of a 63-kev E2 transition, and that the second is the L_I line of a 45-kev M1-E2 transition. The fact that no other electron lines associated with these transitions were observed is consistent with the intensities of the observed lines and the multipole assignments of the transitions. The evidence for the 461-kev state is tenuous, since in the energy region of these lines there are many unassigned lines among which one might expect some coincidental agreement. Some support is given the postulate by the close agreement between the differences of the postulated transitions (17.25 kev) and the measured energy (17.26) of the 3/2+ → 1/2+ transition.

Table XIV

Unassigned electron lines in the decay of Pa^{233}

Film no.[a]	Ee^- (kev)	Possible transition energies[b] (kev) K	L_I	L_{II}	L_{III}	Possible assignments
Relatively certain lines						
48-x	1.90	117.49	23.66	22.84	19.06	(c)
48-x	4.08	119.67	25.84	25.02	21.24	(c)
416	108.3	223.9	130.1	129.2	125.5	130-L_I
416	112.7	228.3	134.5	133.6	129.9	130-L_{III}
419	166.5	282.1	188.3	187.5	183.7	
I. S.	172.4	288.0	194.2	193.4	189.6	(c)
I. S.	226.6	342.2	248.4	247.6	243.8	
I. S.	229.5	345.0	251.2	250.4	246.6	250-L_{II}
412	232.1	347.8	254.0	253.2	249.4	
416	232.3					
I. S.	233.5	349.1	255.2	254.4	250.6	250-L_{III}
416	262.7	378.3	284.5	283.6	279.9	
I. S.	281.1	396.7	302.8	302.0	298.2	
417	292.0	407.6	313.8	312.9	309.2	314-L_I
I. S.	293.0	408.6	314.8	313.9	310.2	314-L_{II}
I. S.	445.4	561.0	467.2	466.3	462.6	
Questionable lines						
48-x	6.84	122.43	28.60	27.78	24.00	
48-x	9.31	124.90	31.07	30.25	26.47	
48-x	9.44	125.03	31.20	30.38	26.60	
419	19.86	135.45	41.62	40.80	37.02	
408	20.25	135.84	42.01	41.19	37.41	
408	20.49	136.08	42.25	41.43	37.65	
50-x	21.30	136.89	43.06	42.24	38.46	
408	21.75	137.34	43.51	42.69	38.91	
408	22.08	137.67	43.84	43.02	39.24	
50-x	23.60	139.19	45.36	44.54	40.76	
50-x	23.84	139.43	45.60	44.78	41.00	
419	24.68	140.27	46.44	45.62	41.84	
48-x	25.70	141.29	47.46	46.64	42.86	

Table XIV (continued)

Film no.[a]	Ee^- (kev)	Possible transition energies[b] (kev) K	L_I	L_{II}	L_{III}	Possible assignments
48-x	28.52	144.11	50.28	49.46	45.68	
419	30.64	146.23	52.40	51.58	47.80	
48-x	35.53	151.12	57.29	56.47	52.69	
408	37.77	153.36	59.53	58.71	54.93	58.8-L_{II}
408	41.67	157.26	63.43	62.61	58.83	58.8-L_{III}
I. S.	47.59	163.18	69.35	68.53	64.75	
48-x	53.86	169.45	75.62	74.80	71.02	
8	54.16	169.75	75.92	75.10	71.32	(d)
48-x	63.91	179.50	85.67	84.85	81.07	
48-x	65.15	180.74	86.91	86.09	82.31	
408	65.83	181.42	87.59	86.77	82.99	
419	67.23	182.82	88.99	88.17	84.39	
48-x	69.42	185.01	91.18	90.36	86.58	
50-x	72.21	187.80	93.97	93.15	89.37	
48-x	74.46	190.05	96.22	95.40	91.62	
48-x	81.73	197.32	103.49	102.67	98.89	
419	105.6	221.2	127.4	126.5	122.8	KM_IM_{III} Auger line
I. S.	217.7	333.3	239.5	238.6	234.9	
I. S.	219.5	335.1	241.3	240.4	236.7	
I. S.	221.5	337.1	243.3	242.5	238.7	
I. S.	227.2	342.8	249.0	248.2	244.4	
903	396.7	512.3	418.5	417.6	413.9	415-L_{III}

a. The films are identified as follows:

(1) 48-x, 50-gauss accelerator spectrograph with 10-kv pre-accerlation.
(2) 50-x same as 48-x without acceleration
(3) I. S. — intensity standards
(4) Remaining films exposed on conventional spectrographs

b. These values were obtained by adding the K, L_I, L_{II}, or L_{III} binding energy (as indicated) to the measured Ee^-.

c. These lines were stronger than others listed in the table. They are designated as weak, most others as vvvw.

d. This line is the low-energy side of the 75-kev L_{II} line, which appeared split on this film. This may indicate two-close lying lines or may be an instrumental effect.

With the assignment of the 5/2 member, it is possible to calculate the rotational constant $\hbar^2/2\mathfrak{J}$ and the decoupling parameter "a" for this K = 1/2 band. These constants are defined by the equation[3,4]

$$E_{rot} = \hbar^2/2\mathfrak{J}\ [I\ (I + 1) + a\ (-)^{I + 1/2}\ (I + 1/2)\ ].$$

Substitution of the measured energies gives $\hbar^2/2\mathfrak{J}$ = 7.41 kev and a = -0.22.

It is interesting to compare these values with those of the same rotational band occurring in other nuclei. In U^{235} the 1/2 + [631] level is a low-lying isomeric state. Albridge and Hollander,[87] using permanent-magnet spectrographs, have determined the energies of the 3/2+ and 5/2+ members of this band in U^{235} by measuring the 5/2+ → 1/2+ and 5/2+ → 3/2+ transition energies from the alpha decay of Pu^{239}. The energies of the 5/2+ and 3/2+ levels were found to be 51.67 kev and 13.00 kev, respectively. These energies lead to values of $\hbar^2/2\mathfrak{J}$ = 6.04 kev and a = -0.28.

The 1/2+ [631] level is the ground state of Pu^{239}. In a study of the decay of Np^{239} Hollander et al. determined values of $\hbar^2/2\mathfrak{J}$ and a for the K = 1/2 band in Pu^{239} as 6.25 kev and -0.58, respectively.[46]

In Table VI are listed two lines assigned as the L_{II} and L_{III} lines of a 57.90-kev transition. In Fig. 5 this transition is placed between the 399- and 341-kev levels. Keller and Cork[52] and Hok and Kramer[49] have reported lines which can be interpreted as L lines of a 58-kev transition; however, other workers have not observed these lines. In this work the electron line of about 41 kev, assigned as the 58-kev K_{III} line, was seen by means of the 50- and 100-gauss spectrographs and by means of the accelerator camera both with and without pre-acceleration. The approximately 37-kev line, assigned as the 58-kev L_{II} line, was seen by means of the 50-gauss instrument and perhaps with the 100-gauss spectrograph. That this line was not observed in the accelerator camera is explained by the fact that it is weaker than the approximately 41-kev line, and this stronger line was just visible on the plates exposed in the accelerator camera. The line of approximately 36 kev reported by Hok and Kramer[49] as the 58-kev L_I line was most likely the 40-kev M_{III} line.

The 58-kev L lines assigned in this work were too weak to be given a numerical intensity. This weakness, in addition to the fact that the transition is thought to be E2 and, therefore, highly converted, is consistent with the fact that Browne failed to detect the gamma ray of this transition.[64] That a 58-kev photon was not detected with the Pasadena spectrometer may not be significant since it is possible that during the sweep of this energy region the discriminator of the detector was set so as not to accept pulses corresponding to this energy. This fact was not discovered until the source had been returned from Pasadena to Berkeley.

The position of the 58-kev transition in the proposed decay scheme requires that this transition be electric quadrupole. The L-conversion coefficients of a 58-kev electric quadrupole transition are given by Rose as 3.3, 70, and 56 for the L_I, L_{II}, and L_{III} shells, respectively.[28] That the L_{III} line is observed as somewhat more intense than the L_{II} line is not necessarily in contradiction to an assignment of E2, since source-absorption and film-efficiency corrections would increase the intensity of the L_{II} line relative to that of the L_{III} line.

d. Other Transitions

There is evidence for the existence of other gamma transitions in the Pa^{233} decay. This evidence is a number of unassigned electron lines (Table XIV) detected by means of the permanent-magnet spectrographs and two photon lines (Table VIII) of energies 41.65 and 145.42 kev detected by means of the Pasadena bent-crystal spectrometer. These new data and possible interpretations are discussed in this section.

The electron lines listed in Table XIV are divided into two groups. Those in the first group are lines whose existence are considered relatively certain because of their intensities or because of their detection on more than one photographic plate. The second group contains lines whose existences are questionable or doubtful. An attempt was made to find lines that could correspond to different conversion lines of the same transition. In Table XIV the K, L_I, L_{II}, and L_{III} binding energies have been added to each of the observed energies and possible transition energies are indicated.

Bisgard et al. have reported weak electron lines of energies approximately 5 kev less than those of the 300-, 312-, and 341-kev K lines (i.e., at approximately 180, approximately 185, and approximately 220 kev).[53] With the exception of a questionable line at approximately 220 kev, lines of these energies were not observed in this work, although they would most likely have been visible were they present in the intensities reported by the Danish workers.

In Table VIII fairly large error limits have been placed on the measured energies of the 42- and 145-kev photons because in the spectrum the photon lines were not well defined and hence the energies were difficult to determine. The 41.65-kev gamma was observed only with the platinum wire source because the line was of too low intensity to be seen with the weaker ThO_2 source. The 145-kev line was observed only with the ThO_2 source because this region of the energy spectrum was not scanned with the platinum wire source.

In Table XIV there is no definite evidence of conversion electrons corresponding to transitions of 42 or 145 kev. One extremely weak line, which was seen at an energy of 19.86 kev, could be the L_I line of a 41.62-kev transition; however, this line is of doubtful existence so the assignment cannot be made with any degree of certainty. The fact that there is no definite evidence of conversion electrons of these two transitions raises the question whether the recorded gamma rays have arisen from impurities in the bent-crystal sources. The source with which the 41-kev gamma was detected underwent the same chemistry as used for the permanent-magnet spectrograph sources; and although the source used for the detection of the 145-kev gamma underwent no chemistry, it is likely that very few fission products were formed, owing to the low fission cross section for thermal neutrons on Th^{232}. At any rate, no gamma ray of 145 kev has been reported as being associated with any fission product isotope. For these reasons the possibility of impurities has been ruled out. The most probable reason for the failure to observe conversion electrons from these transitions is that they have small conversion coefficients. For example, if the transitions were electric dipole it is reasonable that the conversion-electron intensities would have been too small to be detected.

The difference between the energies of the 42- and 145-kev photons is 103.77 ± 0.05 kev. This difference agrees with the energy of the 103.86 ± 0.02-kev transition to within 0.1%, but the agreement is not within the assigned limits of errors. Probably the error limits have been underestimated and the close agreement is a significant one; but a definite answer to this point must await a more precise redetermination of the photon energies. However, for the purpose of the following discussion it is assumed that the difference between the energies of the 42- and 145-kev transitions does correspond to the energy of the 104-kev transition. In this manner one can determine what possibilities are open for the assignment of these lines if the assumption proves correct.

The two new photon lines can be used to define a level at 270.3 kev as shown in Fig. 6a. Thomas et al.[88] have reported a level in U^{233} of approximately 290 kev populated by the alpha decay of Pu^{237}. The energy of the level reported by these workers probably agrees within experimental error with the 270-kev level postulated here. Stephens et al.[83] and Mottelson and Nilsson[89] have discussed the possible Nilsson assignments of this level. The former workers prefer an assignment of 5/2 - [752], the latter, one of 7/2 - [743].

In this work the assignment of 5/2 - [752] to the 270-kev level appears to be the only reasonable choice. With this assignment one can explain our failure to observe electron lines corresponding to transitions associated with this level, since these transitions would be electric dipole, and hence would have small conversion coefficients. Because of its high resolution, the bent-crystal spectrometer was not used to sweep the entire energy spectrum; thus it is not known whether photons associated with this level other than the two reported are observable. In particular, it would be valuable to search for a photon of 270.3 kev which would de-excite the 270.3-kev 5/2- level to ground. With this assignment it is true that the 145-kev transition would be designated as K-forbidden ($\Delta K = 2$); however, it may not be unreasonable to assume that this transition proceeds by an admixture of K values in either the initial or final state.

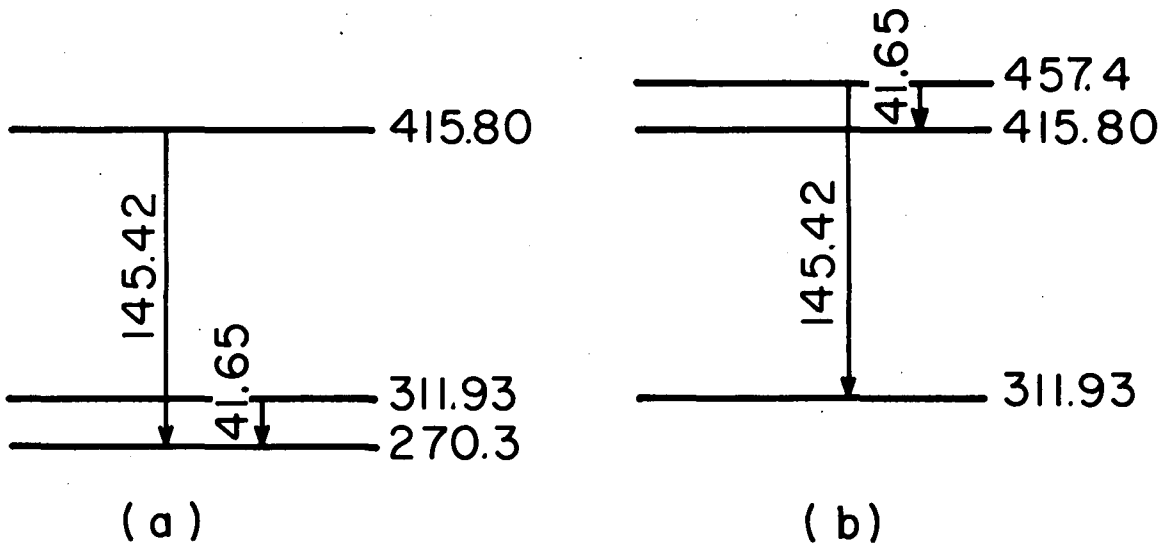

MU-20058

Fig. 6. (a and b) Possible assignments of two new transitions in the decay of Pa^{233}.

An alternative assignment of the new transitions is shown in Fig. 6b, where a level is defined at 457.4 kev. No level of this energy has been postulated for U^{233} previously. The possible Nilsson assignments of this level are the same as those discussed for the 270.3-kev level, with the 5/2 - [752] state again being the only reasonable choice. The arguments for this assignment are the same as those presented in the discussion of the 270-kev level. In Table XIV electron lines are listed that could be assigned to transitions of 58.8 kev (457 → 399) and 117.5 kev (457 → 340). Although with respect only to energy these transitions would fit quite well into the postulated scheme of Fig. 6b, it would be difficult to explain why their electron lines would be seen and not those of the other transitions. For this reason we conclude that the energy fit is fortuitous, and these transitions have not been included in Fig. 6b.

At present there is not enough information to place in the scheme with confidence either the newly discovered gamma rays or the electron data of Table XIV. Additional work with high-resolution gamma spectroscopy and strong Pa^{233} sources is required.

9. Auger Electron Data

The following section is devoted to a discussion of the Auger electron lines of uranium observed in this work. Burhop has presented an excellent review of the Auger process,[90] and a summary of experimental and theoretical data appears in the spectroscopic tables of Nijgh et al.[69] It is not the intention to reproduce here the material already presented in previous publications except as it relates to the data of this work. It should be mentioned that, in general, there is no abundance of detailed experimental information on the energies and intensities of Auger electrons in the heavy-element region. What information is available indicates that theoretical attempts to predict Auger energies and intensities have not been very successful.

a. K-Auger Lines

Uranium K-Auger electron data are presented in Table XV. These data were obtained by means of the permanent-magnet spectrographs. Most

of the lines listed were observed by means of more than one spectrograph (i.e., at more than one field strength). The energies listed are the mean averages of several determinations, and the error limits are standard deviations from the mean values. In those cases in which only a single energy determination was made an estimated error is given in brackets. The intensities were measured by the use of the intensity standards in the same manner as employed for determining electron intensities.

One of the methods of calculating Auger electron energies is that discussed by Bergström and Hill.[91] In this method one defines the Auger energy for a process UVW as $E_{uvw} = U_z - V_z - W(V_z)$, where U_z and V_z are the binding energies of the U and V shells in an atom of atomic number Z, and $W(V_z)$ is the binding energy of the W shell for an atom already ionized in the V shell. Since, in general, $W_z < W(V_z) < W_{z+1}$, an effective charge increment ΔZ is introduced and defined as $\Delta Z = W(V_z) - W_z / W_{z+1} - W_z$, so that the energy may be defined as $E_{uvw} = U_z - V_z - W_{z+\Delta z}$.

Bergström and Hill[91] have used experimentally determined K-Auger energies for mercury (Z = 80) and Mladjenovic and Slätis[92] those of bismuth (Z = 83) to calculate values of ΔZ for KL_pL_q processes. They have found that ΔZ is independent of L_p and depends on L_q in the following manner:

$$\Delta Z = 0.5 \text{ for } L_q = L_I,$$
$$\Delta Z = 0.5 \text{ for } L_q = L_{II},$$
$$\Delta Z = 0.8 \text{ for } L_q = L_{III}.$$

In this work values of ΔZ for uranium K-Auger lines have been calculated, using the binding energies of Hill et al.[93] and are listed in Table XV. The limits of error quoted were calculated from the error limits placed upon the experimental energies. The ΔZ values for the KL_pL_q lines are seen to be approximately the same as those listed above for Z = 80. Little can be said regarding the values of ΔZ for the KL_pM_q lines, since the error limits are so large. Unfortunately the calculated values of ΔZ for these transitions are quite sensitive to the values of the measured energy. For the KL_IM_I and KL_IM_{II} transitions in bismuth Mladjenovic and Slätis[92] report ΔZ values of 0.81 and 0.38, respectively.

The measured intensities of this work are compared in Table XV to the corresponding relative intensities for the Auger lines in the region of Z = 80 measured by several workers. The experimental data from the other workers have been normalized as indicated by brackets for the purpose of comparison. The agreement is good with the exception of the KL_IL_{II} line. Neither the intensity values of previous work nor of this work agree well with the theoretical values of Asaad and Burhop.[94] It has been suggested that this disagreement for high-Z values is due to relativistic effects.[94]

b. L-Auger Lines

Uranium L-Auger lines observed in this work are presented in Table XVI. These lines were detected by means of a 50-gauss permanent-magnet spectrograph employing an extremely clean source which was prepared by dipping a 10-mil platinum wire into an acid solution of Pa^{233}. The source was used in the preaccelerator camera both with and without the application of an accelerating voltage. (For a complete discussion of this source and measurements see Part Two.) If an Auger line listed in Table XVI was detected both with and without acceleration, the average of the two energy measurements is given. In most of these cases the agreement between the two energy determinations is within 0.04 kev.

The observed approximate relative intensities are indicated by a code explained in a footnote to Table XVI. Since more lines were observed by means of the accelerating voltage than without, the intensities listed refer to a plate obtained with the voltage applied. These intensities represent only a visual impression of the line as it appears on the plate; they are not corrected for photographic efficiency or for geometry effects.

The calculated energies listed in Table XVI were obtained by the method outlined in Part One, Section III.B.9.a above, with the assumption that the effective charge increment, ΔZ, is unity. This assumption was made with good results by Sujkowski and Slätis[95] for calculating the energies of the L-Auger lines of bismuth.

The assignments of the L-Auger lines were made solely on the basis of energy agreement with the calculated values. Since a large number of Auger lines may fall within a narrow energy region and since the possible errors in the measured energies can be large in comparison with the

Table XV

Uranium K-Auger lines seen from the decay of Pa^{233}

Auger transition	Observed energy (kev)	ΔZ	Observed[a] intensities Z = 92 (% β decay)	Reported experimental relative intensities[b] Z = 83[c]	Z = 83[d]	Z = 80[e]	Z = 79[f]	Z = 79[g]	Theoretical[h] relative intensities Z ≅ 80
KL_IL_I	71.69 ± 0.10	0.58 ± 0.15	0.095	0.088	0.089	0.10	0.10	0.11	0.032
KL_IL_{II}	72.54 ± 0.10	0.54 ± 0.15	0.25	0.16	[0.16]	0.12	0.17	0.14	0.039
KL_IL_{III}	76.29 ± 0.16	0.84 ± 0.35	~0.093	0.096	0.12	0.07	0.12	0.093	0.074
$KL_{II}L_{II}$	-- --	-- --	--	<0.018	<0.018	0.02	0.03	0.044	0.0049
$KL_{II}L_{III}$	77.13 ± 0.13	0.80 ± 0.29	0.14	[0.14]	0.20	[0.14]	[0.14]	[0.14]	[0.14]
$KL_{III}L_{III}$	-- --	-- --	--	0.07	0.12	0.06	0.08	0.083	0.078
KL_IM_I	87.96 ± (~0.2)	1.68 ± (~1.1)		0.035					0.010
KL_IM_{II}	88.33 ± (~0.2)	1.78 ± (~1.1)		0.044					0.006
$KL_IM_{IV,V}$									0.0002
$KL_{II}M_{III}$	90.02 ± (~0.2)			0.061					0.030
$KL_{III}M_{I,II}$	92.95 ± 0.25								0.010
KM_IM_{III}?	105.6 ± (0.25)								

a. The brackets indicate the lines used to normalize the relative-intensity data from other workers for the purpose of comparison.

b. These intensities were obtained from spectrographic films in the same manner as for the conversion electron intensities.

c. Reference 92.

d. C. D. Ellis, Proc. Roy. Soc. (London) 139A, 336 (1933).

e. Reference 91.

f. J. W. Mihelich, Phys. Rev. 88, 415 (1952).

g. Nall, Baird, and Haynes, private communication to J. O. Rasmussen (Jan. 1960).

h. Reference 94.

Table XVI

Uranium L-Auger lines seen from the decay of Pa^{233}

Auger transition	Intensity[a] Bismuth Sujkowski and Slätis[b]	Intensity[a] Uranium This work	Energy (kev) Uranium, this work Observed	Energy (kev) Uranium, this work Calculated[c]
$L_I L_{III} M_V$	--	vw(b)	0.96	0.94
$L_{II} L_{III} N_I$	--	w	2.24	2.28
$L_{II} L_{III} N_{III}$	--	wm	2.64	2.70
$L_I N_{II} L_{III}$	--	w	2.83	2.88
$L_{II} L_{III} O_I$	--	w	3.48	3.44
$L_I L_{III} N_{III}$	--			3.52
$L_{II} L_{III} O_{II}$	--			3.52
$L_{II} L_{III} O_{IV}$	--	w(b)	3.71	3.68
$L_I L_{III} N_{IV}$	--			3.78
$L_{III} M_I M_{III}$	vw	vw(b)	7.17	7.18
$L_{III} M_{II} M_{III}$	w	?	7.47	7.55
$L_{III} M_I M_{IV}$	vw	?	7.71	7.76
$L_{III} M_I M_V$	vw	--	--	7.95
$L_{III} M_{II} M_V$	vw	?	8.22	8.32
$L_{III} M_{III} M_{III}$	w	w(b)	8.42	8.43
$L_{III} M_{II} M_{IV}$		--	--	8.13
$L_{III} M_{III} M_{IV}$	m	w(b)	8.98	9.01
$L_{III} M_{III} M_V$	m	w(b)	9.12	9.20
$L_{III} M_{IV} M_{IV}$	vw	--	--	9.59
$L_{III} M_{IV} M_V$	vs	m	9.72	9.78
$L_{III} M_V M_V$	s	wm	9.93	9.95
$L_{II} M_I M_{II}$	--	?	10.02	10.03
$L_I M_I M_I$	--	vw(b)	10.47	10.47
$L_{III} M_{II} N_I$	--			10.48
$L_{III} M_I N_V$	vw	vw(b)	10.88	10.83
$L_I M_I M_{II}$	--			10.85
$L_{III} M_{II} N_{III}$	--			10.90
$L_{II} M_I M_{III}$	vw			10.96

Table XVI (continued)

Auger transition	Intensity[a] Bismuth Sujkowski and Slätis[b]	Intensity[a] Uranium This work	Energy (kev) Uranium, this work Observed	Energy (kev) Uranium, this work Calculated[c]
$L_{II}M_{II}M_{III}$	w	(masked by 28-L_{III})		11.33
$L_{III}M_{I}O_{IV}$	--	vw	11.54	11.51
$L_{III}M_{III}N_{II}$	--			11.54
$L_{II}M_{I}M_{IV}$	--			11.54
$L_{III}M_{II}N_{VI,VII}$	w			11.57
$L_{III}M_{III}N_{III}$		--	--	11.78
$L_{I}M_{III}N_{VI,VII}$	vw	--	--	17.05
$L_{II}N_{IV}N_{IV,V}$	w	(masked by 40-L_{II})		19.34
$L_{II}N_{V}N_{V}$				19.42
$L_{II}M_{II}M_{IV}$	w	--	--	11.91
$L_{II}M_{II}M_{V}$	w	(masked by 17-M_{II})		12.10
$L_{I}M_{I}M_{IV}$	--	vvw	12.39	12.36
$L_{III}M_{IV}N_{III}$	--			12.36
$L_{III}M_{III}N_{VI}$	--			12.45
$L_{III}M_{III}O_{II}$	--	vvw	12.59	12.60
$L_{I}M_{II}M_{IV}$	vw	--	--	12.73
$L_{II}M_{III}M_{IV}$	m	wm(b)	12.80	12.79
$L_{III}M_{V}N_{IV}$	--			12.79
$L_{I}M_{II}M_{V}$	vw	(masked by 17-M_{III})		12.92
$L_{III}M_{IV}N_{VI,VII}$	vw	--	--	13.03
$L_{III}M_{IV}O_{II}$	--	vw	13.16	13.18
$L_{II}M_{V}N_{VI,VII}$	m			13.20
$L_{III}M_{IV}O_{IV}$	--	vw	13.34	13.34
$L_{II}M_{IV}M_{IV}$	m			13.37
$L_{II}M_{IV}M_{V}$	vs	wm	13.56	13.56
$L_{II}M_{V}M_{V}$	vw	--	--	13.73
$L_{II}M_{I}N_{III}$	--	w	14.32	14.31
$L_{I}M_{IV}M_{V}$	w			14.38

Table XVI (continued)

Auger transition	Intensity[a] Bismuth Sujkowski and Slätis[b]	Intensity[a] Uranium This work	Energy (kev) Uranium, this work Observed	Energy (kev) Uranium, this work Calculated[c]
$L_{II}M_{I}N_{V}$	w	vvw	14.67	14.61
$L_{II}M_{II}N_{III}$	--			14.68
$L_{II}M_{I}N_{VI,VII}$	w	?	14.98	14.98
$L_{II}M_{II}N_{V}$	--			14.98
$L_{III}N_{I}N_{VI,VII}$	w	vw	15.34	15.31
$L_{II}M_{III}N_{II}$	vw			15.32
$L_{I}M_{I}N_{IV}$	vw			15.39
$L_{III}N_{IV}N_{V}$	--	vvvw	15.60	15.60
$L_{II}M_{III}N_{IV}$	vw	(masked by 17-N_{I})		15.82
$L_{II}M_{V}N_{I}$	w	--	--	15.89
$L_{III}N_{II}N_{V}$		--	--	15.11
$L_{III}N_{VI}N_{VI}$	--	vvw	16.35	16.36
$L_{I}M_{II}O_{IV}$	--	??	16.48	16.48
$L_{II}M_{V}N_{IV}$	w	--	--	16.57
$L_{II}M_{IV}N_{VI,VII}$	w	--	--	16.81
$L_{III}N_{V}N_{VI,VII}$		--	--	16.01

a. The symbols used are w=weak, m=medium, s=strong, v=very, (b)=broad, and ?=questionable.

b. Reference 95.

c. These values were calculated by assuming a ΔZ of unity.

differences between the energies of the L-Auger lines, it is possible that errors in assignments have occurred. For comparison the intensities of L-Auger lines of bismuth reported by Sujkowski and Slätis[95] are also listed in Table XVI. The correspondence between the more intense lines of the bismuth and uranium spectra is obvious.

C. Curium-241

1. Introduction

The levels of Am^{241} have been studied previously from the electron-capture decay of Cm^{241} (35-day half life) by Glass,[17] and from the alpha decay of Bk^{245} (5-day half life) by Chetham-Strode,[96] Hulet et al.,[97] and Magnusson et al.[98] The studies of the alpha decay of Bk^{245} have assigned levels in Am^{241} at 42, 206, and approximately 480 kev. The Cm^{241} electron-capture decay has been observed to populate the approximately 480-kev level, which decays directly to the ground state. In addition to the electron-capture decay, Cm^{241} decays by approximately 1% alpha branch.[17]

The study presented here was undertaken to obtain detailed quantitative information about the Cm^{241} electron-capture decay scheme. This study is a joint project undertaken by Saadia Amiel, Frank Asaro, Charles J. Gallagher, and the author. By means of gamma-gamma coincidence techniques it was possible to obtain the desired information and to set limits on the precision of the data.

In this work the energy of the approximately 480-kev photon was determined to be 467 ± 3 kev. In addition, a photon of 640 ± 7 kev was observed and assigned to a level at 640 kev.

2. Experimental Techniques

The coincidence apparatus used is described in Section II.A. The source was prepared by evaporating the chemically purified curium (see Section II.C) onto a platinum disc.

3. Measurements and Results

Coincidence measurements were taken by using as gate pulses K x-rays, L x-rays, and the 467-kev gamma ray.[99] In addition, a number of "singles" spectra were taken. From the data obtained it is possible to determine a number of features of the decay of Cm^{241}. These determinations involve calculations which in some cases are complicated because of the presence of coincidences other than those being sought. Since each calculation is a separate problem it is thought best to discuss each individually. The equations governing each calculation are given and explained briefly. The photon spectrum in coincidence with K x-rays is shown in Fig. 7.

a. The Fraction of 467-kev Events in Coincidence With K-Capture Events

We desire to determine $\frac{K_{ec} : 467}{T : 467}$, the fraction of 467-kev events in coincidence with K-capture events. This determination is accomplished by recording the spectrum in coincidence with 467-kev photons. The desired coincidences are of the type (467-kev photon) - (K x-ray). The equation giving the desired fraction is

$$\frac{K_{ec} : 467}{T : 467} = \frac{T_{x\text{-}ray}}{T_g \cdot \ell \left(\frac{G_s}{1 - G_g \epsilon_x \cdot \frac{K_{ec} : 467}{T : 467} \cdot \ell} \right)} ,$$

where $T_{x\text{-}ray}$ = total K x-rays in the coincidence spectrum corrected for detector efficiency and background,

T_g = the total number of gates,

ℓ = the K-fluorescence yield for Z = 95,

G_s = the signal-detector geometry,

G_g = the gate-detector geometry,

ϵ_x = the counting efficiency for the gate detector for K x-rays.

The equation is almost self-explanatory: $\frac{K_{ec} : 467}{T : 467}$ is simply the total coincidence events over the total gates, corrected for fluorescent

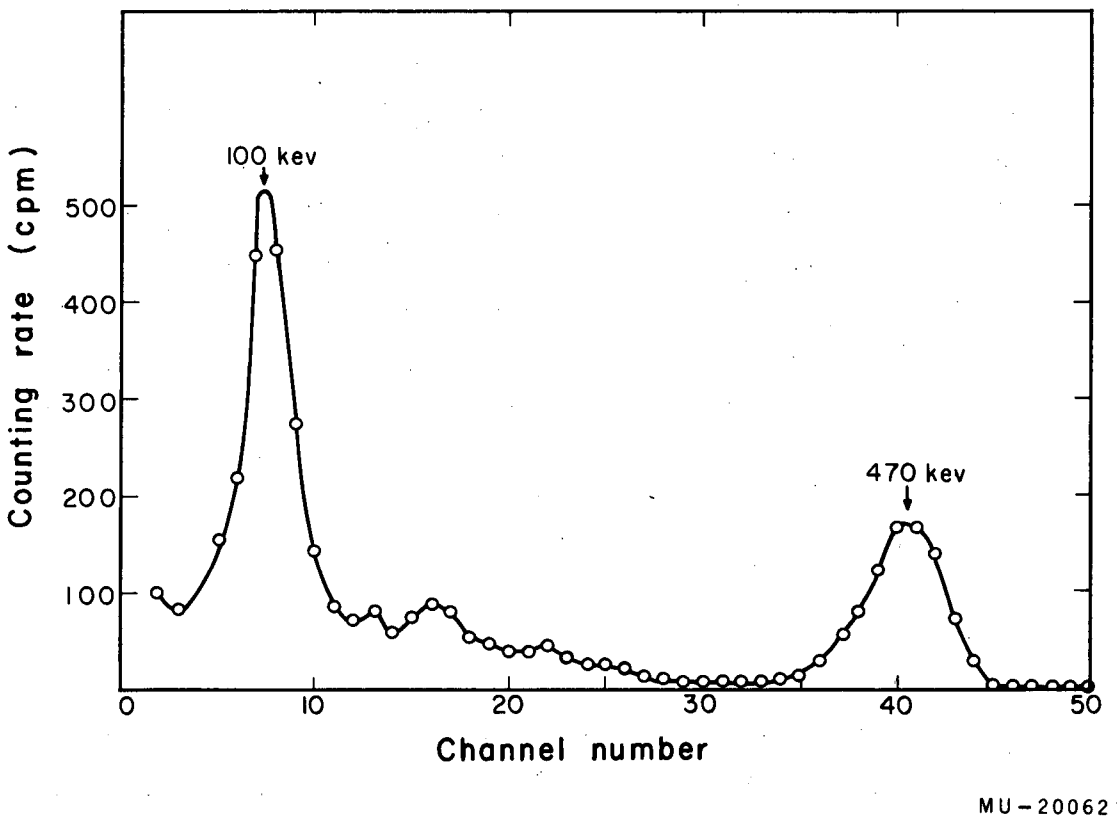

Fig. 7. Photon spectrum of Am^{241} in coincidence with K x-rays.

yield and for geometry effects. The geometry term

$$\frac{G_s}{\left(1 - G_g \; \epsilon_x \cdot \frac{K_{ec} : 467}{T : 467} \cdot \ell\right)}$$

used instead of the signal geometry, G_s, corrects the data for small gate losses from coincidence stack-up in the gate detector. The gate and signal geometries were measured by means of an Am^{241} standard of known disintegration rate. The 60-kev transition was recorded and the ratio of recorded counts to known total counts was taken as the geometry. (The Am^{241} standard was 5100 alpha dpm or 1840 60-kev gamma dpm.) The geometries used in this determination, which are typical of those of all the determinations, are $G_g = 0.077 \pm 0.03$ and $G_s = 0.112 \pm 0.015$.

The equation actually gives the number of 467-kev <u>photons</u> in coincidence with K-capture events; however, this fraction is the same for 467-kev events that are internally converted and, hence, for the total number of 467-kev events. This calculation does not distinguish those coincident events in which cascading gammas from higher levels (in coincidence with K-capture events) populate the 467-kev state. In the calculations to follow, the abundance of such transitions is assumed negligible. It is also assumed that the amount of 640-kev Compton tail in the 467-kev peak is negligible. It is to be noted that the fraction of 467-kev events in coincidence with K-capture <u>x-rays</u> is simply

$$\ell \cdot \frac{K_{ec} : 467}{T : 467} = \frac{K_x : 467}{T : 467} .$$

The most accurate values obtained for the two quantities are

$$\frac{K_{ec} : 467}{T : 467} = 0.67 \pm 0.10, \qquad \frac{K_x : 467}{T : 467} = 0.65 \pm 0.09.$$

A value of 0.965 was assumed for ℓ.[69]

The errors are deduced from the assigned errors of the experimental data by standard statistical methods, assuming all errors are standard deviations.

b. K-Conversion Coefficient of the 467-kev Transition

The K-conversion coefficient of the 467-kev transition, α_K, was determined from the spectrum in coincidence with K x-rays. The desired coincidence events are between the K-capture x-rays and the 467-kev photons, and between the K-capture x-rays and the K-conversion x-rays. In addition to these events there are unwanted coincidences between 467-kev Compton events that are of the correct energy to activate the gate signal and K-capture x-rays, as well as between K-capture x-ray gates and K-conversion x-rays. If it were not for these unwanted coincidences, α_K would be given by the total K x-rays in the coincidence spectrum over the total 467-kev photons in the coincidence spectrum times $1/\ell$. The $1/\ell$ term corrects for K-conversion events which are not accompanied by K x-rays. Since both types of unwanted coincidences produce additional K x-rays in the coincidence spectrum, the true α_K is obtained by introducing correction factors, which reduce the ratio K x-rays/gamma rays. The complete equation for the calculation is

$$\alpha_K = \frac{T_{x\text{-}ray} - T_g R_{comp} G_s \frac{K_x : 467}{T : 467}}{2 T_\gamma \cdot \ell}$$

where the terms not defined previously are

T_γ = total 467-kev photons in the coincidence spectrum corrected for detector efficiency and background,

R_{comp} = the ratio of 467-kev Compton events to total gates in the gate spectrum corrected for gate losses due to coincidence stack-up.

The negative term in the numerator is the number of unwanted K x-rays in the coincidence spectrum produced by Compton gates. The factor 2 is in the denominator because there are just as many coincidences between K-conversion x-ray gates and K-capture x-rays as between K-capture x-ray gates and K-conversion x-rays. The results of several determinations show $\alpha_K = 0.15 \pm 0.01$.

c. Fraction of K Capture to 467-kev Level

This determination is also accomplished by recording the spectrum in coincidence with K x-rays. The number of 467-kev photons recorded in the coincidence spectrum depends upon a number of factors, one of these factors being y, the fraction of K capture which populates the 467-kev level. The number of recorded 467-kev photons also depends upon the total number of K x-ray gates, the fraction c of these gates that are K-capture x-ray gates, and the fraction of the 467-kev events that are photons. This latter fraction is $1/\alpha+1$, where α is the total conversion coefficient of the 467-kev state. The method by which α is determined from the measured value of α_K is described below.

In the calculation two terms are unknown, c and y; hence it is necessary to set up and solve simultaneously two equations in these unknowns. The equations used are

$$\frac{T_x \cdot c \cdot y}{\frac{K_x : 467}{T : 467}} \cdot \frac{\alpha_K}{\alpha + 1} \cdot \ell = T_x \quad (1 - c), \tag{1}$$

$$y \cdot c \cdot \frac{1}{\alpha + 1} \quad T_g \quad \frac{G_s}{1 - G_g \epsilon_\gamma} = T_\gamma , \tag{2}$$

where ϵ_γ is the efficiency of the gate detector for 467-kev photons.

Equation (1) equates the number of K-conversion x-rays expected in an x-ray "singles" peak of total events T_x as computed by two different means. The left-hand side gives the number of K-conversion x-rays expected from the number, $T_x \cdot c$, of K-capture x-ray events taking place; and the right-hand side is the number of K-conversion x-rays computed directly ($1 - c$ is the fraction of the x-rays that are K-conversion x-rays).

The second equation relates the number of 467-kev events (T_γ) recorded in the coincidence spectrum to the number expected from the total number of gates T_g. Appearing on the left is a geometry term similar to the one used previously (Section III.C.1.a) except that

ϵ_γ replaces ϵ_x, since it is 467-kev photons that are now capable of producing stack-up in the gate crystal. The exact geometry term is more complicated than that used here;[100] however, for the geometries employed $G_s/1-G_g\epsilon_\gamma$ is accurate to approximately 1%.

The results of this determination are

$$c = 0.86 \pm 0.17,$$

$$1 - c = 0.14 \pm 0.17,$$

$$y = 1.00 \begin{matrix} +0.00 \\ -0.20 \end{matrix} .$$

The calculation gives a value of $y = 1.09 \pm 0.29$; however, since y cannot exceed 1.00, the value has been recorded as $y = 1.00 \begin{matrix} +0.00 \\ -0.20 \end{matrix}$.

d. Multipolarity of the 467-kev Transition and Total Conversion Coefficient

The multipolarity of the 467-kev transition was determined from the measured value of α_K and from the theoretical conversion coefficients of Rose.[28] The transition was found to be 37% M1 and 63% E2. The total conversion coefficient was determined as the sum of the theoretical K-, L-, M-, etc. conversion coefficients for a transition of this multipole admixture. The contribution of shells higher than M was approximated by assuming that the conversion coefficients decrease as the inverse cube of the principal quantum number.[101] The result is $\alpha = 0.24 \pm 0.02$.

e. Ratio of Total 640-kev Photons to Total 467-kev Photons

This ratio, T : 640/T : 467, was obtained directly from the singles spectrum by integrating the counts under the photon peaks, correcting for counting efficiencies, and forming the ratio. The value determined is $\frac{T : 640}{T : 467} = 0.036 \pm 0.002$.

f. Ratio of 640-kev Photons in Coincidence with K x-rays to 467-kev Photons in Coincidence with K x-rays

This ratio, K_x : 640/K_x : 467, was obtained by integrating the counts under the photon peaks in the spectrum in coincidence with K x-rays and correcting for counting efficiencies. The result is

$$\frac{K_x : 640}{K_x : 467} = 0.0021 \pm 0.0002.$$

g. Ratio of 640-kev Photons in Coincidence with K x-rays to Total 640-kev Photons

This ratio is given by the equation

$$\frac{K_x : 640}{T : 640} = \frac{K_x : 640}{K_x : 467} \cdot \frac{K_x : 467}{T : 467} \cdot \frac{T : 467}{T : 640} .$$

Substituting the quantities as determined above gives

$$\frac{K_x : 640}{T : 640} = 0.038 \pm 0.01 .$$

By dividing this quantity by the fluorescent yield one obtains the fraction of 640-kev events in coincidence with K-capture events, thus:

$$\frac{K_{ec} : 640}{T : 640} = \frac{K_x : 640}{T : 640} \times \frac{1}{\ell} = 0.039 \pm 0.01.$$

h. Ratio of 640-kev Photons in Coincidence with L x-rays to 467-kev Photons in Coincidence with L x-rays

This determination was made by looking at the spectrum in coincidence with L x-rays. The photon peaks were integrated as in the determination of $\frac{K_x : 640}{K_x : 467}$. The result is

$$\frac{L_x : 640}{L_x : 467} = 0.029 \begin{array}{l} +\ 0.001 \\ -\ 0.006 \end{array} .$$

Note that these L x-ray—gamma coincidences arise not only from capture in the L shell but also from K-capture events, which emit L x-rays during the rearrangement of the atomic electrons.

It must also be mentioned that this value has not been corrected for losses in the 467-kev peak due to losses of L x-ray gates. These gate losses can occur when a K-capture event produces simultaneously a K x-ray, an L x-ray, and a 467-kev gamma ray. If both the K x-ray and L x-ray record in the gate detector, the L x-ray gate is lost. Losses

of this nature are of much less importance with the 640-kev transition, for which the fraction of K capture is quite small. It can be shown that the ratio of the 467-kev coincidence counts lost by this means to the total that would be recorded if no losses were present is $\approx 2/3\ G_g$. Unfortunately, the geometry used in making this measurement is unknown; hence the data cannot be corrected for the losses. If a small gate geometry was used, the correction is negligible; however, for large G_g the correction could be as great as approximately 25%. This uncertainty is the reason for the large limit of error placed upon $\frac{L_x : 640}{L_x : 467}$.

i. Ratio of L Capture to K Capture for 467-kev and 640-kev States

The ratios $L_{ec} : 467/K_{ec} : 467$ and $L_{ec} : 640/K_{ec} : 640$ were determined from the values of $K_{ec} : 467/\ T : 467$ and $K_{ec} : 640/T : 640$ and the ratio of L capture to capture from higher shells. Nijgh et al.[69] give the ratio of capture in the X shell (X = M, N, $\cdots$) to that in the L shell as

$$\epsilon_x/\epsilon_L \cong \frac{2^3}{n^3}\left(\frac{Z - Z_x}{Z - Z_L}\right)^3 ,$$

where n and Z_x are the principal quantum numbers and the Slater screening constants, respectively, for the X shell. These authors tabulate values of $\epsilon_m + \epsilon_n + \cdots/\epsilon_L$ as computed from this equation. For Z = 96, $\epsilon_m + \epsilon_n + \cdots/\epsilon_L = 0.294$, which leads to the result that 77% of the electron capture that is not K capture is L capture. The ratios K_{ec}/T given above for the two levels can be used, therefore, to determine the ratios L_{ec}/T and hence the ratios of L capture to K capture. The results are

$$\frac{L_{ec} : 467}{K_{ec} : 467} = 0.38 \pm 0.13, \qquad \frac{L_{ec} : 640}{K_{ec} : 640} = 19 \pm 5.$$

It should be mentioned that the L_{ec}/K_{ec} ratio of the 640-kev level was also calculated in another (probably less accurate) manner.

This method utilizes (L x-ray) – (gamma) coincidence spectra. The equations used are

$$\frac{L_x : 640}{L_x : 467} = \frac{L_x : 640}{T : 640} \times \frac{T : 640}{T : 467} \times \frac{T : 467}{L_x : 467} ,$$

$$\frac{L_x : 640}{T : 640} = \left[\frac{L_{ec} : 640}{T : 640} + \frac{K_{ec} : 640}{T : 640} \chi \right] \ell_L$$

(and similarly for the 467-kev transition), where χ is the number of K vacancies filled by L vacancies, and ℓ_L is the fluorescence yield in the L shell. A value of $\chi = 0.77$ was obtained from the book by Nijgh et al.[69] The values of ℓ_L need not be known for calculating the final result, since ℓ_L cancels out when the equations are combined. Assuming the value of $L_{ec} : 467/K_{ec} : 467 = 0.38 \pm 0.13$, as determined above, and substituting other experimentally determined quantities leads to $L_{ec} : 640/T : 640 = 0.59 \pm 0.16$ and $L_{ec} : 640/K_{ec} : 640 = 15 \pm 5$, in agreement with the value determined above.

It should be noted that this agreement between the values of $L_{ec} : 640/K_{ec} : 640$ as computed by two different means is evidence that the 640-kev photon proceeds to the ground state and not to a low-energy excited state. If the photon did populate an excited state, there would be coincidences between the photon and L x-rays arising from the conversion in the depopulation of the low energy state. If such coincidences were present the value of $L_{ec} : 640/K : 640$ as calculated by the second method above would be larger than that given by the first method. Actually the opposite is true.

j. Total Electron-Capture Disintegration Energy of Cm^{241}

The total electron-capture disintegration energy of Cm^{241} was determined from a graph presented by Brysk and Rose,[102] which relates the nuclear energy difference to the ratio of L_I capture to K capture for allowed transitions. The electron-capture decays to the 467- and 640-kev levels are thought to be first forbidden ($\Delta I = 1$, yes) transitions (see below); however, Hoff and Rasmussen have reported that the

L/K ratio for $\Delta I = 1$, yes type transitions are generally the same as for allowed transitions of the same energy.[103] We have assumed that such is the case in the Cm^{241} decay.

The L/K ratios for the decay were determined from the experimental L/K ratios given above and the theoretical L_{II}/L_I ratios given by Brysk and Rose.[102] For allowed and first-forbidden transitions the L_{III}-shell contribution to electron capture is negligible. The total disintegration energy is $Q_o = W_o + E + 1$, in units of mc^2, where W_o is the nuclear energy difference as given by the graph of Brysk and Rose,[102] E is the energy of the level populated in the daughter nucleus, and 1 is the equivalent rest-mass energy of an electron.

The most accurate value of Q_o was obtained with the data for decay to the 640-kev level, because for large values of L_I/K the value of W_o is quite insensitive to small changes in the ratio of L_I/K. For $L_{ec} : 640/K_{ec} : 640 = 19 \pm 5$, $L_I/K = 17 \pm 4$, $W_o = -370$ kev, $Q_o = 781 \pm 7$ kev.

The error in Q_o resulting from the error in L_I/K is negligible. The error limit quoted is due to the possible error in E_{640} (see Section III.C.1.ℓ below).

The value of Q_o determined from the L/K ratio of 0.38 ± 0.13 for decay to the 467-kev level is $850 \begin{smallmatrix}+380\\-75\end{smallmatrix}$-kev.

k. Log ft Values

Electron-capture f values for allowed transitions are given by[102,104]

$$f = \pi/4\ [n_K\ g^2_K\ q^2_K + n_{L_I}\ g^2_{L_I}\ q^2_{L_I} + n_{L_{II}}\ f^2_{L_{II}}\ q^2_{L_{II}}],$$

where

n_i = the number of electrons in the ith shell available for capture,

g_i and f_i = the "large" and "small" component Dirac radial wave functions of the ith shell,

q_i = the neutrino energy for capture from the ith shell.

For Cm, $n_K = n_{L_I} = n_{L_{II}} = 2$; hence

$$f = \pi/2\ [g^2_K\ q^2_K + g^2_{L_I}\ q^2_{L_I} + f^2_{L_{II}}\ q^2_{L_{II}}].$$

Brysk and Rose[102] have published graphs of g_i and f_i as functions of Z for i = K, L_I, L_{II}, and L_{III}. For Z = 96, we have $g_K = 3.6$, $g_{L_I} = 1.5$ and $F_{L_{II}} = -0.53$. These values, with the decay energies determined above, have been used to calculate the f values for the decay to the 467- and 640-kev levels. The results are

$$f_{467} = 4.02 \qquad \text{and} \qquad f_{640} = 0.223.$$

The ft value is the product of the f value and the partial half life (in seconds) for the branch of decay under consideration. In this work the percent populations of the 467- and 640-kev states were not determined directly; however, the values are assumed to be approximately 96% and approximately 4%, respectively. The assumption is that the populations of the two levels are in the same ratio as the intensities of the photons depopulating them. (It is known experimentally that there is negligible decay to levels other than the 467- and 640-kev ones; hence the sum of the populations of the 467- and 640-kev levels must be approximately 100%.) The assumption is valid only if the conversion coefficients of the two transitions are equal and if no transition proceeds from the 640- to the 467-kev level. The 640-kev transition is most likely an M1 or M1-E2 mixture, as is the 467-kev transition; hence the first condition is approximately satisfied.

From the photon spectrum in coincidence with the 467-kev gamma ray it was possible to set an upper limit on the photon intensity of a transition (≈ 173 kev) between the 640- and 467-kev levels. This upper limit was determined to be approximately equal to the photon intensity of the 640-kev transition. If such a transition does take place with this intensity, then the percent error in the assumed population of the 467-kev level is small; however, the estimated population of the 640-kev level (4%) would be too small by a factor of approximately two.

The total half life of Cm^{241} is 35 days and, approximately 99% of the decay is electron capture. If the populations of the 467- and 640-kev levels are 96% and 4% of the electron capture, respectively, the partial half lives are $t_{467} = 3.18 \times 10^6$ seconds and $t_{640} = 7.65 \times 10^7$ seconds. It follows that $(\log ft)_{467} \cong 7.11$ and $(\log ft)_{640} \leqq 7.2$. The value of 7.2 is the upper limit of $(\log ft)_{640}$, because a lower limit was assumed for the percent population of this level. If the population were twice the value assumed (8% instead of 4%) the log ft would be calculated as 6.93.

Hoff and Rasmussen have reported that it is permissible to calculate ft values for $\Delta I = 1$, yes electron capture using an allowed f to compare with ft values for $\Delta I = 1$, yes beta minus decay calculated with an allowed f.[103] As pointed out by Hoff and Rasmussen, this leads to the conclusion that $\Delta I = 1$, yes electron capture decay should have log ft values around 7.5, since the correlation by King and Peaslee shows the log ft values of $\Delta I = 1$, yes beta minus transitions are around 7.5.[85] It is not unlikely, therefore, that in the electron capture of Cm^{241} the transitions to the 640- and 467-kev levels are of the type $\Delta I = 1$, yes; however, on the basis of log ft values alone one cannot rule out the possibilities that the transitions may be hindered allowed or $\Delta I = 0$, yes.

ℓ. Energies of Gamma Transitions

Energies of 467 ± 3 and 640 ± 7 kev for the two observed gamma transitions in Am^{241} were determined from the scintillation spectra. Na^{22}, Cs^{137}, and Hg^{203} were used as energy calibration standards. The limits of errors are based upon estimates of the precision with which the positions of the gamma-ray peaks on the graph of the spectrum could be determined.

The gamma-ray energy of 467 ± 3 kev reported here is to be compared with values of 470 ± 10 kev reported by Glass[17] from the electron capture of Cm^{241} and 480 ± 5 kev reported by Chetham-Strode[96] from the alpha decay of Bk^{245}.

When lead absorbers were used in this work to reduce the simultaneous counting of 467-kev photons and K x-rays in the same detector, no photon peak as reported by Glass[17] was observed at 592 kev. Hence we

agree with the suggestion of Chetham-Strode[96] that the peak reported at 592 kev was most likely a sum peak of 467-kev photons and K x-rays.

4. Discussion of Results

Information on the electron-capture decay of Cm^{241} is summarized in Fig. 8. The quantum assignments shown have already been discussed in regard to the data presented here.[83]

The ground-state spin of Am^{241} has been measured as 5/2.[105,106] The Nilsson assignment of 5/2 - [523] was made from a study of the alpha decay to Np^{237}.[107] The 1/2 + [631] assignment of the ground state of Cm^{241} was made by Stephens et al. on the basis that the favored alpha decay of Cm^{241} populates this same state in Pu^{237}.[108]

The M1-E2 character of the 467-kev transition along with the 5/2- assignment of the ground state fixes the parity of the 467-kev level as odd and the spin as 3/2, 5/2, or 7/2. If the ground state of Cm^{241} is 1/2 +, as assigned, then the log ft of 7.11 for electron capture to the 467-kev level allows only the choice 3/2- for this level. The two most reasonable choices of Nilsson assignments for this state are 1/2 - [530] (3/2- member lying lowest) and 3/2 - [521]. Stephens et al. prefer the former assignment,[83] whereas Mottelson and Nilsson prefer the latter.[89]

The log ft of 7.2 for decay to the 640-kev level indicates a $\Delta I = 1$, yes, a hindered allowed, or a $\Delta I = 0$, yes transition; thus the spin of this level is either 1/2 or 3/2 with either even or odd parity. The Nilsson states available are 3/2- [521], 3/2+ [651], and 1/2- [530].

If the 1/2- [530] state is assigned to the 467-kev level, the choice is restricted to the 3/2- or 3/2+ state. Stephens et al. prefer the assignment 3/2 - [521] because no transition from this level to the 5/2+ state at 206-kev has been observed.[83] (The 206-kev state that is populated in the alpha decay of Bk^{245} has been assigned as 5/2+ [642].) The log ft of ≤ 7.2 determined in this work is consistent with either assignment since the choice 3/2- [521] indicates a $\Delta I = 1$, yes transition (log ft $\cong 7.5$), and the choice 3/2+ [651] indicates a hindered-allowed transition ($\Delta n_z = 2$).

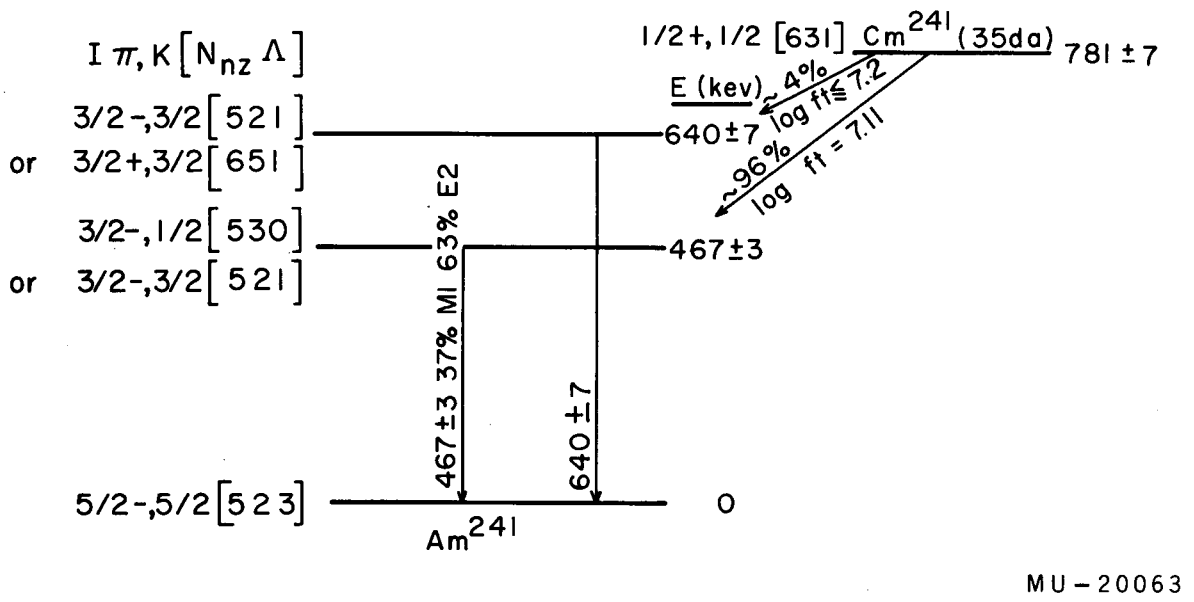

Fig. 8. The electron capture decay of Cm^{241}.

The total decay energy determined here as 781 ± 7 kev is to be compared with the value of 0.80 Mev calculated by Foreman and Seaborg from closed cycles.[109]

IV. CONCLUSION

In the work discussed here detailed experimental information of the nuclear decays of some heaviest element nuclides was obtained and analyzed with respect to the unified model of Bohr and Mottelson. The reasonably close correlation between the experimental data and theoretical predictions is evidence for the usefulness of the unified model in describing the dynamical aspects of nuclear structure in this region of the periodic table. That agreement between experiment and theory was not always obtained and that in some cases this lack of agreement cannot be explained by experimental errors points up the need for further theoretical development and illustrates the increasing importance of detailed empirical data.

Part Two

AN ACCELERATING ELECTRON SPECTROGRAPH

I. INTRODUCTION

The difficulties associated with accurate measurements of the energies and intensities of low-energy electrons is a major problem in nuclear spectroscopy. In beta spectrometers low-energy electrons are absorbed by counter windows and by the mass of the source itself. This absorption makes detection of such electrons difficult or impossible and -- at least -- makes necessary the application of absorption corrections, which can be quite large. Failure to recognize the importance and magnitude of such corrections created many problems for the early spectroscopists when they attempted to analyze their data.

The use of spectrographs employing photographic film as a detector is hampered by the poor detection efficiency of emulsions for low-energy electrons. A plot[110] of the efficiency vs electron energy is shown in Fig. 9. Note how rapidly the efficiency drops off at energies less than approximately 40 kev.

Since a great deal of basic information can be obtained from beta spectra, conversion-electron spectra, and Auger-electron spectra in the low-energy region, it is only natural that considerable work has been done to improve the means of observing low-energy electrons. This work has been directed at improving the techniques of source preparation and toward increasing the efficiency of detectors. In the latter case, for example, techniques are now available for producing counter windows of thickness 10 $\mu g/cm^2$ or less.[111] In addition, effort has been directed toward artifically accelerating low-energy electrons to energies at which detection and measurement are easier. This method has been employed in both spectrometers and spectrographs.

Accelerating spectrometers and spectrographs employ an electrostatic field incident across a slit system or grid system through which the electrons pass. If the acceleration takes place before the electrons are resolved in energy the technique is called preacceleration; if after the energy resolution, postacceleration.

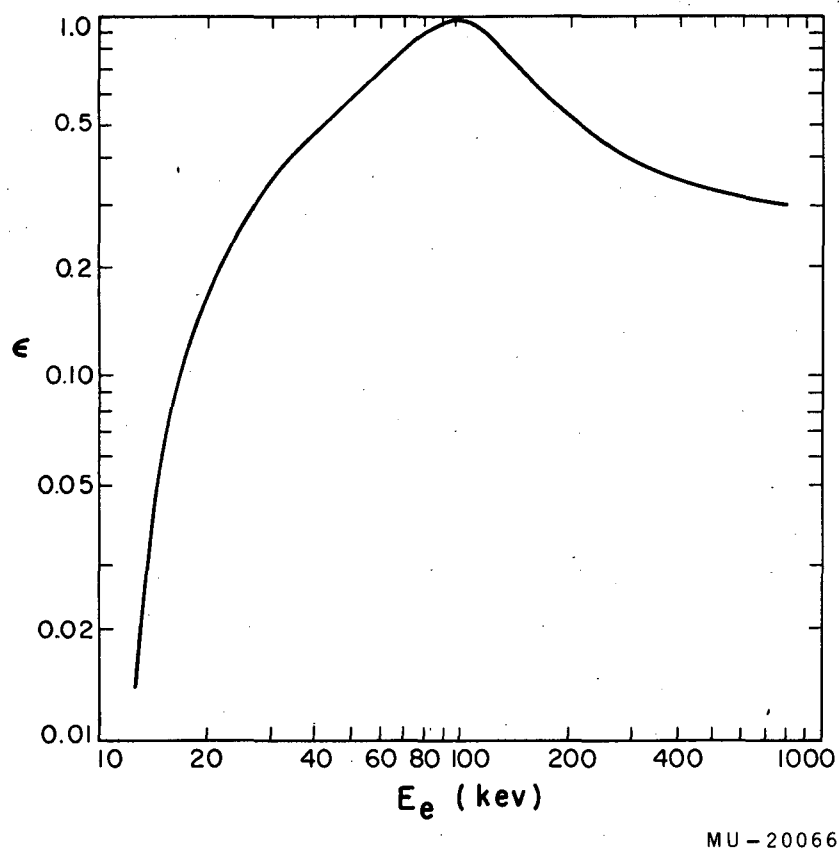

Fig. 9. The efficiency of Eastman Kodak (No Screen) x-ray film.

A number of workers have used the accelerating technique in beta spectrometers to improve the counting efficiencies of low-energy electrons.[112] Rosenblum, Sant'Anna Dionisio, and Valadares[113] and Delesalle[114] have adopted the techniques to photographic recording spectrographs. It was the reports of these French workers that inspired the undertakings described here.

Since permanent-magnet spectrographs are used extensively by the nuclear spectroscopy group at this Laboratory, it was thought worth while to determine the potentialities of an accelerating spectrograph. It was also of interest to attempt the use of a radial electrostatic accelerating field rather than the uniform parallel field employed in spectrographs by the previous workers. It was decided that initially an existing conventional spectrograph would be modified to the accelerating type so that information could be obtained from its performance which would be helpful in designing a completely new instrument. The camera of the spectrograph was modified so that it could be employed as either a pre- or postaccelerator type. Both types of acceleration proved successful; however, the preaccelerator proved to be the more useful device. Since the camera was designed to fit into a narrow opening between the pole faces of the magnets, and hence is only approximately one inch high, it was difficult to insulate the high voltages employed. These difficulties were harder to overcome for the postacceleration method because of the more complex instrumentation involved. By means of the preaccelerator it was possible to detect and measure the energies of electron lines of less than 1 kev. With the conventional spectrographs at this Laboratory it is virtually impossible to detect lines of energies less than approximately 7 kev.

II. THE INSTRUMENT

A. Vacuum Chamber and System

Over-all views of the spectrograph are shown in Figs. 10 and 11. Figure 10 shows the camera in place, Fig. 11 shows the vacuum chamber with the rubber O-ring seal. Immediately above and below the vacuum chamber are the permanent magnets; these produce a field of approximately 50 gauss. The vacuum chamber and magnets are enclosed by the yoke of the magnet. A description of the magnets and vacuum chamber are given by Smith.[6]

The vacuum system consists of a mechanical roughing and forepump (immediately below the spectrograph), a fractionating oil diffusion pump (Consolidated Electrodynamics, Model MCF-300), a liquid nitrogen trap, and a dry ice—alcohol trap. The white tank and hose in Figs. 10 and 11 are part of the liquid nitrogen system, which automatically fills the cold trap. The pipes to the left of the spectrograph that are wrapped in heavy black insulation are part of the chilled-water cooling system for the diffusion pump.

The glass tube behind and above the system is an ion gauge for pressure measurements. Since this tube is incandescent when operating and since the camera containing the photographic film must be kept dark, it was necessary to connect this tube to the system by means of a connection containing a number of light baffles. The vacuum system is made of nonmagnetic stainless steel.

With this system it was possible to obtain pressure readings on the ion gauge of 4×10^{-6} mm Hg. Since these readings were taken at the back part of the spectrograph and through a system of light baffles, it is impossible to say what pressures were obtained within the camera itself. In order to insure that minimum pressure would be achieved, the lid designed to cover the camera was left off; however, there were a number of places within the camera in which air could be trapped.

It is true that the conventional spectrographs can be successfully operated at pressures as high as 10^{-2} mm Hg; however, the lower pressure

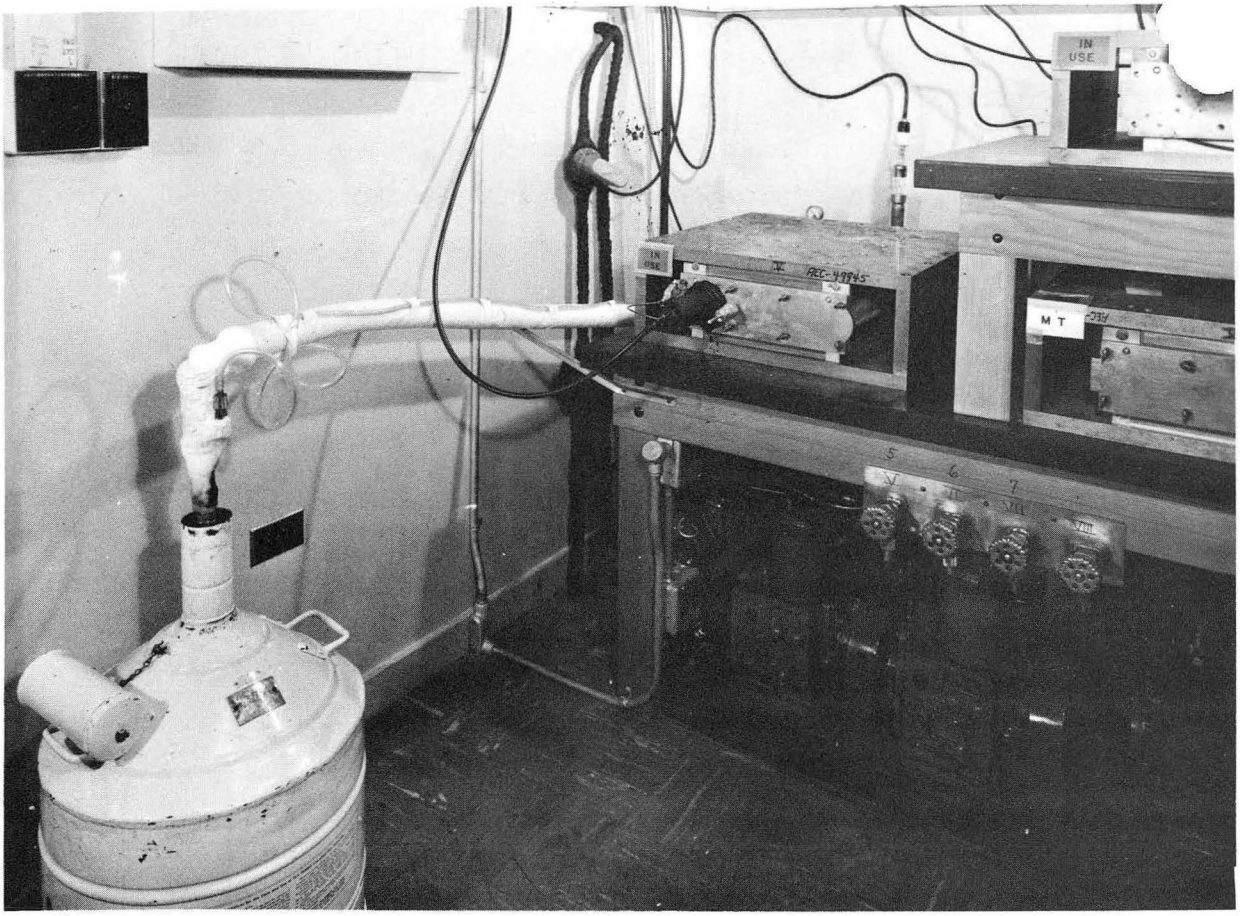

ZN-2409

Fig. 10. Accelerator spectrograph – camera in position.

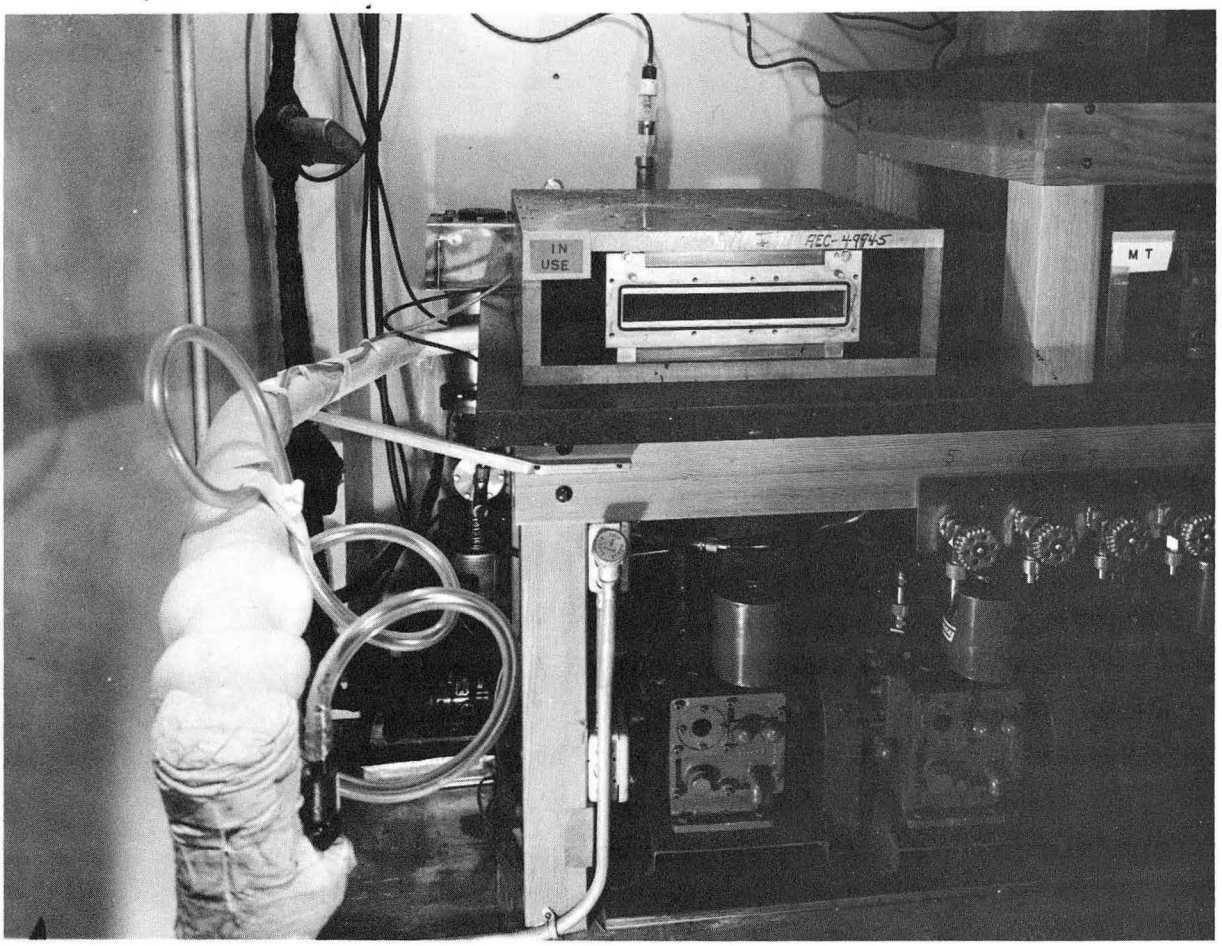

ZN-2410

Fig. 11. Accelerator spectrograph — camera removed.

is required in the accelerating spectrograph in order to avoid arcing of the high voltage. In order to maintain voltages of from 3 to 20 kv within the small space available, it was necessary to obtain pressures lower than 10^{-5} mm Hg. With the pressures obtainable the equipment could be run successfully at the desired potentials. When, on occasion, the high voltage did produce an arc the photographic film was blackened by the light.

B. The Camera

An over-all view of the camera is shown in Fig. 12. This camera is a modification of the instruments built by Smith and Hillander.[20] The picture shows the camera with both the pre- and postaccelerators attached and with the source in position. The source and slit system are located in the upper left portion of the camera. Figure 13 is a close-up of this section.

The "source" is a 10-mil platinum wire mounted in narrow positioning grooves of an aluminum source holder by means of small brass screws and washers. The aluminum source holder fits into the milled slot of a lucite mount and is held in place with a metal set screw. The set screw serves as the electrical contact for the preaccelerator voltage. The lucite mount, which electrically insulates the source holder from the rest of the camera, is slotted around its periphery near the source holder in order to increase the electrical leakage path length along its surface.

The high voltage is brought into the camera by means of a Kovar seal mounted in the brass faceplate. When the camera is operating as a preaccelerator, this voltage is negative with respect to ground. A small metal spring, attached between the Kovar and the source-holder set screw, carries the potential to the source holder. With the source at a negative potential relative to the rest of the camera, the acceleration takes place between the source and the slit system. This slit system is circular, with the center located at the source so that an approximately radial field will be produced. Previous workers have not employed this arrangement, but have produced accelerating fields between parallel plates. The slit is

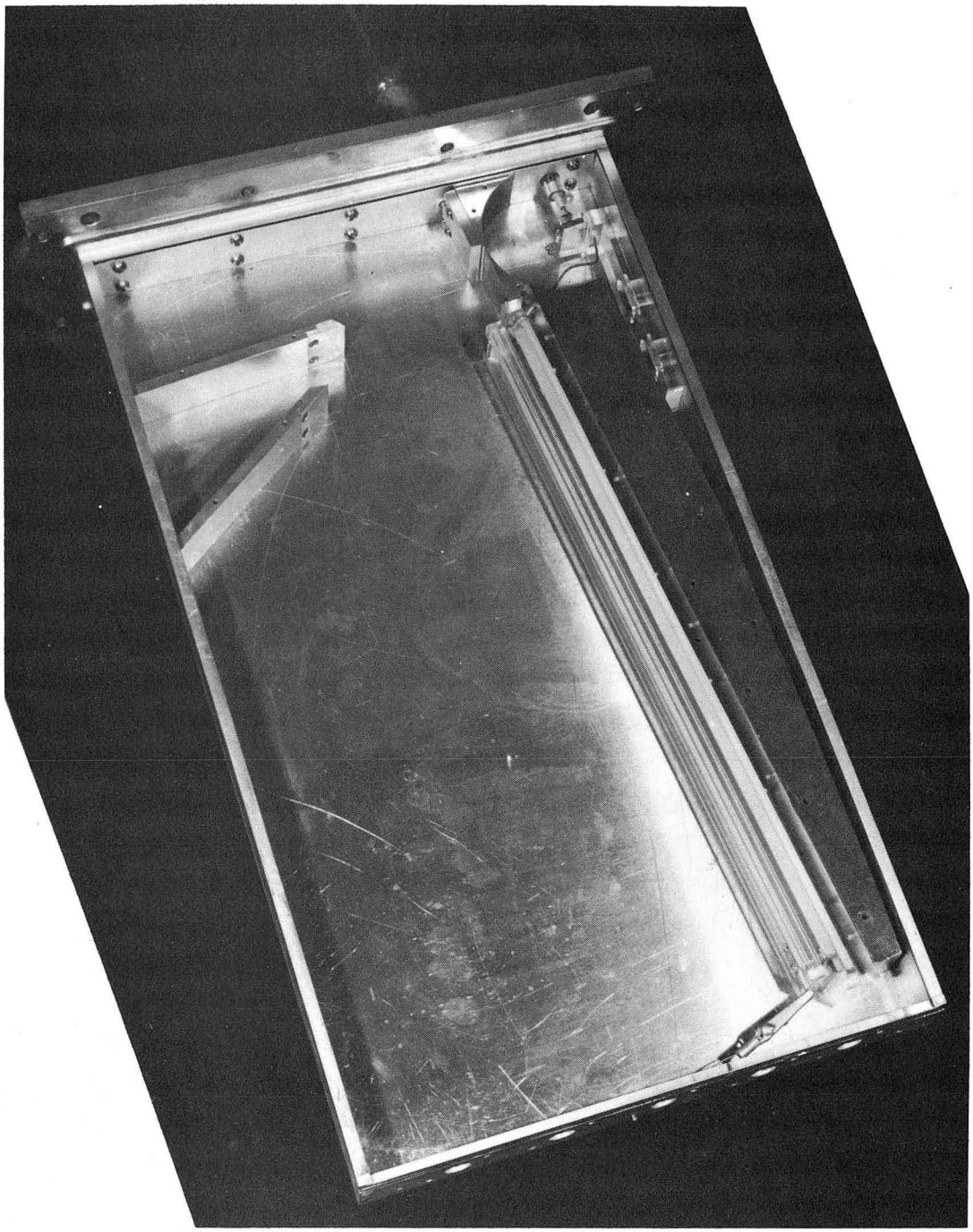

ZN-2411

Fig. 12. Accelerator spectrograph camera — over-all view.

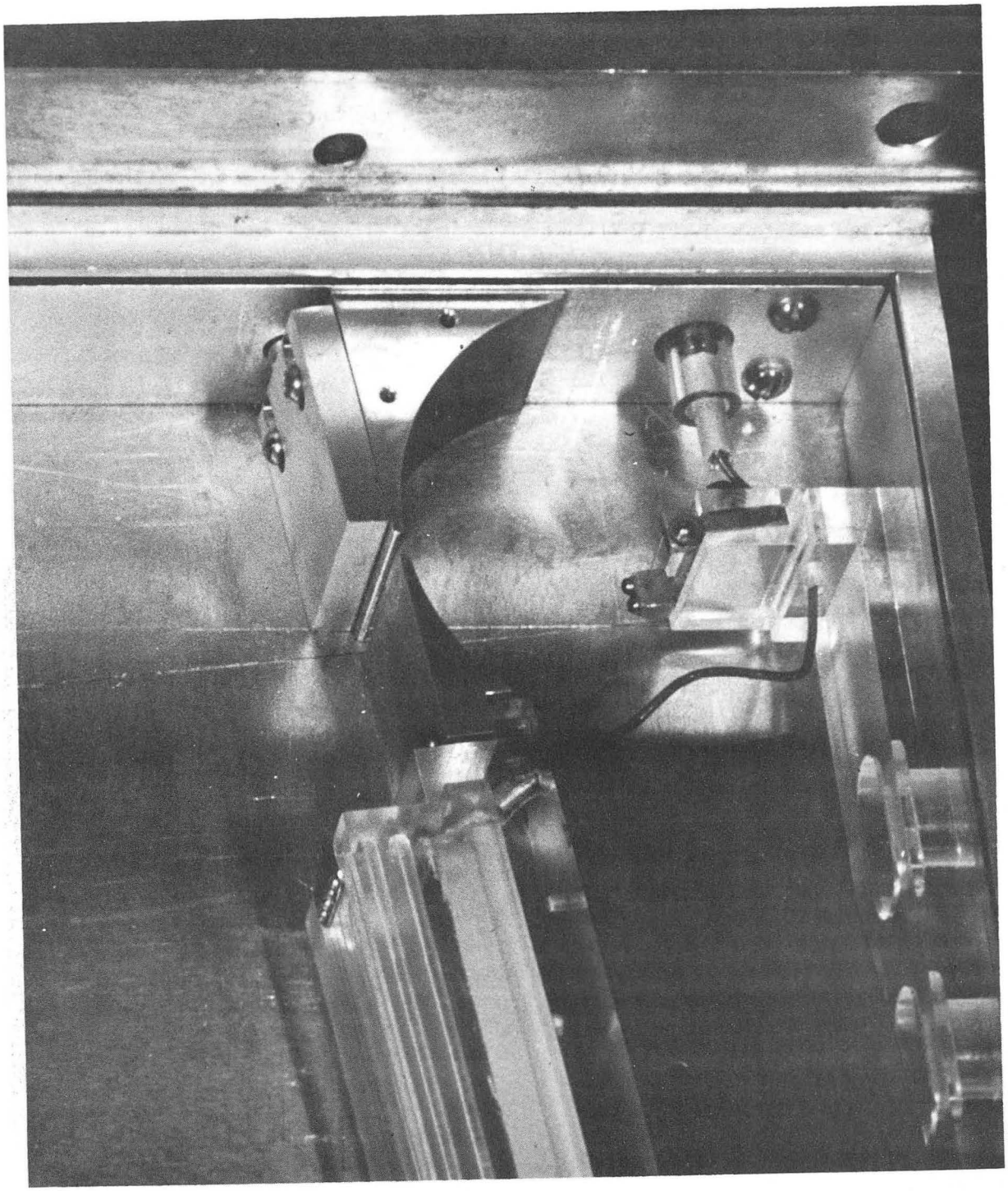

ZN-2412

Fig. 13. Accelerator spectrograph camera — source and slit system.

fitted with a sliding shutter which is kept closed until the system is brought down to vacuum and the voltage has stabilized. This shutter is operated manually through a vacuumtight Wilson seal.

In Fig. 12 the long dark bar across the upper edge of the camera is a lead shield which absorbs gamma radiation from the source. The film is held in a film holder which is positioned by a lucite mount attached to the lower edge of the lead shield. In this picture the postaccelerator film-holder mechanism is in place.

Figure 14 is a close-up of the film holders used in the camera. From top to bottom the pieces shown are: (a) lucite backing plate for postaccelerator film holder, (b) photographic film, (c) lucite postaccelerator film holder with metal grid system, (d) aluminum preaccelerator film-holder plate, (e) aluminum preaccelerator backing plate. The film holder used with the preaccelerator is the same as those used in the conventional spectrographs at this Laboratory. The notches on this piece produce notches in the background on the plate, and these serve as calibration marks. The film is held in place in the film holder by the backing plate, which sets firmly behind it. The film holder slips into the lucite slotted mount on the lead shield assembly.

The postaccelerator system accelerates electrons between the two grid networks of the film holder. Each grid network consists of four tungsten wires (0.002 inch in diameter) mounted lengthwise on the lucite holder. Small springs produce a tension to keep the wires rigid. The grids furthest from the film (the first ones the electrons see as they enter the system) are maintained at ground potential by electrical contact with the camera wall. This contact is established by means of an alligator clip which is attached to the grid network after the holder is mounted in the camera. The clip can be seen to the right in Fig. 12.

The grid network closest to the film is held at a positive potential. This potential enters the system by means of a small attachment located in the base of the holder and attached to the second grid. The attachment is the male portion of an electrical connection; the female portion attaches to a wire which passes through a hole in the lead shield and source-holder mount. When the postaccelerator is operating

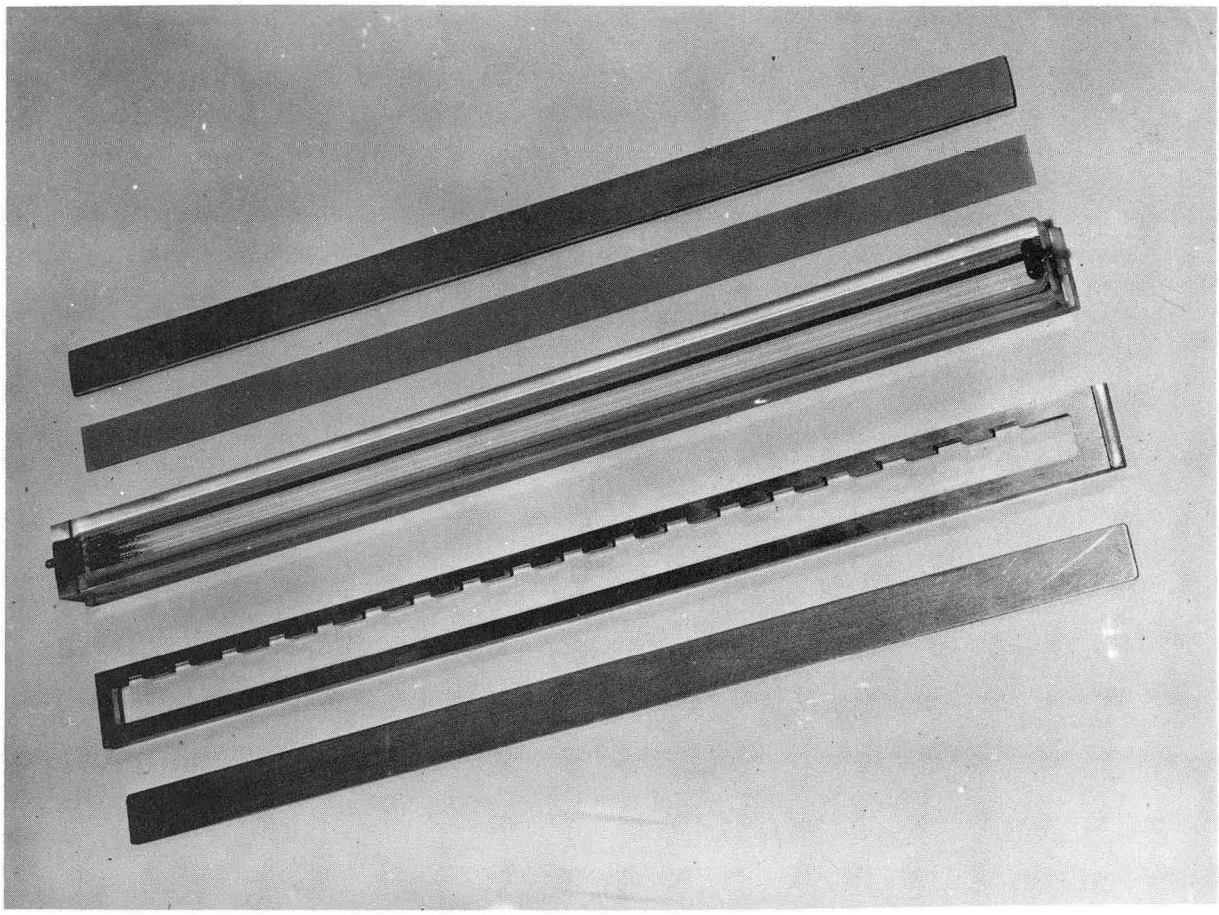

ZN-2413

Fig. 14. Film holders for accelerator camera.

the wire is attached to the Kovar seal input. Since only one Kovar seal was installed, both the pre- and postaccelerators cannot be operated at the same time.

The postacceleration of the electrons takes place between the ground-potential grid and the grid held at positive potential (approximately 5 kv). It is also necessary to maintain the photographic film itself at the positive potential. This is accomplished by coating with silver conducting paint the inner surface of the film holder from the second grid back to the film. In addition, the inner surface of the lucite film-backing plate is coated so that the film is entirely surrounded by a conducting medium.

C. Instrumentation and High-Voltage Supplies

Three high-voltage supplies were used with the spectrograph. The first of these is shown on the right in Fig. 15. This instrument is a radiofrequency voltage regulator constructed at this Laboratory. It was designed to give a continuous range of voltages between 5 and 50 kv with a regulation of 0.01%. The instrument with the chart recorder on top of the voltage regulator monitors the output voltage against a standard reference voltage. Either a mercury cell or a Zener diode could be used for the reference voltage. It was found that for operating in the region of 10 to 20 kv (the normal operating range) the voltage would remain constant to within approximately 0.01% for a period of at least 12 hours, following a period of drift during warm-up.

The second voltage supply (not shown) is a 10-ma regulated dc power supply for voltages from 500 v to 4 kv. This supply is rated for only approximately 1% voltage regulation -- which was sufficient, since this supply was used only with the postaccelerator. The requirements on voltage regulation are less stringent with the postaccelerator than with the preaccelerator, since in the former case the applied voltage does not affect the energy of the electrons until after momentum selection and resolution have taken place.

The third voltage supply consisted of 50 Burgess dry cells (300 v each) connected in series. This unit is shown in Fig. 16. The batteries

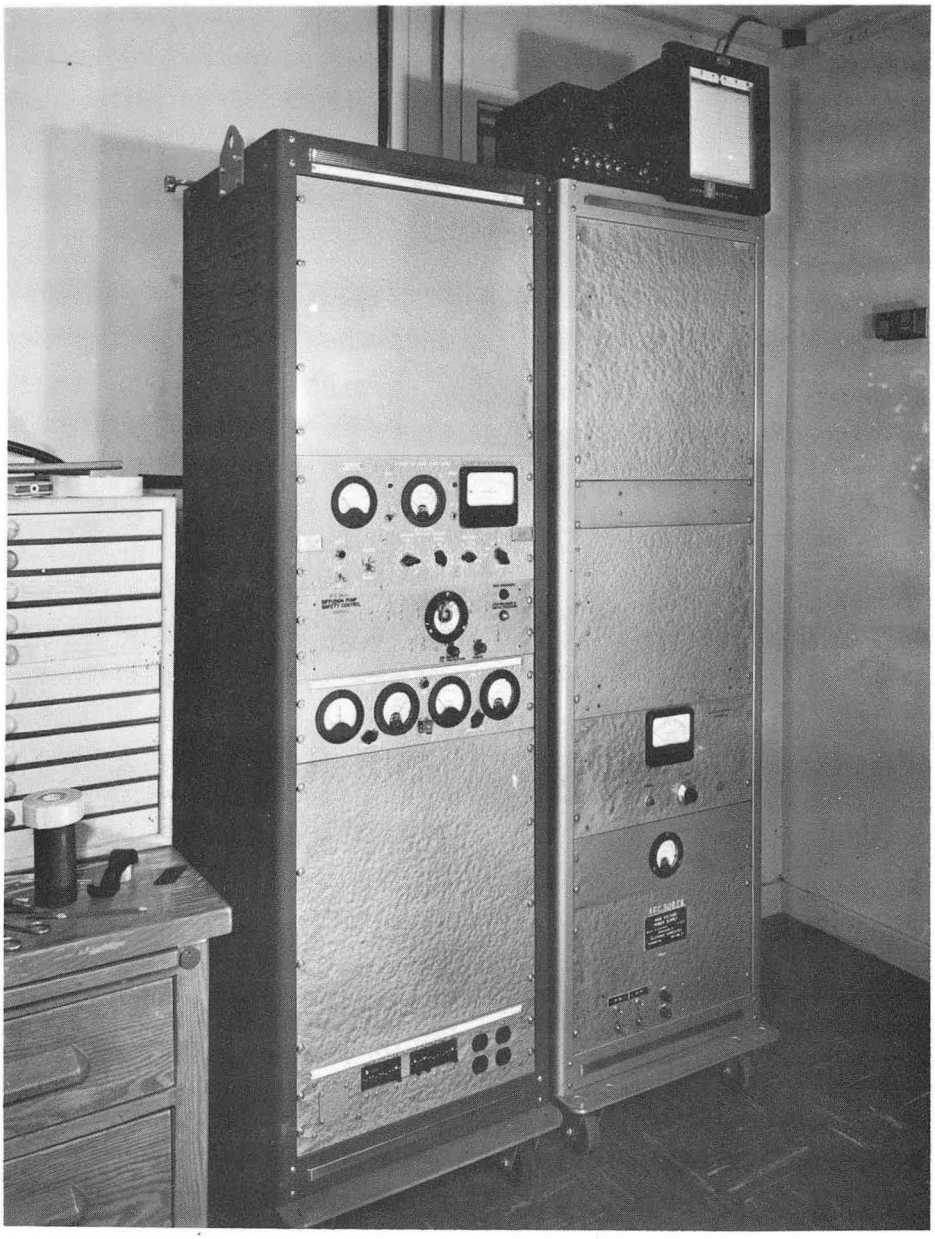

ZN-2414

Fig. 15. Instrumentation and high voltage supply for accelerator spectrograph.

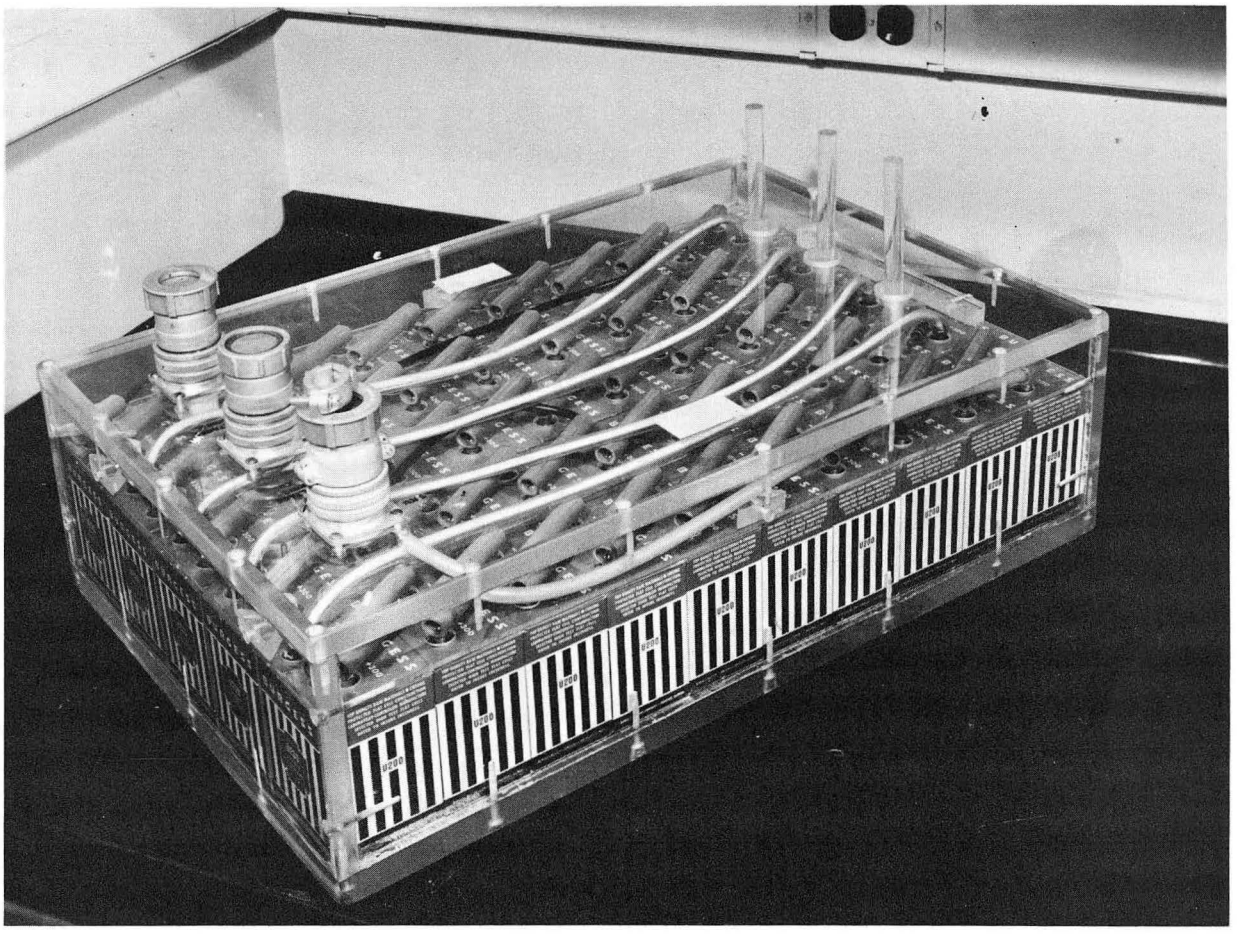

ZN-2415

Fig. 16. Dry cell high voltage supply for preaccelerator.

were packaged in a lucite box which was held together by tygon screws. The batteries were connected in series by means of resistors, which can be seen in the picture. The three outlets at the left top of the box are taps for obtaining 5, 10 or 15 kv. The lucite rods at the right are switches for breaking the circuit of those batteries not in use. This unit was used only with the preaccelerator and proved to be quite successful.

There was no method available for checking the constancy of the voltage of the battery supply other than examining the width of the conversion lines observed on the photographic plate. There was no noticeable line broadening produced either by the battery supply or by the electronic regulator used with the preaccelerator. This method of checking the voltage regulation is quite sensitive, since, for operation at 10 kv, a 0.1% drift in the voltage would produce a 0.2% change in the measured energy of a 5-kev electron line. Such a drift could produce a noticeable line broadening.

An insulated cable carried the voltage from the supply to the spectrograph. In Fig. 10 this cable can be seen leading to the brass faceplate of the camera. The large black cylinder attached to the faceplate is a lucite housing enclosing the Kovar seal. Inside this housing the cable is attached to the Kovar seal by means of a banana jack which plugs into a corona ball.

The auxiliary instrumentation of the spectrograph is contained in the left-hand cabinet of Fig. 15. This cabinet contains the ion-gauge power supply, thermocouple gauges which monitor the forepump pressure, and cutoff switches which turn off the current to the diffusion pump if either the chilled-water system fails or the pressure of the system increases beyond a safe point. The blank lower panel of this cabinet housed the postaccelerator voltage regulator (which was not present at the time the picture was taken.

III. RADIOACTIVE SOURCES

All sources used were deposits of the active material on 10-mil platinum wires. Three methods of depositing the source were attempted. The first was the electrodeposition method described by Smith and Hollander.[20] This method has been the standard procedure for preparing spectrograph sources at this Laboratory; however, for low-energy work this method is not always satisfactory, since one often obtains a coating of black material (presumably platinum black) on the wire during plating. This coating causes a broadening of the lines of low-energy conversion and Auger electrons.

Since mass-free sources are obtained routinely by means of vacuum vaporization at this Laboratory, an attempt was made to vacuum evaporate a sample of Np^{237}, Np^{238} onto 10- and 20-mil platinum wires.[115] The routine procedure consists of evaporating a drop of the active solution in a narrow (approximately 1/16 x 1 inch) groove pressed into a tungsten filament, and vaporizing the activity in vacuo onto a platinum disc placed immediately above the filament. The vaporization is accomplished by electrically heating the filament to white heat. This same method was employed in this work except that platinum wires were used in place of the platinum discs. These wires were mounted as close as possible to the filament without touching, and the groove in the filament was narrowed to a width approximately the size of the wire. In this manner it was possible to deposit approximately 20% of the activity on one side of the wire, leaving the other side nearly clean. Since the spectrograph sees only one side of the wire, this yield is as menaingful as a 40% electrodeposition yield with the activity deposited uniformly around the surface of the wire.

The third method involved dipping a platinum wire into a mass-free and quite active solution of Pa^{233} and drying the wire under a heat lamp. After this dipping and drying process was repeated several times an extremely clean source was obtained which registered approximately 20 mr on a beta-gamma survey meter.

IV. RESULTS

A. Preaccelerator

Figure 17 shows enlarged photographs of the same region of the Pa^{233} electron spectrum obtained with (Plate 48-X) and without (Plate 50-X) a preacceleration voltage (10 kv) applied. The source used was the "dipped" source described in Section III, above. The exposure times of the two plates were approximately the same. Electron lines in the region of approximately 80 kev (not shown in Fig. 17) are noticeably darker on Plate 50-X (no acceleration) than on Plate 48-X; however in the low energy region (Fig. 17) the lines on Plate 48-X have been enhanced by the preacceleration so that they are darker and more clearly defined than the corresponding lines on Plate 50-X. On Plate 50-X the energy of the least energetic line observed was 6.78-kev; whereas lines of approximately 1-kev and less were observed on Plate 48-X.

In Table XVII the observed energies and the observed intensities of the lines seen with and without the preaccelerator voltage applied are compared. For the purpose of energy determinations the more pronounced Pa^{233} conversion-electron lines on Plate 50-X were used to calibrate the magnetic field. The calibration data are plotted in Fig. 18. In this plot the effective magnetic field is plotted against the radius of curvature of the electron path. Used in this calibration were the energy values of the photons listed in Table VIII, Part One, of this dissertation, and the binding energies of Hill et al.[93]

In order to calculate the energies of the lines detected with the preaccelerator voltage turned on (Plate 48-X), it was necessary to determine the magnitude of the applied voltage. Since it was known that the applied voltage was approximately 10 kv and since it was easy to identify the more pronounced conversion lines in the spectrum, this determination was not difficult. The radii of curvature of the electron paths were determined in the conventional manner and the effective magnetic field was read from the graph in Fig. 18. It was assumed that the accelerating voltage did not perturb the electron path to an extent that would

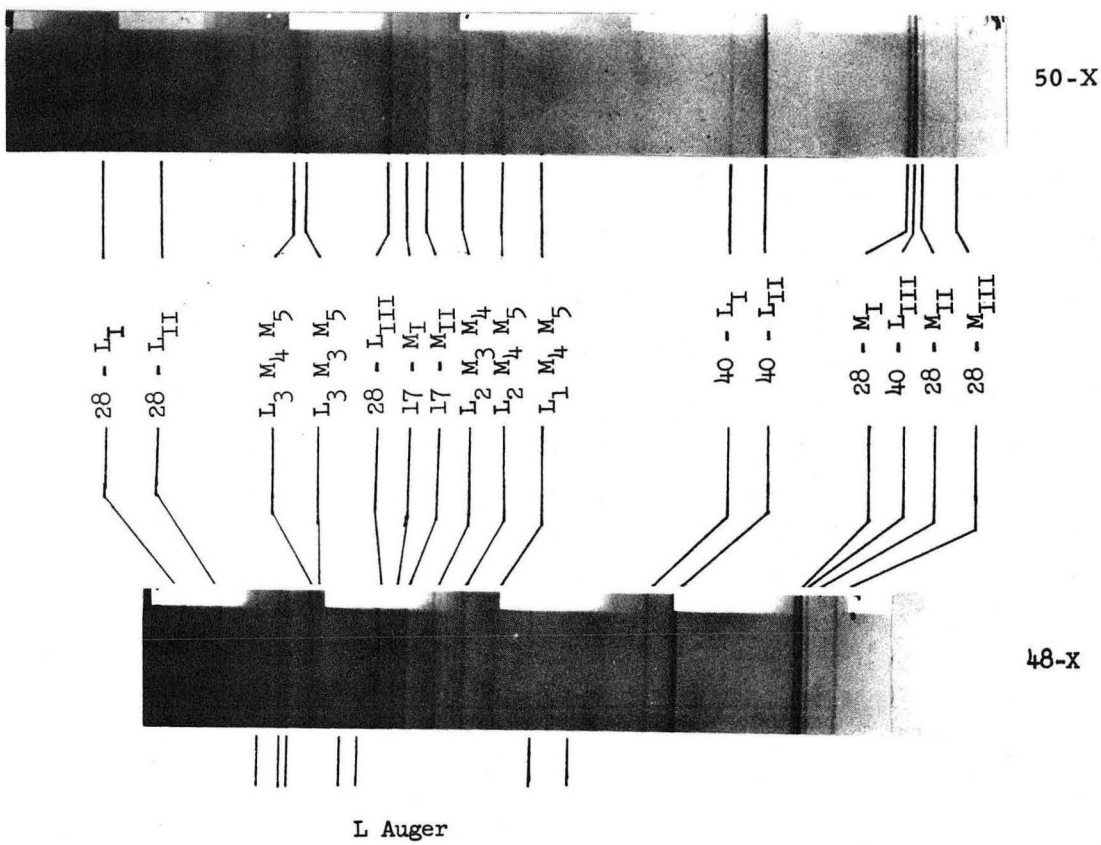

ZN-2417

Fig. 17. A comparison of the low energy electron spectrum of Pa^{233} obtained with and without preacceleration. (Plate 48-X was obtained with a 10-kev preacceleration voltage applied).

Table XVII

Low-energy conversion and Auger-electron data of Pa^{233} obtained with and without preacceleration

Intensity[a] (arb. units)	$\mathcal{H}\rho$ (gauss-cm)	Ee (kev)	Accepted[b] energy (kev)	ΔEe[c] (kev)	Ee-10.25[d] (kev)	Energy[e] on plate 50-x (kev)	Assignment[f]
w→m	316.0	8.71			-1.54		
w→m	320.0	8.93			-1.32		
s	325.1	9.21			-1.04		
vs (b)	340.5	10.10			-0.15		
vw (vb)	359.0	11.21			0.96		L-Auger
w	373.9	12.15			1.90		
w	379.1	12.49			2.24		L-Auger
w→m	385.2	12.89			2.64		L-Auger
w	388.1	13.08			2.83		L-Auger
w?	397.8	13.73			3.48		L-Auger
w (vb)	401.2	13.96			3.71		L-Auger
w	406.5	14.33			4.08		
s	443.2	16.99	6.78	10.21	6.74	6.78	28.50-L_I
?	444.5	17.09			6.84		
vw (b)	448.8	17.42			7.17		L-Auger
?	452.7	17.72			7.47		L-Auger
m→s	453.8	17.80	7.60	10.20	7.55	7.59	28.49-L_{II}
?	455.9	17.96			7.71		L-Auger
?	462.4	18.47			8.22		L-Auger
w (b)	464.5	18.64			8.39	8.45	L-Auger
w (b)	471.7	19.21			8.96	9.00	L-Auger
w (b)	473.5	19.35			9.10	9.13	L-Auger
?	476.1	19.56			9.31		
?	477.7	19.69			9.44		
m	481.1	19.97			9.72	9.72	L-Auger
w→m	483.2	20.14			9.89	9.96	L-Auger
?	484.8	20.27			10.02		L-Auger
vw (b)	490.3	20.72			10.47		L-Auger

Table XVII (cont.)

Intensity[a] (arb. units)	$\mathcal{H}\rho$ (gauss-cm)	Ee (kev)	Accepted[b] energy (kev)	ΔEe[c] (kev)	Ee-10.25[d] (kev)	Energy[e] on plate 50-x (kev)	Assignment[f]
vw (b)	495.3	21.14			10.89	10.87	L-Auger
m→s	501.1	21.62	11.38	10.24	11.37	11.37	28.53-L_{III}
vw	503.0	21.79			11.54		
w (b)	505.1	21.96			11.71	11.73	17.26-M_I
w→m(b)	509.0	22.30			12.05	12.08	17.23 M_{II}
vvw	513.0	22.64			12.39		
vvw	515.3	22.84			12.59	12.59	
w→m(b)	517.5	23.03			12.78	12.81	
vw	519.3	23.19			12.94	12.97	17.24-M_{III}
vw	521.4	23.37			13.12	13.19	
vw	523.8	23.58			13.33	13.34	
w→m	526.4	23.81			13.56	13.56	
w	535.1	24.59			14.34	14.31	
vvw	538.8	24.92			14.67		
?	542.2	25.23			14.98		
vw	546.1	25.59			15.34		
vvvw	549.0	25.85			15.60		
vvvw	550.9	26.03			15.78		17.22-N_I
vvvw	553.0	26.22			15.97		17.24-N_{II}
vvw	557.2	26.61			16.36	16.34	
??	558.5	26.73			16.48		
m	580.4	28.81	18.59	10.22	18.56	18.58	40.32-L_I
s	589.0	29.65	19.41	10.24	19.40	19.39	40.34-L_{II}
m→s	625.1	33.28	22.99	10.29	23.03	23.01	28.58-M_I
s	626.7	33.45	23.19	10.26	23.20	23.16	40.36-L_{III}
w	628.5	33.63	23.36	10.27	23.38	23.37	28.56-M_{II}
w→m	636.9	34.51	24.24	10.27	24.26	24.29	28.56-M_{III}
w	663.5	37.35	27.10	10.25	27.10	27.13	28.54-N_I
vw	665.4	37.56	27.27	10.29	27.31	27.30	28.58-N_{II}
vw	667.2	37.75	27.50	10.25	27.50	27.52	28.54-N_{III}

Table XVII (cont.)

Intensity[a] (arb. units)	$H\rho$ (gauss-cm)	Ee (kev)	Accepted[b] energy (kev)	ΔEe[c] (kev)	Ee-10.25[d] (kev)	Energy[e] on plate 50-x (kev)	Assignment[f]
vw (b)	674.3	38.53	28.22	10.31	28.28	28.27	28.60-O_I
?	676.4	38.77			28.52		
vw	731.4	45.06	34.80	10.26	34.81	34.81	40.36-M_I
m→ s	734.3	45.40	35.17	10.23	35.15	35.29	40.33-M_{II}
?	737.5	45.78			35.53		
m→ s	741.7	46.28	36.05	10.23	36.03	36.02	40.33-M_{III}
w	767.2	49.38	39.08	10.30	39.13	39.09	40.40-N_{II}
w	768.8	49.57	39.31	10.26	39.32	39.35	40.36-N_{III}
vw	774.6	50.29	40.10	10.19	40.04	40.11	40.29-O_{II}
vvw	781.2	51.11			40.86	40.77	58.02-L_{III}
vvvs	878.1	63.82	53.52	10.30	53.57	53.50	75.33-L_I
??	880.2	64.11			53.86		
m	883.9	64.62	54.34	10.28	54.37	54.34	75.31-L_{II}
vvw	910.2	68.29	58.12	10.17	58.04		75.20-L_{III}
vvvw?	951.0	74.16			63.91		
vvvs	957.4	75.09	64.83	10.26	64.84	64.91	86.60-L_I
??	959.5	75.40			65.15		
m	962.6	75.86	65.65	10.21	65.61	65.67	86.55-L_{II}
??	988.2	79.67			69.42		
m→ s	990.5	80.02	69.73	10.29	69.77	69.76	75.32-M_I
w	992.9	80.38	70.10	10.28	70.13	70.17	75.31-M_{II}
vvw	1002.9	81.89			71.64	71.79	KL_IL_I
vvw	1009.2	82.85			72.60	72.58	KL_IL_{II}
m	1017.4	84.11	73.84	10.27	73.86	73.85	75.30-N_I
vvw(b)?	1021.3	84.71			74.46		
w	1024.5	85.20	74.96	10.24	74.95	74.98	75.27-O_I
vvvw	1034.0	86.67			76.42		KL_IL_{III}
vvvw	1039.0	87.45			77.20	77.14	$KL_{II}L_{III}$
s	1063.5	91.31	81.04	10.27	81.06	81.06	86.61-M_I

Table XVII (cont.)

Intensity[a] (arb. units)	$\mathcal{H}\rho$ (gauss-cm)	Ee (kev)	Accepted[b] energy (kev)	ΔEe[c] (kev)	Ee-10.25[d] (kev)	Energy[e] on plate 50-x (kev)	Assignment[f]
w	1065.8	91.67	81.41	10.26	81.42	81.45	86.60-M_{II}
?	1067.7	91.98			81.73		
w	1070.1	92.36	82.10	10.26	82.11	82.09	103.9-L_{I}
w	1075.1	93.16	82.92	10.24	82.91	82.94	103.9-L_{II}
w→m	1089.0	95.39	85.15	10.24	85.14	85.16	86.58-N_{I}
vw	1096.4	96.59	86.27	10.32	86.34	86.30	86.66-O_{I}
vvw	1098.8	96.98	86.70	10.28	86.73		103.9-L_{III}

a. Units used are: s-strong; m-medium; w-weak; v-very; (b)-broad; and ?-questionable.

b. The accepted energies are those considered as the best values on the basis of the electron and gamma ray data of this work.

c. ΔEe is the difference between the measured energy of the accelerated electron and the accepted energy.

d. The average value of ΔEe is 10.25 ± 0.03.

e. These energies are from another exposure of the same source without acceleration.

f. For the specific assignments of the L-Auger lines see Part I, Table XVI.

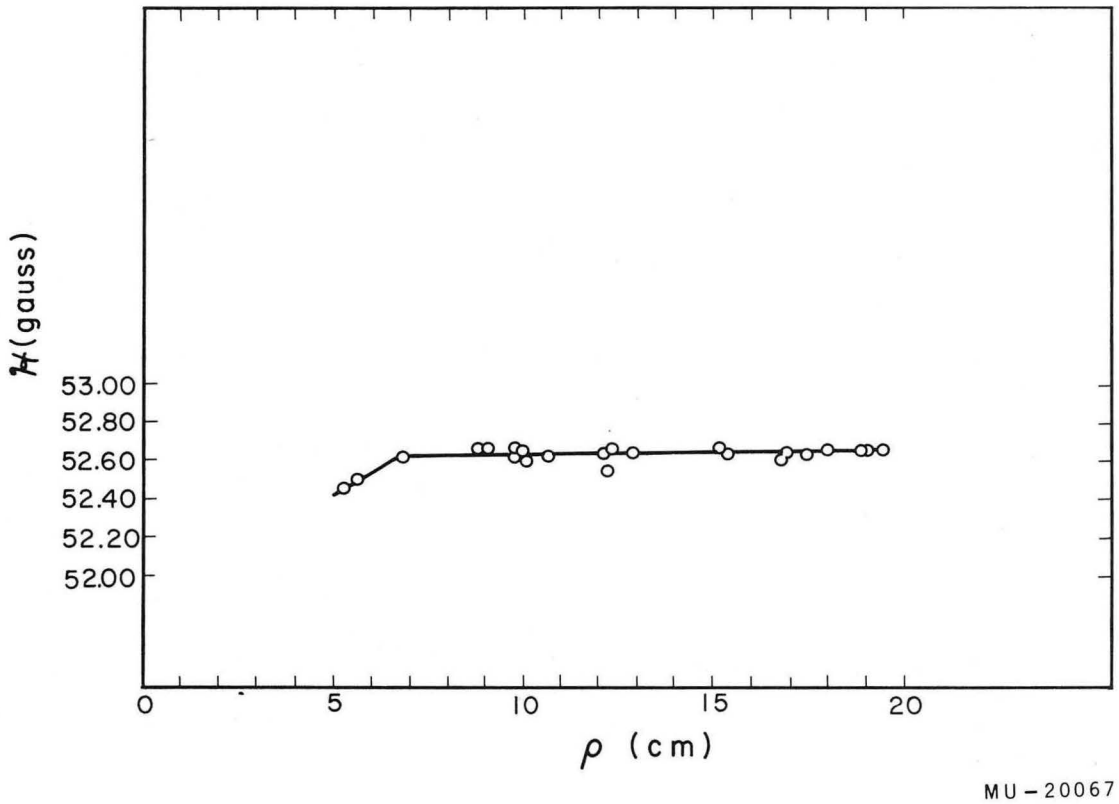

Fig. 18. Magnetic field calibration curve for accelerating spectrograph.

cause the electron to see an effective field appreciably different from that seen by an unaccelerated electron of the same energy as that of the accelerated one. Figure 18 shows that the effective field is essentially constant for radii greater than 7 cm so that this assumption is valid at least for electrons whose radii of curvature are greater than this value.

The energies calculated in this way are listed in Table XVII. Also listed for the more prominent lines are the differences between these energies and the accepted energies. The difference is the energy increment produced by the applied accelerating voltage. This increment is fairly constant over the spectrum, the average value being 10.25 ± 0.03 kev. The corrected energies of the lines, obtained by subtracting 10.25 kev from the measured energies, are listed in Table XVII and compared to the energies obtained without acceleration (Plate 50-X). The agreement is quite good.

Many lines were seen on Plate 48-X that were undetected on Plate 50-X. Most of these new lines appear in the low-energy region. Although some of these lines may not be real, the majority of them are surely conversion lines or Auger lines. Only four lines were detected on Plate 50-X and unseen on Plate 48-X, and these are all marked as questionable.

The assignments of lines listed in Table XVII have been discussed in Section III.B of Part One. The detection and analysis of these low-energy electron lines (particularly the L-Auger spectrum) are proof of the usefulness of the preaccelerator camera.

The four lines observed on Plate 48-X with energies less than the accelerating potential of 10.25 kev are obviously not conversion or Auger lines. It is believed that these are electrons removed by the accelerating potential from bound states in the platinum wire.

B. Postaccelerator

Two plates taken with and without the postacceleration voltage (5 kv) applied are shown in Fig. 19. The source was an electroplated sample of Am^{241}. Both plates were exposed for the same length of time (34 hr), and the plates were developed together to insure that differences in line intensities would not result from different development conditions.

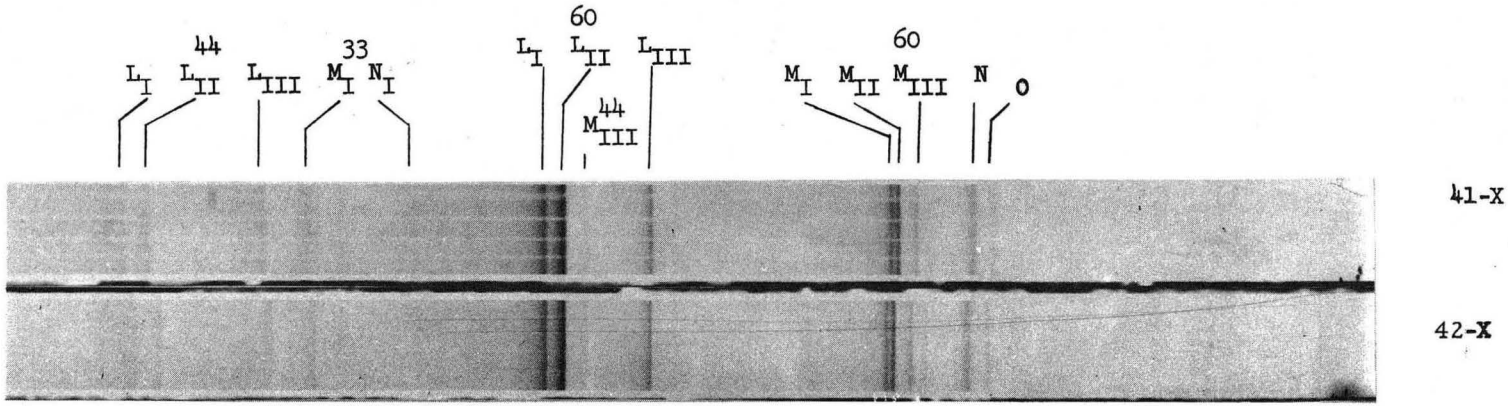

ZN-2418

Fig. 19. A comparison of the low energy electron spectrum of Am^{241} obtained with and without postacceleration. (Plate 41-X was obtained with a 5-kev postacceleration voltage applied.)

It can be seen that the lines on the plate taken with postacceleration are somewhat darker than those on the other plate. This is more evident on the original plates than in the reproduction. The lowest-energy lines shown are in the region of 21 kev. It is encouraging that even at these relatively high energies an increase in energy of only 5 kev produces a noticeable effect. For conversion lines of lower energies the effect would be even greater. Higher accelerating potentials could not be used because of the difficulties in maintaining high potentials in the limited space available, as mentioned in the Introduction, Part Two.

It should be noted that the increase in intensity obtained here is not nearly as large as that apparently obtained by Delesalle with a postacceleration of 1 kv on the L and M lines (approximately 30 kev) of the 46-kev transition in the decay of Ra.D.[114] He presents a reproduction of a photographic plate in which the lines obtained with postacceleration (1 kv) are much stronger than those obtained without acceleration. He does not say, however, if the times of exposures with and without acceleration were the same. If these exposure times were equal, it is difficult to understand the large difference in intensities, since, according to Fig. 9, an increase of 1 kev at approximately 30 kev total energy produces a very small difference in the film efficiency. (It is certainly reasonable to assume that the relative efficiencies of the film used by Delesalle do not differ greatly from those of the film used in this work.)

Two other comments should be made about Fig. 19. First, note the horizontal light lines running lengthwise on the plates. These lines are produced by the grid system of the accelerator. The lines are wider on the plate taken with the voltage turned on -- presumably because the grid wires deflect the electrons electrically as well as mechanically. Note also that the conversion-electron lines on the upper plate are displaced relative to those on the lower plate. This displacement occurs because the electrons do not enter the accelerator normal to the planes of the grid networks; thus the electrons experience a component of acceleration which shifts their position sideways. Plans were developed to narrow the

defining slit and move the source closer to the slit so that the instrument would more nearly resemble a 180-degree spectrograph. For this type of instrument the electron paths strike the photographic plate normal to the plane of the plate, hence the displacement of the lines would be made smaller by such a modification. At the time of this writing these plans have not been carried out.

The postaccelerator film holder was not notched as was the preaccelerator holder, so that no calibration marks were produced on the film. It was impossible, therefore, to make accurate energy measurements. The notches were not machined in the holder initially because it was considered unnecessary to complicate further an already difficult machining job until the holder had proven itself worth-while to use.

V. INTENSITY MEASUREMENTS

It was mentioned in the Introduction of Part Two that the efficiency of photographic film for low-energy electrons is quite small. Also, this efficiency at low energies is not known very well, so that accurate intensity measurements are difficult to obtain for electron lines of less than approximately 15 kev. One of the purposes of the accelerator camera is to raise the energies of the electrons to an energy region where the film efficiency is greater and better known; however, with the preaccelerator camera another uncertainty in the measured intensity is introduced if, by the process of accelerating, the effective geometry of the instrument is altered (i.e., if the electric potential causes more electrons to enter the slit than would otherwise). In the preacceleration the electron intensities are also affected by the increased radius of curvature (ρ) of the electron paths; however, corrections for ρ are made in the same manner as for unaccelerated electrons. If accurate intensity measurements of low-energy lines are to be made, it is necessary to determine the effect of the voltage on the effective geometry of the spectrograph.

Delesalle determined the magnitude of this effect for his spectrograph by making exposures of the same source with first preacceleration, then postacceleration.[114] The same accelerating potential was used in each case so that the increase in intensity due to increased film efficiency would be equal for both exposures. After ρ corrections were made, the intensities obtained with pre- and postacceleration were compared to determine the effect of the preaccelerating voltage on the effective geometry of the spectrograph. For two different conversion-electron lines in the decay of Ra D, Delesalle lists his results as follows:

Acceleration voltage (kv)	$\Delta N/N$ (%)	
	$E_e \cong 30$ kev	$E_e \cong 43$ kev
1	1.3	0.8
2	2.7	1.6
3	4.0	2.4
4	5.3	3.2

($\Delta N/N$ is the percent increase in intensity attributed to an increase in the effective geometry of the preaccelerating spectrograph.)

In this work an attempt was made to determine this effect empirically by means of Ilford G·5 nuclear track emulsion film. Faler has used this film to measure electron intensities directly by counting the individual electron tracks produced per energy interval along the film.[116] Since in this method the number of electron tracks, rather than the number of emulsion grains developed (i.e., the darkening of the film), is determined, the measured intensity does not depend upon the film efficiency. It should be possible, therefore, to determine the relative effective geometry of the spectrograph at different values of the preaccelerator voltage by measuring the intensity of a given conversion-electron line by the electron-track method at the various voltage settings.

The attempts to make such measurements were unsuccessful because the backgrounds of the developed nuclear track plates were too dark. Low background is required for successful counting of the electron tracks. In most instances the developed plates were quite black at the end nearest the source, the blackness tapering off in intensity along the plate until near the center the undarkened yellow emulsion was visible. The cause of this darkness was undetermined, but it is felt that with additional work this difficulty could be overcome and good-relative-geometry measurements achieved.

It is possible that the effect of the electrostatic field on the geometry of the instrument could be calculated from knowledge of the paths of electrons of various energies in crossed electric and magnetic fields; however, because of the close spacings within the camera, the electric field is undoubtedly complex in nature and would be difficult to estimate.

As a very rough approximation it could be assumed that the electric field is radial as in a magnetron. With this approximation the equations derived by Hull[117] could be used to calculate the electron paths; however, it is felt that this approximation for the source arrangement used here would be too poor to lead to any useful results.

It would be instructive to construct an instrument in which the accelerating potential is more nearly radial so that the effective geometry could be calculated accurately. Because the potential distribution in such an arrangement is logarithmic, an electron would experience the majority of its acceleration after traveling only a fraction of the distance between source and slit, and this acceleration would be radial. Thus, the path of the electron should not deviate greatly from that of an unaccelerated electron starting from the source with an energy equal to the final energy of the accelerated electron. It is believed, therefore, that the variation of effective geometry with electric field strength would not be as great for this arrangement as reported by Delesalle for his parallel-plate accelerator.[114] To avoid problems imposed by the small space available between the magnet pole faces it would be possible to establish the accelerating unit outside the magnetic field.

VI. CONCLUSION

The accelerating spectrograph described here was successful as both a pre- and postaccelerator. The preaccelerator proved more useful, however, since the acceleration of the low-energy electrons as they leave the source lessens the effect of source absorption, increases their radius of curvature so that the focusing is better, and raises the electrons to energies at which reasonable film efficiencies are realized. The postaccelerator has only the last advantage.

The use of the preaccelerator in studying the L-Auger spectrum and the low-energy conversion spectrum of the decay of Pa^{233} illustrates the large amount of information -- undetectable by the conventional instruments -- that can be obtained by means of the preaccelerator spectrograph.

It was shown that good focusing can be obtained with the use of an approximately radial accelerating field. Because of the possible advantage of a radial field (discussed above), a worth-while project would be to construct a new preaccelerator in which a radial field is more nearly realized than in this work.

ACKNOWLEDGMENTS

Sincere thanks are extended to Dr. Jack Hollander, who capably and unselfishly supervised this study, and to Professor Isadore Perlman, under whose direction the work was undertaken.

Many helpful discussions with Professor John Rasmussen and Dr. Frank Asaro are greatly appreciated. In addition, the assistance of Dr. Asaro with certain phases of the experimental work is gratefully acknowledged.

Mr. George Kilian, Mr. Milton Firth, and Mr. Donald Paxton have contributed much to this study by developing the electric and electronic components of the accelerator spectrograph.

Also appreciated are the suggestions and comments of Mr. Fred Reynolds and Dr. Maynard Michel.

The assistance and advice of Dr. Charles Gallagher and Professor Jesse DuMond have been most helpful.

Special recognition is accorded my wife, Ulla, for her constant interest and encouragement and for typing this original manuscript.

The assistance of the health chemists, the inspection technicians, and the secretarial staff is greatly appreciated.

Thanks are also due my parents, who have been a source of encouragement throughout my college career.

This work was performed under the auspices of the United States Atomic Energy Commission.

APPENDIX

CALCULATION OF SOURCE ABSORPTION FOR THE Pa^{233} GAMMA-RAY SOURCES

I. Wire Source

The activity is evenly distributed around the surface of a 10-mil platinum wire. The detection apparatus is on the negative Y axis (Fig. 20), and it is assumed that the detection geometry is small enough so that only rays leaving the source parallel to the Y-axis enter the detector (i.e., the detector is at $y = -\infty$). Since the cross section of the source is uniform, the problem can be considered in two dimensions. Let I_o be the total activity leaving the wire in the negative y direction. The activity on the side of the wire facing the detector ($1/2\ I_o$) will not be absorbed by the wire. Some fraction f of the activity ($1/2\ I_o$) leaving the back side of the wire will be absorbed by the wire; and f will depend on the angular position (θ) of the small area of source being considered. The total activity capable of entering the detector is, then, $I_t = 1/2\ I_o + 1/2\ fI_o$.

We define the "angular density" of the activity on the wire as $I_o/2\pi$. The small increment of activity, dI_o, leaving the source in the negative y direction from a small increment of angle, $d\theta$, on the back side of the wire is given by the expression

$$dI_o = I_o/2\pi \quad d\theta \ .$$

The fraction of this activity that penetrates the wire is

$$f = e^{-\mu\rho(2y)} = e^{-2\mu\rho r \sin\theta}$$

where, μ is the mass absorption coefficient, ρ the density of the wire, and r the radius of the wire. Thus,

$$dI = I_o/2\pi \quad e^{-2\mu\rho r \sin\theta}$$

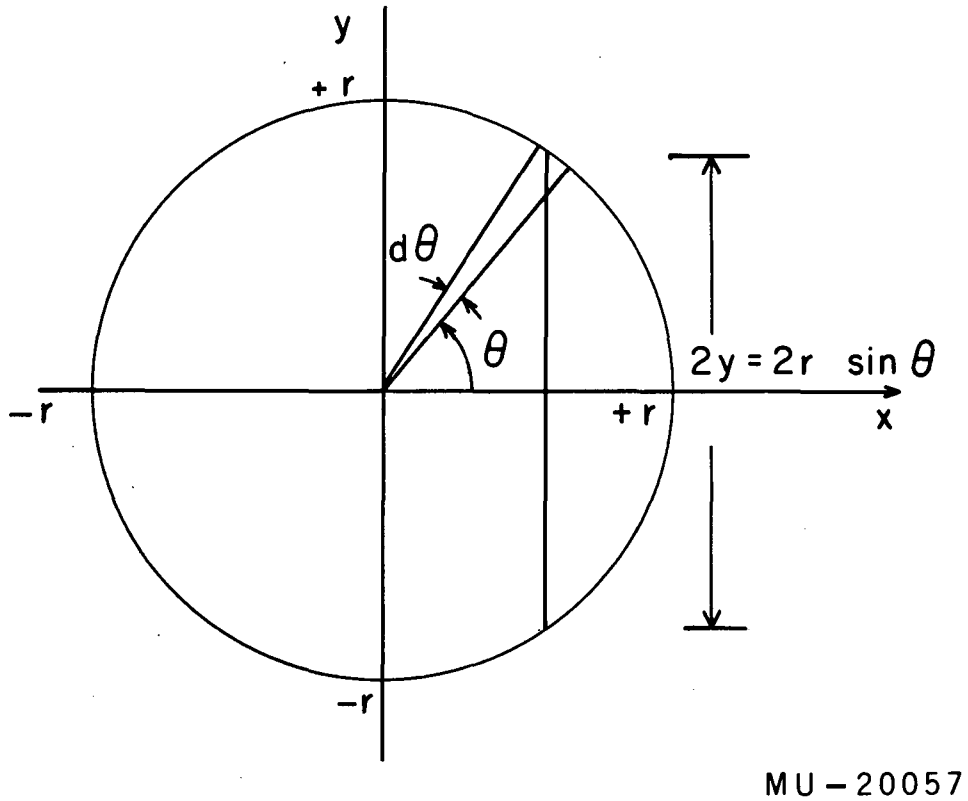

Fig. 20. Source absorption - activity evenly distributed around surface of wire (detector is at y = - ∞).

Integrating from $\Theta = 0$ to $\Theta = \pi$ gives

$$I = I_o/2\pi \int_o^{\pi} e^{-2\mu\rho r \sin \Theta} \, d\Theta.$$

Thus

$$I_t = 1/2\, I_o + I_o/2\pi \int_o^{\pi} e^{-2\mu\rho r \sin \Theta} \, d\Theta,$$

and

$$I_t/I_o = 1/2 + 1/2\pi \int_o^{\pi} e^{-2\mu\rho r \sin \Theta} \, d\Theta.$$

In this work the integration was performed graphically.

II. ThO_2 Source

In this case the activity is uniformly distributed through a volume of uniform circular cross section (Fig. 21). The assumptions concerning the detector are the same as those in Appendix I; hence, again, only rays leaving the source in the negative y direction are capable of entering the detector. We consider I_o, the total activity leaving the source in the desired direction. The "area density" of this activity is $I_o/\pi r^2$. At the point x,y is located an increment of area, dxdl, where l is the distance, parallel to the y axis, from the "front side" of the source to the point y. The small increment of activity, dI_o, leaving this area is

$$dI_o = I_o/\pi r^2 \quad dxdl .$$

The fraction of this activity that is not absorbed by the source is $e^{-\mu\rho l}$; hence

$$dI = I_o/\pi r^2 \quad e^{-\mu\rho l} \quad dxdl.$$

The total activity not absorbed is

$$I = \int_{-r}^{r} \int_{o}^{2y} I_o/\pi r^2 \quad e^{-\mu\rho l} \quad dldx,$$

where $y = r \sin \theta$ is constrained to the circumference of the circle:

$$I = - I_o/\mu\rho\pi r^2 \int_{-r}^{r} (e^{-2\mu\rho y} - 1) \quad dx.$$

Transforming to polar coordinates gives

$$I = I_o/\mu\rho\pi r \int_{o}^{\pi} (1 - e^{-2\mu\rho r \sin \theta}) \sin \theta \, d \theta.$$

Performing the integration on the first term gives

$$I = I_o/\mu\rho\pi r \quad \{2 - \int_{o}^{\pi} e^{-2\mu\rho r \sin \theta} \sin \theta \, d \theta\} .$$

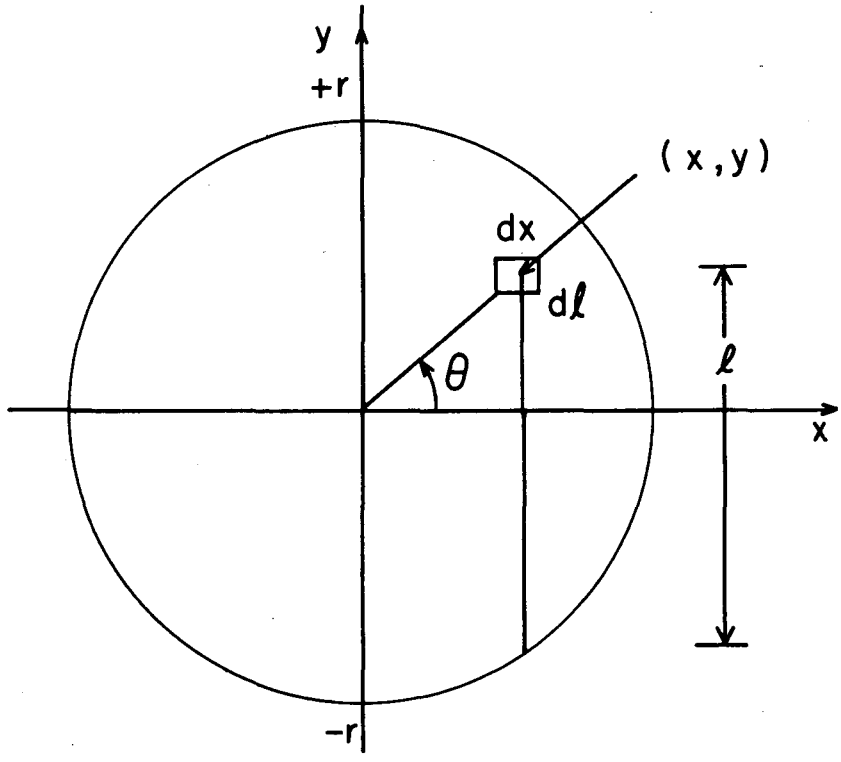

MU-20059

Fig. 21. Source absorption - activity uniformly distributed throughout cylindrical volume (detector is at $y = -\infty$).

The equation in this form is undesirable, since in the present application the integral is very near unity. The term in brackets, being the small difference between two nearly equal numbers, is therefore subject to large error. Recognizing the relation

$$e^{-a \sin \theta} \sin \theta = d/d\theta \left(- \cos \theta \, e^{-a \sin \theta}\right) - a \cos^2 \theta \, e^{-a \sin \theta}$$

leads to

$$I/I_o = 4/\pi \int_o^{\pi/2} \cos^2 \theta \, e^{-2\mu\rho r \sin \theta} \, d\theta.$$

In this work the integration was performed graphically. Dixon has arrived at the same equation by a different reasoning and has expanded the integral in series for the purpose of evaluation.[118]

REFERENCES

1. M. G. Mayer, Phys. Rev. 78, 16 (1950).

2. Haxel, Jensen, and Suess, Ergeb. exakt. Naturw. 26, 244 (1952).

3. A. Bohr and B. R. Mottelson, Collective and Individual-Particle Aspects of Nuclear Structure, Kgl. Danske Videnskab. Selskab., Mat.-fys. Medd. 27: No. 16 (ed. 2, 1957).

4. A. Bohr and B. R. Mottelson, in Beta- and Gamma-ray Spectroscopy, edited by Kai Siegbahn (Interscience Publishers, Inc., New York, 1955), Chap. 17.

5. Earl K. Hyde, The Unified Nuclear Model and Its Application to Heavy Element Nuclides, UCRL-8783, June 1959.

6. Warren G. Smith, I. Neutron-Deficient Isotopes in the Nobel Metal Region. II. Conversion-Electron Spectra of Some Heavy Elements (Thesis), UCRL-2974, June 1955.

7. G. D. O'Kelley, The Spectrometric Determination of Some Beta-Particle and Conversion-Electron Energies (Thesis), UCRL-1243, 1951.

8. Jesse W. M. Du Mond, Office of Naval Research Special Technical Report No. 28 and Atomic Energy Commission Special Technical Report No. 8, March 1954.

9. The author is grateful to Dr. J. W. M. Du Mond, Dr. Charles J. Gallagher, and Dr. Felix Böhm for the use of their equipment and for their cooperation and assistance.

10. G. D. O'Kelley and J. L. Olsen, A Ring-Focused, Long Magnetic Lens Beta-Ray Spectrometer, California Research and Development Company Report MTA-38, May 1954.

11. Manufactured by the Pacific Electro-Nuclear Company, Culver City, California.

12. R. C. Pilger, Nuclear Decay Schemes in the Actinium Family (Thesis), UCRL-3877, July 1957.

13. Manufactured by the Harry W. Dietart Co., Detroit 4, Michigan.

14. M. Mladjenovic and H. Slätis, Arkiv Fysik 8, 65 (1954).

15. Walter M. Gibson, Fission and Spallation Competition from the Intermediate Nuclei Americium-241 and Neptunium-235 (Thesis), UCRL-3493, Nov. 1956.

16. Max W. Hill, Nuclear Decay Studies of Protactinium Isotopes (Thesis), UCRL-8423, Aug. 1958.

17. Richard A. Glass, Studies in the Nuclear Chemistry of Plutonium, Americium, and Curium, and the Masses of the Heaviest Elements (Thesis), UCRL-2560, April 1954.

18. For a review of previous work see I. Perlman and J. O. Rasmussen, Handbuch der Physik 42 (Springer-Verlag, Berlin, 1957).

19. Asaro, Thompson, and Perlman, Phys. Rev. 92, 694 (1953); Asaro, Harvey, Stephens, and Perlman, unpublished data.

20. W. G. Smith and J. M. Hollander, Phys. Rev. 101, 746 (1956).

21. Rasmussen, Slätis, and Passell, Phys. Rev. 99, 42 (1955).

22. Rasmussen, Stephens, Strominger, and Åström, Phys. Rev. 99, 47 (1955).

23. Freedman, Jaffey, and Wagner, Phys. Rev. 79, 410 (1950).

24. Slätis, Rasmussen, and Atterling, Phys. Rev. 93, 646 (1954).

25. S. A. Baranov and K. N. Shlyagin, Atomnia Energia 1, 52 (1956).

26. This is the Bohr-Mottelson notation for ($I\pi$, K).

27. A description of the electroplating procedure is given in References 6 and 20. Preparation of the ammonium oxalate plating solution is described by Moore and Smith, Nucleonics 13, No. 4, 66 (1955).

28. M. E. Rose, Internal Conversion Coefficients (North Holland Publishing Co., Amsterdam; Interscience Publishing Co., New York, 1958).

29. O. Nathan, Nuc. Phy. 4, 125 (1957).

30. Alder, Bohr, Huus, Mottelson, and Winther, Revs. Modern Phys. 28, 433 (1956).

31. R. K. Sheline, in Nuclear Structure, Proceedings of the University of Pittsburgh Conference, edited by Sidney Meshkov, June 1957.

32. C. J. Gallagher, Electron-Spectroscopic Studies of Neutron-Deficient Rhenium Isotopes (Thesis), UCRL-3928, Sept. 1957.

33. Bäckstrom, Lindskog, Bergman, Bashandy, and Bäcklin, Arkiv Fysik 15, 121 (1959).

34. Bjørnholm, Nathan, Nielsen, and Sheline, Nuclear Phys. 4, 313 (1957).

35. F. S. Stephens, Jr. (Lawrence Radiation Laboratory), private communication.

36. Perlman, Asaro, Harvey, and Stephens, Electric Monopole Transitions in Pu^{238} and U^{234}, Bull. Am. Phys. Soc. II, 2, 394 (1957).

37. A. S. Reiner, Structure Effects in the Interaction Between Nuclei and Atomic Electrons (Thesis), University of Amsterdam, 1958 (unpublished).

38. D. C. Peaslee, Nuclear Monopole Matrix Elements, UCRL-3523, 1957, (unpublished).

39. J. O. Rasmussen, Theory of E0 Transitions in Spheroidal Nuclei, UCRL-9084, Feb. 1960.

40. Brink, Hubbs, Nierenberg, and Worcester, Phys. Rev. 107, 189 (1957).

41. Albridge, Hubbs, and Marrus, Phys. Rev. 111, 1137 (1958).

42. Alaga, Alder, Bohr, and Mottelson, Kgl. Danske Videnskab. Selskab. Mat.-fys. Medd. 29, No. 9 (1955).

43. L. A. Nordheim, Revs. Modern Phys. 23, 322 (1951).

44. C. J. Gallagher and S. A. Moszkowski, Phys. Rev. 111, 1282 (1958).

45. For a discussion of the asymptotic quantum numbers see B. R. Mottelson and S. G. Nilsson, Kgl. Danske Videnskab. Selskab. Mat.-fys Skr. Danske Videnskab 1, No. 8 (1959).

46. Jack M. Hollander, Phys. Rev. 105, 1518 (1957).

47. D. Strominger and J. O. Rasmussen, Nuclear Phys. 3, 197 (1957).

48. Rasmussen, Canavan, and Hollander, Phys. Rev. 107, 141 (1957).

49. Ong Ping Hok and G. J. Sizoo, Physica 20, 77 (1954) and Ong Ping Hok and P. Kramer, Physica 21, 676 (1955).

50. L. G. Elliott and A. B. Underhill, Report HAR 761, 1952.

51. W. A. Brodie, Proc. Phys. Soc. 67-A, 397 (1954).

52. H. B. Keller and J. M. Cork, Phys. Rev. 79, 1030 (1950).

53. Bisgard, Dahl, and Olesen (preprint).

54. G. Albouy and M. Valadares, J. phys. radium (to be published).

55. J. O. Newton, Nuclear Phys. 5, 218 (1958).

56. D. Saxon, Phys. Rev. 81, 639 (1951).

57. J. M. Hollander and J. H. Hamilton, private communication.

58. K. Siegbahn and K. Edvarson, Nuclear Phys. 1, 137 (1956).

59. The accepted energies were deduced from the electron binding energies tabulated in Reference 69.

60. The ThO_2 source was prepared at this Laboratory by the author, who was unable to accompany the source to the California Institute of Technology. Dr. Gallagher very kindly agreed to perform the intensity measurements with this source.

61. Detector efficiencies and photopeak-to-total ratios were calculated for the 3 x 2-in. and 5 x 3-in. sodium iodide cyrstals by means of equations given by M. J. Berger and J. Doggett, J. Research Nat'l. Bur. Standards 56, 355 (1956); Research Paper No. 2686.

62. G. W. Grodstein, X-Ray Attenuation Coefficients from 10-kev to 100-Mev; Nat'l. Bur. of Standards Research Paper No. 583.

63. Lind, West, and Du Mond, Phys. Rev. 77, 475 (1950).

64. C. I. Browne, Jr., Precision Measurements of x-Rays and Gamma-Rays in Radioactive Decay (Thesis), UCRL-1764, 1952.

65. Olof Beckman, Arkiv. Fysik 9, 495 (1955).

66. For a discussion of lifetimes and energy widths of atomic states see M. Mladjenovic, Arkiv. Fysik 8, 27 (1954).

67. The author is grateful to Professor J. W. M. Du Mond for his helpful discussion of this problem.

68. C. J. Gallagher, private communication to Prof. J. W. M. DuMond (1960).

69. Nijgh, Wapstra, and Van Lieshout, Nuclear Spectroscopy Tables North Holland Publishing Co., Amsterdam, 1959.

70. R. L. Heath, Scintillation Spectrometry Gamma-Ray Catalogue, AEC Research and Development Report 1DO-16408, July, 1957.

71. F. K. McGowan and E. C. Campbell, Phys. Rev. 92, 523 (1953).

72. A. H. Wapstra, Arkiv Fysik 7, 279 (1954).

73. L. A. Sliv and I. M. Band, Coefficients of Internal Conversion of Gamma Radiation -- Part I, K-Shell (issued in U. S. A. as University of Illinois Report 57ICCK1).

74. ΣL_i refers to the sum of the measured L-subshell intensities. It differs from the total L intensity when one or more of the subshells were not measured.

75. S. A. Moszkowski, Phys. Rev. 82, 35 (1951).

76. K. L. Vander Sluis and P. M. Griffin, J. Opt. Soc. Am. 45, 1087 (1955).

77. K. L. Vander Sluis and J. R. McNally, Jr., J. Opt. Soc. Am. 45, 65 (1955).

78. N. I. Kaliteevskii and M. P. Chaika, Doklady Akad, Nauk S. S. S. R. 103, 49 (1955); Optika i Spektroskopiya 1, 809 (1956).

79. L. A. Korostyleva, A. R. Stringanov, and N. M. Iashin, Zhur. Eksptl. i Teoret. Fiz. 28, 471 (1955); [translation: Soviet Phys. JETP 1, 310 (1955)]; Izvest. Akad. Nauk. S. S. S. R. Ser. Fiz. 19, 31 (1955).

80. A. G. Zimin and N. M. Yashin, Doklady Akad. Nauk. S. S. S. R. 109, 283 (1956); [translation: Soviet Phys. Doklady 1 419 (1957)].

81. J. C. Hubbs and J. Winocur, Bull. Am. Phys. Soc. II, 3, 319 (1958).

82. Hamilton, Hollander, and Pettersson, to be published.

83. Stephens, Asaro, and Perlman, Classification of the Energy Levels of Odd-Mass Nuclei in the Heavy-Element Region [UCRL-8376, 1958], Phys. Rev. 113, 212 (1959).

84. G. Alaga, Phys. Rev. 100, 432 (1955); Nuclear Phys. 4, 625 (1957).

85. R. W. King and D. C. Peasley, Phys. Rev. 94, 1284 (1954).

86. Stephens, Asaro and Perlman, unpublished data (1957).

87. Albridge and Hollander, unpublished data (1956).

88. Thomas, Vandenbosch, Glass, and Seaborg, Phys. Rev. 106, 1228 (1957).

89. B. R. Mottelson and S. Nilsson, Mat.-fys. Skr. Sanske Videnskab Selskab 1, No. 8 (1959).

90. E. H. S. Burhop, The Auger Effect and Other Radiationless Transitions, (Cambridge University Press, Cambridge, 1952).

91. I. Bergström and R. D. Hill, Arkiv Fysik 8, 21 (1954).

92. M. Mladjenovic and H. Slätis, Arkiv. Fysik 9, 41 (1955).

93. Hill, Church, and Mihelich, Rev. Sci. Instr. 23, 523 (1952).

94. W. N. Asaad and E. H. S. Burhop, Proc. Phys. Soc. (London) 71, 369 (1958).

95. Z. Sujkowski and H. Slätis, Arkiv. Fysik 14, 101 (1958).

96. A. Chetham-Strode, Jr., Light Isotopes of Berkelium and Californium (Thesis), UCRL-3322, June 1956.

97. Hulet, Thompson, Ghiorso, and Street, Phys. Rev. 84, 366 (1951).

98. Magnusson, Friedman, Engelkemeir, Fields, and Wagner, Phys. Rev. 102, 1097 (1956).

99. The coincidence measurements were performed by Dr. Frank Asaro.

100. The exact term is $\dfrac{Gs}{1 - Gg \frac{cy}{1+\alpha} (\varepsilon_\gamma + 2\alpha_K \ell \varepsilon_K)}$

where Gg is the gate detector geometry.

101. Brysk and Rose (Ref. No. 102) have discussed the n^{-3} dependence of electron-capture transition probabilities. We have assumed here that the probability of internal conversion varies in a like manner.

102. H. Brysk and M. E. Rose, Theoretical Results on Orbital Capture, Oak Ridge National Laboratory Report - ORNL 1830, Jan. 1955.

103. R. W. Hoff and J. O. Rasmussen, Concerning ft Values and L/K Ratios for Orbital Electron Capture, UCRL-4511, May 1955; Phys. Rev. 101, 280 (1956).

104. J. K. Major and L. C. Biedenharn, Revs. Modern Phys. 26, 321 (1954).

105. M. Fred and F. S. Tomkins, Phys. Rev. 89, 318 (1953).

106. R. Thorne, Nature 178, 484 (1956).

107. See Reference 83 for a discussion of this assignment.

108. Stephens, Asaro, Amiel, and Perlman, Phys. Rev. 107, 1456 (1957).

109. B. M. Foreman, Jr., and G. T. Seaborg, J. Inorg. Nuclear Chem. 7, 305 (1958).

110. This plot, which is used at this Laboratory for film efficiency corrections, is a composite of the data of R. A. Dudley, Nucleonics 12, No. 5, 24 (1954); Cranberg and Halpern, Rev. Sci. Instr. 20, 641 (1949); and F. Canavan, Lawrence Radiation Laboratory, unpublished data, 1956.

111. See, for example, Hamilton, Langer, and Smith, Phys. Rev. 112, 2010 (1958).

112. For a review of this previous work and for references see References 113 and 114 below.

113. S. Rosenblum, J. Sant'Anna Dionisio, and M. Valadares, J. Phys. et Rad. 17, 112 (1956).

114. J. Delesalle, Contribution á l' étude de la conversion interne dans le sous-couches L, par spectrographie magnétique semi-circulaire avec pré et post-accélération (Thesis), Université de Paris, 1958; J. Phys. Radium 19, 111 (1958).

115. Many thanks are due Dr. Frank Asaro for his advice and assistance in preparing the vaporized samples.

116. Kenneth T. Faler, Nuclear Decay-Scheme Studies of Some Tantalum and Terbium Isotopes (Thesis), UCRL-8664, April 1959.

117. A. W. Hull, Phys. Rev. 18, 31 (1921).

118. W. R. Dixon, Nucleonics 8, No. 4, 68 (1951).

This report was prepared as an account of Government sponsored work. Neither the United States, nor the Commission, nor any person acting on behalf of the Commission:

A. Makes any warranty or representation, expressed or implied, with respect to the accuracy, completeness, or usefulness of the information contained in this report, or that the use of any information, apparatus, method, or process disclosed in this report may not infringe privately owned rights; or

B. Assumes any liabilities with respect to the use of, or for damages resulting from the use of any information, apparatus, method, or process disclosed in this report.

As used in the above, "person acting on behalf of the Commission" includes any employee or contractor of the Commission, or employee of such contractor, to the extent that such employee or contractor of the Commission, or employee of such contractor prepares, disseminates, or provides access to, any information pursuant to his employment or contract with the Commission, or his employment with such contractor.